FINAL TECHNICAL REPORT
NASA GRANT NUMBER NAG3-1844

PROJECT TITLE:

DETERMINATION OF INTERFACIAL RHEOLOGICAL PROPERTIES THROUGH MICROGRAVITY OSCILLATIONS OF BUBBLES AND DROPS

PI INFORMATION:

Professor Ali Nadim
(with graduate student: Brian M. Rush)
Department of Aerospace and Mechanical Engineering
Boston University
110 Cummington Street
Boston, MA 02215 USA
Email: nadim@bu.edu
Phone: 617-353-3951
Fax: 617-353-5866

Contents

1 Introduction 1

2 Theory 3
- 2.1 Motivating example: An oscillating flat plate . . . 3
  - 2.1.1 Exact solution using Laplace transforms . . . 4
  - 2.1.2 Approximate solution using an averaging method . . . 5
- 2.2 Drop oscillations: equations and boundary conditions . . . 6
- 2.3 The total mechanical energy equation . . . 7
- 2.4 Analysis of total mechanical energy equation . . . 9
  - 2.4.1 Base flow: inviscid oscillations . . . 10
  - 2.4.2 Case 1: "negligible" surfactant effects . . . 13
  - 2.4.3 Case 2: "small" surfactant effects . . . 19
  - 2.4.4 Case 3: "medium" surfactant effects . . . 25
  - 2.4.5 Case 4: "large" surfactant effects . . . 29

3 Numerics 32
- 3.1 Governing equations and boundary conditions . . . 32
  - 3.1.1 Regularized boundary integral representation . . . 32
  - 3.1.2 Boundary conditions . . . 34
- 3.2 Numerical procedure . . . 34
  - 3.2.1 Base flow: inviscid oscillations . . . 35
- 3.3 Modified boundary conditions . . . 36
  - 3.3.1 Case 1: "negligible" surfactant effects . . . 38
  - 3.3.2 Case 2: "small" surfactant effects . . . 44
  - 3.3.3 Case 3: "medium" surfactant effects . . . 47
  - 3.3.4 Case 4: "large" surfactant effects . . . 51

4 Summary and conclusions 54

A Surface theorems 57

B Constants in matched asymptotics 58
- B.1 Case 1: "negligible" surfactant effects . . . 58
- B.2 Case 2: "small" surfactant effects . . . 58
- B.3 Case 3: "medium" surfactant effects . . . 59

C Local coordinate system 60

D Explicit kernels in numerics 61

Bibliography 62

List of Figures

2.1 Schematic of oscillating plate system 3
2.2 Integration contour for solution using Laplace transforms 5

3.1 Schematic of the local coordinate system 33
3.2 Example inviscid calculation 37
3.3 Numerical instability seen when including bulk viscous effects 43
3.4 Example calculation for a clean drop including bulk viscous effects 44
3.5 Example calculation including weak bulk viscous and surfactant effects 48
3.6 Example calculation including weak bulk viscous and surfactant effects 49
3.7 Example calculation including large surfactant effects 53

A.1 Material surface bounded by a material line. 57

Executive Summary

This report summarizes our derivations of analytical expressions for the frequencies and damping constants for small-amplitude axisymmetric shape oscillations of a liquid drop suspended in an immiscible fluid host in microgravity. In particular, this work addresses large Reynolds number shape oscillations and focuses on the surface rheological effects that arise from the presence of insoluble surfactants at the interface. Parameters characterizing viscous effects from the bulk phases, surface viscous effects, Marangoni effects from the surface advection and diffusion of surfactants, and the Gibbs elasticity are all considered and analyzed to determine the relative importance of each contribution.

Supplementing the analytical treatment for small-amplitude oscillations, a numerical boundary integral equation formulation is developed for the study of large-amplitude axisymmetric oscillations of a drop in vacuum. The boundary integral formulation is an extension of classical potential flow theory and approximately accounts for viscous effects in the bulk fluid as well as the surface viscous and Marangoni effects resulting from an insoluble surfactant contaminating the interface.

Theoretical and numerical results are presented for four distinct cases. These range from the case when the effects of the surfactants are "negligible" to "large" when compared to the viscous effects in the bulk phases. The feasibility of the non-contact measurement of the surface parameters, using experimental observations for the oscillation frequencies and damping constants of drops and bubbles, is discussed.

Inventions:

This research has *not* resulted in any invention.

Publications resulting from this grant:

- A. Nadim, "Shape Oscillations of Gas Bubbles with Newtonian Interfacial Properties," in Proceedings of the Third Microgravity Fluid Physics Conference, NASA Lewis Research Center, Cleveland, OH (June 1996).
- B. M. Rush, H. Azuma and A. Nadim, "Forced Oscillations of a Sessile Mercury Drop," Proceedings of FEDSM'98, 1998 ASME Fluids Engineering Division Summer Meeting, Washington, DC (June 1998).
- A. Nadim and B. M. Rush, "Mechanisms Contributing to the Damping of Shape Oscillations of Liquid Drops," Proceedings of ICMF'98, The Third International Conference on Multiphase Flow, Lyon, France (June 1998).
- B. M. Rush and A. Nadim, "Damping of Drop Oscillations by Surfactants and Surface Rheology," in Proceedings of the Fourth Microgravity Fluid Physics and Transport Phenomena Conference, pp. 615–620, NASA Lewis Research Center, Cleveland, OH (August 1998).
- B. M. Rush and A. Nadim, "The Shape Oscillations of a Two-Dimensional Drop Including Viscous Effects," *Engineering Analysis with Boundary Elements*, **24**, 43–51 (2000).

Forthcoming publications:

- B. M. Rush and A. Nadim, "Energetics of Viscous Drop Oscillations," (In preparation for *Phys. Fluids*).
- B. M. Rush and A. Nadim, "Effects of Surfactants and Interfacial Rheology on Oscillating Drops, Part I: Analysis Based on the Energy Equation, Part II: Simulations Using the Boundary Integral Method," (In preparation for *J. Fluid Mech.*).

Conference papers:

- Shape Oscillations of Gas Bubbles with Newtonian Interfacial Properties, A. Nadim, Third Microgravity Fluid Physics Conference, NASA Lewis Research Center, Cleveland, OH (June 1996).
- Nonlinear Oscillations of Two-Dimensional Drops, B. M. Rush, A. Nadim and H. Azuma, American Physical Society, Division of Fluid Dynamics, Annual Meeting, Syracuse, NY (November 1996). [*Bull. Am. Phys. Soc.*, **41**, 1793 (1996).]
- A Comparison of Several Boundary Integral Methods for Inviscid Drop Oscillations, B. M. Rush and A. Nadim, Fourth U.S. National Congress on Computational Mechanics, San Francisco, CA (August 1997).
- Nonlinear Oscillations of Two-Dimensional Drops with Surface Rheology, B. M. Rush and A. Nadim, American Physical Society, Division of Fluid Dynamics, Annual Meeting, San Francisco, CA (November 1997). [*Bull. Am. Phys. Soc.*, **42**, 2160 (1997).]
- A Comparison of Several Boundary Integral Methods for Inviscid Drop Oscillations, B. M. Rush and A. Nadim, IABEM International Symposium on Boundary Element Methods, Ecole Polytechnique, Palaiseau (Paris), France, (May 1998).
- Mechanisms Contributing to the Damping of Shape Oscillations of Liquid Drops, A. Nadim and B. M. Rush, 3rd International Conference on Multiphase Flow, Lyon, France (June 1998).
- Forced Oscillations of a Sessile Mercury Drop, B. M. Rush, H. Azuma and A. Nadim, Symposium on the Manipulation of Particles by External Forcing, ASME Fluids Engineering Division Summer Meeting, Washington, DC (June 1998).
- Damping of Drop Oscillations by Surfactants and Surface Rheology, B. M. Rush and A. Nadim, Fourth Microgravity Fluid Physics and Transport Phenomena Conference, Cleveland, Ohio (August 1998).
- Shape Oscillations of Surfactant-Laden Viscous Drops with Marangoni and Interfacial Rheological Effects, B. M. Rush and A. Nadim, American Institute of Chemical Engineering, Annual Meeting, Dallas, TX (November 1999).
- Added Mass and Dissipation in Oscillatory Boundary Layers, B. M. Rush and A. Nadim, American Physical Society, Division of Fluid Dynamics, Annual Meeting, New Orleans, LA (November 1999). [*Bull. Am. Phys. Soc.*, **44**, 193 (1999).]
- The Shape Oscillations of Drops and Bubbles in the Presence of Surfactants, B. M. Rush and A. Nadim, American Physical Society, Division of Fluid Dynamics, Annual Meeting, Washington, DC (November 2000).

Chapter 1

Introduction

The dynamics of the shape deformations of drops and bubbles are important in a wide variety of practical applications including heat-transfer [7], chemical engineering [16], multiphase flow [24], and nuclear physics [13]. Any system in which the surface area to volume ratios are high may be greatly influenced by the presence of surfactants. Surfactants are long molecules with separated hydrophilic and hydrophobic segments that preferentially adsorb to an interface and give it viscoelastic properties. For a Newtonian interfacial fluid these viscoelastic properties are characterized by surface tension, a Gibbs elasticity, and surface shear and dilatational viscosities. Since the dynamics of drops and bubbles depend on these viscoelastic properties, experiments have been proposed for the non-contact measurement of these properties through the observations of forced and freely oscillating drops and bubbles [48, 20, 9, 25, 15]. The present work aims to determine analytical expressions for the dependence of the frequency and damping constants on these viscoelastic interfacial properties, needed for extracting their values from the experimental data.

The study of the small-amplitude shape oscillations of drops and bubbles has a long history. By using a normal-mode analysis to separate the time variable, Rayleigh [39] determined the small-amplitude linear frequencies of an inviscid drop oscillating in vacuum. This analysis was generalized to treat the case of an inviscid drop submerged in an inviscid medium by Lamb [23], who also used the inviscid velocity solutions to estimate the rate of damping of a weakly viscous drop in vacuum or a gas bubble immersed in a weakly viscous medium. A similar dissipation estimate was obtained for arbitrary viscosities by Reid [40] for a drop in a vacuum or low density gas, and by Valentine *et al.* [53] for a drop submerged in a fluid medium. Miller and Scriven [29] used a normal-mode analysis of the linearized Navier-Stokes equations to identify the primary role of boundary layer dissipation on the frequency shift and damping rate for the weakly viscous drop and medium system. Their formulation also included viscoelastic surface properties, but they limited their analysis to the case of free and inextensible interfaces. Prosperetti [37, 38] used a more general technique based on Laplace transforms to study the transient regimes of a weakly viscous drop and medium system and showed that the normal-mode results are recovered in the asymptotic limit for long times. Higher-order corrections to Miller and Scriven's normal-mode analysis have been obtained by Marston [28] and Asaki and Marston [6] for free and acoustically forced shape oscillations of a weakly viscous drop and medium system. Lu and Apfel [25] have extended Miller and Scriven's normal-mode analysis to include the effects of a soluble surfactant in the outer medium. A similar normal-mode analysis has been used by Tian *et al.* [45] to analyze the effects of a soluble surfactant on a drop oscillating in vacuum in the quadrupole mode.

Due to its relative complexity, the large-amplitude analysis of drops and bubbles has been limited to inviscid or numerical models. Tsamapoulos and Brown [51, 52] and Natarajan and Brown [33, 34] have used inviscid models to study nonlinear shape oscillations and mode coupling. Foote [19] and Alonzo [2] analyzed the nonlinear oscillations of a viscous drop in vacuum using the marker-and-cell numerical method. The large-amplitude oscillations of a viscous drop has also been studied by Basaran [7] using a finite-element method. The boundary integral numerical method for potential flow has been used by Lundgren and Mansour [26] and Shi and Apfel [44] to simulate high Reynolds number drop oscillations, where weak viscous effects were included in the formulation by a modification of the normal stress boundary condition. The weakly viscous analysis using the boundary integral numerical method has been extended for the case of charged drop forced in an electric field by Feng and Beard [18] and an acoustically forced drop incorporating the effects

of constant surface viscoelastic properties by Chen *et al.* [15].

The shape oscillation experiments of an acoustically levitated drop or bubble began with Marston and Apfel [27]. Trinh *et al.* [46, 47, 48] have also used acoustic forcing to study the small and large-amplitude shape oscillations of a neutrally buoyant drop submerged in an outer medium. Asaki and Marston [6, 5] have analyzed acoustically positioned gas bubbles oscillating in the presence of insoluble and soluble surfactants and Trinh *et al.* [49] have studied the combined effects of acoustic and electric field forcing on charged drops in air. Recently Apfel *et al.* [3] have studied large-amplitude oscillations for a surfactant contaminated drop in air in microgravity.

The present work considers high Reynolds number shape oscillations of a drop and medium system and extends the knowledge of small-amplitude shape oscillations in the presence of surfactants with the derivation and analysis of a total mechanical energy equation for the system. The analysis of this total mechanical energy equation with matched asymptotic expansion techniques generalizes the energy approaches of Lamb [23] and Hsu and Apfel [20] for the determination of the oscillation frequency and damping constants for the system and provides physical insight into the origin and significance of resulting terms. The understanding of large-amplitude shape oscillations of a drop in vacuum is also improved in the present work with the development and analysis of an efficient boundary integral numerical method for high Reynolds number shape oscillations that incorporates, in an approximate way, the viscous effects in the bulk fluid and surface viscoelastic effects arising from the presence of an insoluble surfactant at the interface.

Chapter 2

Theory

2.1 Motivating example: An oscillating flat plate

Figure 2.1 shows a flat plate of mass m submerged in a fluid of density ρ and viscosity μ and attached to a wall by a spring of stiffness k. The equations and boundary conditions describing the one-dimensional time-dependent displacement of the plate $x(t)$ from equilibrium and fluid velocity $u(y,t)$ are given by

$$m\ddot{x}(t) + kx(t) = A\mu\frac{\partial u}{\partial y}(0,t)\,, \tag{2.1}$$

$$x(0) = x_o\,, \quad \dot{x}(0) = 0\,, \tag{2.2}$$

and

$$\rho\frac{\partial u}{\partial t}(y,t) = \mu\frac{\partial^2 u}{\partial y^2}(y,t)\,, \tag{2.3}$$

$$u(y,0) = 0\,, \quad u(0,t) = \dot{x}(t)\,, \quad u(\infty,t) = 0\,. \tag{2.4}$$

Gravity and end effects have been neglected. Equation (2.2) corresponds to the plate being released from an initial displacement x_o. The right-hand side of (2.1) represents the total viscous force on the plate with total surface area A. The above equations and boundary conditions may be nondimensionalized with the time scale $\omega_o^{-1} = (k/m)^{1/2}$ and the length scale x_o. The distance normal to the plate is scaled with the Stokes' boundary layer thickness $(\mu/\rho\omega_o)^{1/2}$ and the nondimensional form of the equations and boundary conditions are

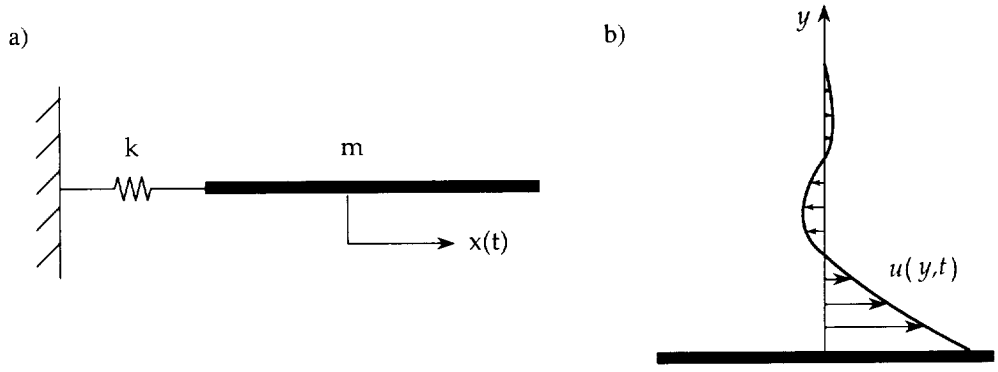

Figure 2.1: a) Schematic of oscillating plate system. b) Stokes' boundary layers above plate.

$$\ddot{x}(t) + x(t) = \varepsilon \frac{\partial u}{\partial y}(0,t)\,, \tag{2.5}$$

$$x(0) = 1\,, \quad \dot{x}(0) = 0\,, \tag{2.6}$$

and

$$\frac{\partial u}{\partial t}(y,t) = \frac{\partial^2 u}{\partial y^2}(y,t)\,, \tag{2.7}$$

$$u(y,0) = 0\,, \quad u(0,t) = \dot{x}(t)\,, \quad u(\infty,t) = 0\,. \tag{2.8}$$

Equations (2.5-2.8) contain the single parameter

$$\varepsilon = \frac{\rho A}{m}\sqrt{\frac{\mu}{\rho\omega_o}}\,, \tag{2.9}$$

which may be interpreted as the ratio of the mass of the fluid in the boundary layer to the mass of the plate.

In the following sections the motion of the plate $x(t)$ when $\varepsilon \ll 1$ is analyzed using two methods. Comparisons are made with shape oscillations of the drop/medium system.

2.1.1 Exact solution using Laplace transforms

Equations (2.5-2.8) may be solved exactly using Laplace transforms in the time variable. The Laplace transform is defined such that

$$\overline{x}(s) = \mathcal{L}\{x(t)\} = \int_0^\infty x(t)e^{-st}dt\,. \tag{2.10}$$

Equations (2.5-2.8) and (2.10) give the solutions for the plate and fluid motion in transform space as

$$\overline{x}(s;\varepsilon) = \frac{s + \varepsilon\sqrt{s}}{(1+s^2) + \varepsilon s\sqrt{s}} \tag{2.11}$$

$$\overline{u}(y,s;\varepsilon) = (s\overline{x} - 1)e^{-\sqrt{s}y}\,. \tag{2.12}$$

When $\varepsilon = 0$, the motions of the plate and fluid are time harmonic with the fluid motion above the plate corresponding to Stokes' 2nd Problem:

$$x(t) = \mathcal{L}^{-1}\{\overline{x}(s;0)\} = \cos(t) \tag{2.13}$$

$$u(y,t) = \mathcal{L}^{-1}\{\overline{u}(y,s;0)\} = e^{-y/\sqrt{2}}\cos(t - y/\sqrt{2})\,. \tag{2.14}$$

If $\varepsilon > 0$, the time-dependent motion of the plate may be expressed in terms of an inverse Laplace transform

$$x(t) = \mathcal{L}^{-1}\{\overline{x}(s;\varepsilon)\} = \frac{1}{2\pi i}\int_{c-i\infty}^{c+i\infty} \frac{(s+\varepsilon\sqrt{s})e^{st}\,ds}{(1+s^2)+\varepsilon s\sqrt{s}} \tag{2.15}$$

and evaluated in the complex s-plane using residue theory. See Figure 2.2 for a description of the integration contour. Note that for small ε, the poles of the integrand in (2.15) are shifted from $\pm i$ by terms of $\mathcal{O}(\varepsilon)$ which are readily calculated. With a total solution of the form $x(t) = x_{\rm sp}(t) + x_{\rm br}(t)$, the leading-order contribution from the two simple poles is

$$x_{\rm sp}(t) = e^{-\varepsilon t/2\sqrt{2}}\cos[(1 - \varepsilon/2\sqrt{2})t] + \mathcal{O}(\varepsilon e^{-\varepsilon t})\,. \tag{2.16}$$

Here $x_{\rm sp}(t)$ is an exponentially damped time harmonic oscillation with a frequency slightly shifted from unity. The leading-oder contribution from the branch cut

$$x_{\rm br}(t) = \frac{-\varepsilon}{\pi}\int_0^\infty \frac{\sqrt{r}e^{-rt}}{(1+r^2)^2 + \varepsilon^2 r^3}\,dr \tag{2.17}$$

$$\sim \frac{-\varepsilon}{2\sqrt{\pi}}\frac{1}{t^{3/2}} \quad \text{as} \quad t \to \infty;\ \varepsilon \to 0\,. \tag{2.18}$$

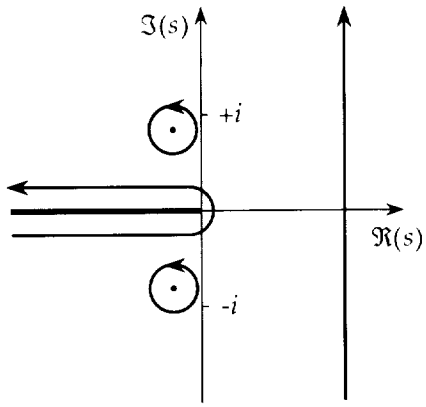

Figure 2.2: Contours around two simple poles and a branch cut in the complex s-plane.

Here $x_{\rm br}(t)$ provides a small correction that decays algebraically for long times. Its contribution dominates that from the simple poles for long times, but by that time the motion of the plate is negligibly small.

Similar behavior has been seen in the analysis of the shape oscillations of drops and bubbles using Laplace transforms. Prosperetti [37, 38] has shown that the time dependent amplitude of the shape oscillations of drop/medium system is composed of a discrete spectrum of exponentially decaying functions and a small continuous spectrum. Roberts and Wu [41] have shown that the continuous spectrum for the shape oscillations of a bubble has an algebraic decay and therefore dominates the total solution for long times. Each of these treatments contains a level of analysis that is impractical when applied to the much more complicated case of the shape oscillations of drops and bubbles when surfactants are present. The following section outlines an averaging method which allows for the calculation of the leading order solutions in a simple way.

2.1.2 Approximate solution using an averaging method

The analysis using the averaging method [21] begins with the derivation of a total mechanical energy equation for the system. For the plate and fluid system this involves multiplying the plate equation (2.5) by $\dot{x}(t)$ and the fluid equation (2.7) by $u(y,t)$ and integrating over y to yield

$$\frac{d}{dt}\left[\frac{\dot{x}^2}{2}+\frac{x^2}{2}\right] = \varepsilon\dot{x}\frac{\partial u}{\partial y}(0,t) \tag{2.19}$$

and

$$\begin{aligned}\frac{d}{dt}\int_0^\infty \frac{u^2}{2}\,dy &= \int_0^\infty u\frac{\partial^2 u}{\partial y^2}\,dy \\ &= -\dot{x}\frac{\partial u}{\partial y}(0,t) - \int_0^\infty \left(\frac{\partial u}{\partial y}\right)^2 dy\,.\end{aligned} \tag{2.20}$$

These two equations may now be combined to form the total mechanical energy equation for the system

$$\frac{d}{dt}\left[\frac{\dot{x}^2}{2}+\varepsilon\int_0^\infty \frac{u^2}{2}\,dy+\frac{x^2}{2}\right] = -\varepsilon\int_0^\infty \left(\frac{\partial u}{\partial y}\right)^2 dy\,. \tag{2.21}$$

The left-hand side of (2.21) is the time rate of change of the total energy of the system, which consists of the kinetic energy of the plate and fluid and the potential energy in the spring. The right-hand side of (2.21) is the the total viscous dissipation in the fluid. For $\varepsilon = 0$, this equation shows that the total energy in the system is conserved.

The averaging method uses the time-periodic solutions of the plate and fluid to find the time-average of the quantities of kinetic energy, potential energy, and dissipation rate. An energy equation is then

constructed which yields terms with equivalent time averages. This new energy equation is then simplified to form a linear oscillator equation that captures the leading order behavior of the plate. This procedure is demonstrated below.

Suppose in general that $\dot{x}(t) = \Re\{Ue^{it}\}$ and $u(y,t) = \Re\{U\exp[-(1+i)y/\sqrt{2}+it]\}$, where U is a complex amplitude. (For the particular boundary conditions above $U = 1$.) It is easily shown that

$$\left\langle \int_0^\infty \frac{u^2}{2}\,dy \right\rangle = \frac{1}{4\sqrt{2}}|U|^2 = \left\langle \frac{\dot{x}^2}{2\sqrt{2}} \right\rangle \tag{2.22}$$

$$\left\langle \int_0^\infty \left(\frac{\partial u}{\partial y}\right)^2 dy \right\rangle = \frac{1}{2\sqrt{2}}|U|^2 = \left\langle \frac{\dot{x}^2}{\sqrt{2}} \right\rangle . \tag{2.23}$$

Here the angular brackets $\langle\rangle$ denote the time average over one period of oscillation. Replacing the fluid terms in (2.21) with terms involving $\dot{x}$ on the right-hand sides of (2.22) and (2.23), which have the same time average, yields

$$\frac{d}{dt}\left[\frac{\dot{x}^2}{2} + \varepsilon\frac{\dot{x}^2}{2\sqrt{2}} + \frac{x^2}{2}\right] = -\varepsilon\frac{\dot{x}^2}{\sqrt{2}} . \tag{2.24}$$

Taking the time derivative of the left-hand side of (2.24) and dividing through by $\dot{x}(t)$ gives the following oscillator equation

$$(1 + \frac{\varepsilon}{\sqrt{2}})\,\ddot{x} + \frac{\varepsilon}{\sqrt{2}}\,\dot{x} + x = 0 , \tag{2.25}$$

which contains added mass and damping terms. The leading order solution is

$$x(t) = e^{-\varepsilon t/2\sqrt{2}}\cos[(1 - \varepsilon/2\sqrt{2})t] + \mathcal{O}(\varepsilon^2) . \tag{2.26}$$

Comparing equations (2.16) to (2.26) shows that the averaging method captures the leading order contributions to the time dependent motion of the plate, but fails to capture the additional $\mathcal{O}(\varepsilon)$ corrections from the branch cut.

2.2 Drop oscillations: equations and boundary conditions

Returning to the problem of drop oscillations, consider a liquid drop of density ρ and viscosity μ suspended in an infinite fluid medium of density $\hat{\rho}$ and viscosity $\hat{\mu}$, in the absence of gravity. Both fluids are assumed to be incompressible and Newtonian. The continuity and momentum equations in each phase take the forms

$$\boldsymbol{\nabla}\cdot\mathbf{v} = 0 , \quad \rho\frac{D\mathbf{v}}{Dt} = \boldsymbol{\nabla}\cdot\boldsymbol{\Pi} \quad \text{for } \mathbf{x} \in V_m(t) , \tag{2.27}$$

$$\boldsymbol{\nabla}\cdot\hat{\mathbf{v}} = 0 , \quad \hat{\rho}\frac{D\hat{\mathbf{v}}}{Dt} = \boldsymbol{\nabla}\cdot\hat{\boldsymbol{\Pi}} \quad \text{for } \mathbf{x} \in \hat{V}_m(t) . \tag{2.28}$$

Here $\mathbf{v}$ and $\hat{\mathbf{v}}$, respectively, refer to the drop and medium velocity fields, $V_m(t)$ and $\hat{V}_m(t)$ are the material volumes of the drop and medium, and the stress tensors $\boldsymbol{\Pi}$ and $\hat{\boldsymbol{\Pi}}$ are given by

$$\boldsymbol{\Pi} = -p\mathbf{I} + 2\mu\mathbf{E} , \quad \mathbf{E} = \frac{1}{2}[(\boldsymbol{\nabla}\mathbf{v}) + (\boldsymbol{\nabla}\mathbf{v})^T] , \tag{2.29}$$

$$\hat{\boldsymbol{\Pi}} = -\hat{p}\mathbf{I} + 2\hat{\mu}\hat{\mathbf{E}} , \quad \hat{\mathbf{E}} = \frac{1}{2}[(\boldsymbol{\nabla}\hat{\mathbf{v}}) + (\boldsymbol{\nabla}\hat{\mathbf{v}})^T] . \tag{2.30}$$

In (2.29) and (2.30), p and $\hat{p}$ represent the pressures in the two fluids, $\mathbf{I}$ is the isotropic unit tensor, and $\mathbf{E}$ and $\hat{\mathbf{E}}$ are the symmetric and traceless rate-of-strain tensors.

These field equations need to be supplemented by boundary conditions at infinity and at the material interface $S_m(t)$ between the drop and medium. At infinity, the velocity field vanishes and the pressure tends to a constant value. The interface is assumed to be covered with surfactants and therefore possesses its own

rheological properties, which may be characterized by the surface stress tensor $\mathbf{\Pi}_s$ [16]. The no-slip and stress balance boundary conditions at the interface thus assume the respective forms [16]

$$\left.\begin{array}{rcl} \mathbf{v} & = & \hat{\mathbf{v}} \\ \hat{\mathbf{n}} \cdot (\hat{\mathbf{\Pi}} - \mathbf{\Pi}) & = & -\nabla_s \cdot \mathbf{\Pi}_s \end{array}\right\} \quad \text{for } \mathbf{x} \in S_m(t)\,. \tag{2.31}$$

The velocity of the interface is equal to the fluid velocity in the drop or medium evaluated at $S_m(t)$. For convenience, this velocity is subsequently denoted by $\mathbf{v}$. The surface stress tensor is also assumed to be "Newtonian" and defined by a Boussinesq-Scriven constitutive relationship of the form [16, 31, 43]

$$\mathbf{\Pi}_s = \sigma \mathbf{I}_s + 2\mu_s \mathbf{E}_s + \kappa_s \mathbf{I}_s (\nabla_s \cdot \mathbf{v})\,. \tag{2.32}$$

Here σ, μ_s, and κ_s, respectively, refer to interfacial tension, surface shear viscosity, and surface dilatational viscosity. Also, $\mathbf{I}_s = \mathbf{I} - \hat{\mathbf{n}}\hat{\mathbf{n}}$ is the surface unit tensor and $\hat{\mathbf{n}}$ is a unit vector normal to the interface pointing into the surrounding fluid medium. $\nabla_s = \mathbf{I}_s \cdot \nabla$ is the surface gradient, and $\mathbf{E}_s$ is the symmetric and traceless surface rate-of-strain tensor defined by

$$\mathbf{E}_s = \frac{1}{2}[(\nabla_s \mathbf{v}) \cdot \mathbf{I}_s + \mathbf{I}_s \cdot (\nabla_s \mathbf{v})^T] - \frac{1}{2}\mathbf{I}_s (\nabla_s \cdot \mathbf{v})\,. \tag{2.33}$$

In this work μ_s and κ_s are taken to be constant. The surface tension σ, however, depends on local surfactant concentration Γ. For small-amplitude drop oscillations the concentration of surfactants Γ is assumed to vary only slightly from the equilibrium concentration Γ_{eq} and the surface tension is approximated as a linearly decreasing function of the surfactant concentration [16]

$$\sigma(\Gamma) = \sigma_{eq} - \frac{e_s}{\Gamma_{eq}}(\Gamma - \Gamma_{eq})\,. \tag{2.34}$$

Here σ_{eq} is a constant equilibrium surface tension and e_s is the Gibbs elasticity.

The surfactant transport equation for an insoluble surfactant is given by [31]

$$\frac{\partial \Gamma}{\partial t} + \nabla_s \cdot (\mathbf{v}\Gamma) = D_s \nabla_s{}^2 \Gamma\,, \tag{2.35}$$

where D_s is the surface diffusivity of surfactants and $\mathbf{v}$ is the velocity of the interface. The surfactant transport equation is coupled to the equations governing the bulk fluid motions through (2.34).

2.3 The total mechanical energy equation

The total mechanical energy equation is obtained by dot multiplying the momentum equation in (2.27) by $\mathbf{v}$, the momentum equation in (2.28) by $\hat{\mathbf{v}}$, integrating over the respective material volumes $V_m(t)$ and $\hat{V}_m(t)$, and adding the resulting equations. With the aid of the bulk Reynolds Transport and Divergence Theorems [4, 31], the no-slip boundary condition (2.31), and the incompressibility conditions (2.27) and (2.28), the following equation is obtained

$$\begin{aligned} \frac{d}{dt}\left\{\int_{V_m} \frac{1}{2}\rho|\mathbf{v}|^2\, dV + \int_{\hat{V}_m} \frac{1}{2}\hat{\rho}|\hat{\mathbf{v}}|^2\, dV\right\} = & \\ & - \int_{V_m} 2\mu(\mathbf{E} : \mathbf{E})\, dV - \int_{\hat{V}_m} 2\hat{\mu}(\hat{\mathbf{E}} : \hat{\mathbf{E}})\, dV \\ & - \int_{S_m} \hat{\mathbf{n}} \cdot (\hat{\mathbf{\Pi}} - \mathbf{\Pi}) \cdot \mathbf{v}\, dS\,. \end{aligned} \tag{2.36}$$

The integrand in the last term on the right-hand side of (2.36) may be simplified using the stress balance boundary condition (2.31):

$$\begin{aligned} \hat{\mathbf{n}} \cdot (\hat{\mathbf{\Pi}} - \mathbf{\Pi}) \cdot \mathbf{v} &= (-\nabla_s \cdot \mathbf{\Pi}_s) \cdot \mathbf{v} \\ &= \mathbf{\Pi}_s^T : \nabla_s \mathbf{v} - \nabla_s \cdot (\mathbf{\Pi}_s \cdot \mathbf{v}) \\ &= 2\mu_s(\mathbf{E}_s : \mathbf{E}_s) + \kappa_s(\nabla_s \cdot \mathbf{v})^2 \\ &\quad + \sigma(\nabla_s \cdot \mathbf{v}) - \nabla_s \cdot (\mathbf{\Pi}_s \cdot \mathbf{v})\,, \end{aligned} \tag{2.37}$$

so that

$$\frac{d}{dt}\left\{\int_{V_m}\frac{1}{2}\rho|\mathbf{v}|^2\,dV+\int_{\hat{V}_m}\frac{1}{2}\hat{\rho}|\hat{\mathbf{v}}|^2\,dV\right\}=$$
$$-\int_{V_m}2\mu(\mathbf{E}:\mathbf{E})\,dV-\int_{\hat{V}_m}2\hat{\mu}(\hat{\mathbf{E}}:\hat{\mathbf{E}})\,dV$$
$$-\int_{S_m}2\mu_s(\mathbf{E}_s:\mathbf{E}_s)\,dS-\int_{S_m}\kappa_s(\boldsymbol{\nabla}_s\cdot\mathbf{v})^2\,dS$$
$$-\int_{S_m}\sigma(\boldsymbol{\nabla}_s\cdot\mathbf{v})\,dS-\int_{S_m}\boldsymbol{\nabla}_s\cdot(\boldsymbol{\Pi}_s\cdot\mathbf{v})\,dS\,. \tag{2.38}$$

The last term on the right-hand side of this expression is zero by the the Surface Divergence Theorem [31], and the second to last term may be simplified using (2.34) and the Surface Reynolds Transport Theorem [31]. The general forms of the Surface Reynolds Transport and Surface Divergence Theorems are given in the Appendix A. The final form for the total mechanical energy equation is

$$\frac{d}{dt}\left\{\int_{V_m}\frac{1}{2}\rho|\mathbf{v}|^2\,dV+\int_{\hat{V}_m}\frac{1}{2}\hat{\rho}|\hat{\mathbf{v}}|^2\,dV+\int_{S_m}\sigma_{eq}\,dS\right\}=$$
$$-\int_{V_m}2\mu(\mathbf{E}:\mathbf{E})\,dV-\int_{\hat{V}_m}2\hat{\mu}(\hat{\mathbf{E}}:\hat{\mathbf{E}})\,dV$$
$$-\int_{S_m}2\mu_s(\mathbf{E}_s:\mathbf{E}_s)\,dS-\int_{S_m}\kappa_s(\boldsymbol{\nabla}_s\cdot\mathbf{v})^2\,dS$$
$$+\int_{S_m}\frac{\mathrm{e}_s}{\Gamma_{eq}}(\Gamma-\Gamma_{eq})(\boldsymbol{\nabla}_s\cdot\mathbf{v})\,dS\,. \tag{2.39}$$

The terms on the left-hand side represent the time rate of change of the total kinetic energies in each phase and the potential energy. The first two terms on the right-hand side of (2.39) represent the viscous dissipation rate in the bulk phases. The next two terms are similarly identified as dissipation terms arising from surface shear and dilatational viscosities. The last term on the right-hand side of (2.39) contains the surface tension gradient, or Marangoni, effects and couples the total mechanical energy equation to the surfactant transport equation. Its interpretation is less obvious and is discussed below.

If the bulk and surface viscosities $\mu, \hat{\mu}, \mu_s, \kappa_s$ and the Gibbs elasticity e_s are set to zero, then equation (2.39) shows that the total energy of the system is conserved. If only the Gibbs elasticity is set to zero, total viscous dissipation rate has contributions from each of the bulk phases with additional contributions from the surface phase.

An interpretation of the Marangoni term may be seen through an analysis of the surfactant transport equation (2.35), which may be equivalently expressed in the following form

$$\begin{aligned}\Gamma_{eq}(\boldsymbol{\nabla}_s\cdot\mathbf{v}) &= -\frac{\partial}{\partial t}(\Gamma-\Gamma_{eq})-\mathbf{v}\cdot\boldsymbol{\nabla}_s(\Gamma-\Gamma_{eq})\\ &\quad -(\Gamma-\Gamma_{eq})(\boldsymbol{\nabla}_s\cdot\mathbf{v})+D_s\nabla_s{}^2(\Gamma-\Gamma_{eq})\,.\end{aligned} \tag{2.40}$$

After multiplying this equation by $\mathrm{e}_s(\Gamma-\Gamma_{eq})/\Gamma_{eq}^2$, integrating over the material surface $S_m(t)$, and using the Surface Reynolds Transport and Surface Divergence Theorems, the Marangoni term in (2.39) may be re-expressed as

$$\begin{aligned}\int_{S_m}\frac{\mathrm{e}_s}{\Gamma_{eq}}(\Gamma-\Gamma_{eq})(\boldsymbol{\nabla}_s\cdot\mathbf{v})\,dS &= -\frac{d}{dt}\int_{S_m}\frac{\mathrm{e}_s}{2\Gamma_{eq}^2}(\Gamma-\Gamma_{eq})^2\,dS\\ &\quad -\int_{S_m}\frac{\mathrm{e}_s D_s}{\Gamma_{eq}^2}\left|\boldsymbol{\nabla}_s(\Gamma-\Gamma_{eq})\right|^2 dS\\ &\quad -\int_{S_m}\frac{\mathrm{e}_s}{2\Gamma_{eq}^2}(\Gamma-\Gamma_{eq})^2(\boldsymbol{\nabla}_s\cdot\mathbf{v})\,dS\,.\end{aligned} \tag{2.41}$$

The Marangoni term must therefore be interpreted as having several contributions. The first contribution is the time rate of change of an additional energy storage term arising from the non-equilibrium distribution of

surfactants. The second contribution is dissipative and arises from the irreversible diffusion of surfactants. The last term on the right-hand side of (2.41) is not clearly identifiable as a dissipative or energy storage term. For small-amplitude oscillations this term will be shown to be negligibly small compared to the other two. Depending on the surface Peclet number characterizing the surfactant transport, the leading-order behavior of the Marangoni term can be shown to be dissipative, provide an additional energy storage, or give a combination of these [32].

2.4 Analysis of total mechanical energy equation

In this section the averaging method is used to analyze the total mechanical energy equation of the drop/medium system performing small-amplitude shape oscillations.

Nondimensionalization is based on the inertial scales from the drop fluid properties:

$$\text{length} = R\,, \quad \text{time} = \omega^{-1} = \left(\frac{\rho R^3}{\sigma_{eq}}\right)^{1/2}\,, \quad \text{mass} = \rho R^3\,. \tag{2.42}$$

Surface tension and surfactant concentration are scaled on their equilibrium values σ_{eq} and Γ_{eq}. The nondimensional forms for the total mechanical energy equation and surfactant transport equation are thus

$$\begin{aligned}\frac{d}{dt}\{\text{K.E.} + \text{P.E.}\} &= -\alpha^2\{\text{Bulk Diss.}\} \\ &\quad -\mu_s^*\{\text{Surf. Diss.}\} \\ &\quad +e_s^*\{\text{Marangoni}\}\end{aligned} \tag{2.43}$$

and

$$\frac{\partial \Gamma}{\partial t} + \boldsymbol{\nabla}_s \cdot (\mathbf{v}\Gamma) = \frac{1}{\mathrm{Pe}_s}\nabla_s{}^2\,\Gamma\,, \tag{2.44}$$

where

$$\text{K.E.} = \int_{V_m} \frac{1}{2}|\mathbf{v}|^2\,dV + \frac{\hat{\rho}}{\rho}\int_{\hat{V}_m} \frac{1}{2}|\hat{\mathbf{v}}|^2\,dV \tag{2.45}$$

$$\text{P.E.} = \int_{S_m} dS \tag{2.46}$$

$$\text{Bulk Diss.} = \int_{V_m} 2(\mathbf{E}:\mathbf{E})\,dV + \frac{\hat{\mu}}{\mu}\int_{\hat{V}_m} 2(\hat{\mathbf{E}}:\hat{\mathbf{E}})\,dV \tag{2.47}$$

$$\text{Surf. Diss.} = \int_{S_m} 2(\mathbf{E}_s:\mathbf{E}_s)\,dS + \frac{\kappa_s^*}{\mu_s^*}\int_{S_m} (\boldsymbol{\nabla}_s\cdot\mathbf{v})^2\,dS \tag{2.48}$$

$$\text{Marangoni} = \int_{S_m} (\Gamma - 1)(\boldsymbol{\nabla}_s\cdot\mathbf{v})\,dS\,. \tag{2.49}$$

Equations (2.45)–(2.49) represent, respectively, the total nondimensional kinetic and potential energy, the bulk and surface viscous dissipation rate, and the Marangoni term.

The nondimensional Marangoni term can be re-expressed as

$$\begin{aligned}\{\text{Marangoni}\} &= -\frac{d}{dt}\{\text{Mar. E.}\} \\ &\quad -\frac{1}{\mathrm{Pe}_s}\{\text{Mar. Diss.}\} \\ &\quad -\{\text{Remainder}\}\end{aligned} \tag{2.50}$$

where

$$\text{Mar. E.} = \int_{S_m} \frac{1}{2}(\Gamma - 1)^2\,dS \tag{2.51}$$

$$\text{Mar. Diss.} = \int_{S_m} |\nabla_s(\Gamma - 1)|^2 \, dS \tag{2.52}$$

$$\text{Remainder} = \int_{S_m} (\Gamma - 1)^2 (\nabla_s \cdot \mathbf{v}) \, dS \, . \tag{2.53}$$

Mar. E. represents the nondimensional Marangoni stored energy term. Mar. Diss. is a dissipation rate. The remainder term will be shown to be negligible for small oscillations.

In addition to $\hat{\mu}/\mu$ and $\hat{\rho}/\rho$, the dimensionless parameters in (2.43)–(2.53) are defined to be

$$(\alpha^2, \mu_s^*, \kappa_s^*, \mathrm{e}_s^*, \mathrm{Pe}_s) \equiv \left(\frac{\mu}{\omega \rho R^2}, \frac{\mu_s \omega}{\sigma_{eq}}, \frac{\kappa_s \omega}{\sigma_{eq}}, \frac{\mathrm{e}_s}{\sigma_{eq}}, \frac{\omega R^2}{D_s} \right) . \tag{2.54}$$

These represent, respectively, the inverse of the Reynolds number, the dimensionless surface shear and dilatational viscosities, the Gibbs elasticity, and the surface Peclet number.

In order to analyze the drop/medium system with the averaging method, the time-periodic velocity profiles in each phase must be determined. The shape oscillations are assumed to be small and axisymmetric, and the Reynolds number is assumed to be large so that deviations from potential flow are confined to thin Stokes boundary layers near the interface. The velocity and pressure fields in each phase are therefore found by the solution of a singular perturbation problem, which may be approximated using matched asymptotic expansion techniques. For this purpose, the nondimensional shape of the interface and surfactant concentration are taken to be

$$r(\theta, t; \varepsilon) = 1 + \varepsilon a_\ell(t) P_\ell(\cos\theta) + \mathcal{O}(\varepsilon^2) \tag{2.55}$$

$$\Gamma(\theta, t; \varepsilon) = 1 + \varepsilon g_\ell(t) P_\ell(\cos\theta) + \mathcal{O}(\varepsilon^2) \, . \tag{2.56}$$

Here ε is a small dimensionless parameter used to linearize the equations and P_ℓ is the Legendre polynomial of order ℓ, where θ represents the polar angle measured from the axis of symmetry. The time-dependent amplitudes for the axisymmetric perturbations in shape $a_\ell(t)$ and surfactant concentration $g_\ell(t)$ are given by the real parts of the complex quantities

$$a_\ell(t) = \Re\{A e^{i\Omega_{\ell 0} t}\} \tag{2.57}$$

$$g_\ell(t) = \Re\{G e^{i\Omega_{\ell 0} t}\} \, . \tag{2.58}$$

Here A and G are complex amplitudes. Since the Reynolds number is assumed to be large, the assumed nondimensional frequency $\Omega_{\ell 0}$ is taken to be the base frequency for small-amplitude inviscid oscillations of a drop/medium system given by the Lamb formula [23]

$$\Omega_{\ell 0}^2 = \frac{\ell(\ell - 1)(\ell + 1)(\ell + 2)}{[(\ell + 1) + \ell \hat{\rho}/\rho]} \, . \tag{2.59}$$

Using the approximate forms for the velocity profiles found from the asymptotic analysis, order-of-magnitude estimates are used to identify the dominant contributions to each term in the total mechanical energy equation. Time-averaging these dominant contributions over one oscillation period further simplifies the terms and allows for the derivation of a damped harmonic oscillator equation. The characteristic frequencies for this equation capture the leading-order behavior of the drop/medium system influenced by the effects of viscosity. When surfactants are introduced, the damped harmonic oscillator equation is coupled to the surfactant transport equation through the Marangoni term. For that case, the leading-order behavior of the system is described by the simultaneous solution of two coupled equations.

The following sections begin with an analysis of the base potential flow for the shape oscillations of the drop/medium system. The succeeding four cases include the effects of viscosity in the system with increasingly greater effects from the presence of an insoluble surfactant at the interface.

2.4.1 Base flow: inviscid oscillations

This section describes the analysis of the inviscid drop/medium system with no surfactants. All the dissipation terms on the right-hand side of the total mechanical energy equation (2.43) are zero and the total energy

of the system is conserved. This case serves as the base flow for large Reynolds number shape oscillations and demonstrates the application of the averaging method to the drop/medium system.

For the shape perturbation in (2.55), the inviscid flow fields in each phase are given by the solution of a regular perturbation problem. If the flow is irrotational, the scalar velocity potentials (scaled with ωR^2) for the flow in each phase may be expanded in regular perturbation series in the small parameter ε

$$\phi(r,\theta,t;\varepsilon,\alpha) \sim \varepsilon\phi_0(r,\theta,t) + \mathcal{O}(\varepsilon^2) \tag{2.60}$$

$$\hat{\phi}(r,\theta,t;\varepsilon,\alpha) \sim \varepsilon\hat{\phi}_0(r,\theta,t) + \mathcal{O}(\varepsilon^2)\,, \tag{2.61}$$

Here the arbitrary constant in the scalar velocity potentials has been set to zero in both phases. These potentials are found by solving Laplace's equation within each phase

$$\nabla^2\,\phi_0 = 0 \quad \text{for} \quad r < 1 \tag{2.62}$$

$$\nabla^2\,\hat{\phi}_0 = 0 \quad \text{for} \quad r > 1\,. \tag{2.63}$$

The potentials are subject to the $\mathcal{O}(\varepsilon)$ kinematic boundary conditions

$$\frac{\partial\phi_0}{\partial r} = \frac{\partial\hat{\phi}_0}{\partial r} = i\Omega_{\ell 0}Ae^{i\Omega_{\ell 0}t}P_\ell(\cos\theta) \quad \text{at} \quad r = 1 \tag{2.64}$$

and the conditions that the potential in each phase remain finite.

The nondimensional pressure (scaled with $\rho\omega^2R^2$) is related to the potential in each phase through the linearized unsteady Bernoulli equation

$$p = p_{eq} - \varepsilon\frac{\partial\phi_0}{\partial t} + \mathcal{O}(\varepsilon^2) \tag{2.65}$$

$$\hat{p} = \frac{\hat{\rho}}{\rho}\left(\hat{p}_{eq} - \varepsilon\frac{\partial\hat{\phi}_0}{\partial t}\right) + \mathcal{O}(\varepsilon^2)\,. \tag{2.66}$$

Here p_{eq} and $\hat{p}_{eq}$ are the equilibrium pressures in each phase satisfying the nondimensional Young-Laplace equation $p_{eq} - \hat{p}_{eq}(\hat{\rho}/\rho) = 2$.

Time-periodic solutions

For $a_\ell(t) = \Re\{Ae^{i\Omega_{\ell 0}t}\}$, the potential flow equations may be readily solved. The resulting velocity components $\mathbf{v} = \boldsymbol{\nabla}\phi = \hat{\mathbf{e}}_r v_r + \hat{\mathbf{e}}_\theta v_\theta$ and pressure in the drop phase are the real parts of

$$v_{r0}(r,\theta,t;\varepsilon) = \varepsilon i\Omega_{\ell 0}Ae^{i\Omega_{\ell 0}t}P_\ell(\cos\theta)r^{\ell-1} + \mathcal{O}(\varepsilon^2) \tag{2.67}$$

$$v_{\theta 0}(r,\theta,t;\varepsilon) = \varepsilon i\Omega_{\ell o}Ae^{i\Omega_{\ell 0}t}\frac{1}{\ell}\frac{dP_\ell}{d\theta}(\cos\theta)r^{\ell-1} + \mathcal{O}(\varepsilon^2) \tag{2.68}$$

$$p(r,\theta,t;\varepsilon) - p_{eq} = \varepsilon\Omega_{\ell o}^2Ae^{i\Omega_{\ell 0}t}\frac{1}{\ell}P_\ell(\cos\theta)r^\ell + \mathcal{O}(\varepsilon^2) \tag{2.69}$$

The velocity components $\hat{\mathbf{v}} = \boldsymbol{\nabla}\hat{\phi} = \hat{\mathbf{e}}_r\hat{v}_r + \hat{\mathbf{e}}_\theta\hat{v}_\theta$ and pressure in the medium phase are similarly

$$\hat{v}_{r0}(r,\theta,t;\varepsilon) = \varepsilon i\Omega_{\ell 0}Ae^{i\Omega_{\ell 0}t}P_\ell(\cos\theta)r^{-(\ell+2)} + \mathcal{O}(\varepsilon^2) \tag{2.70}$$

$$\hat{v}_{\theta 0}(r,\theta,t;\varepsilon) = -\varepsilon i\Omega_{\ell 0}Ae^{i\Omega_{\ell 0}t}\frac{1}{(\ell+1)}\frac{dP_\ell}{d\theta}(\cos\theta)r^{-(\ell+2)} + \mathcal{O}(\varepsilon^2) \tag{2.71}$$

$$\hat{p}(r,\theta,t;\varepsilon)(\rho/\hat{\rho}) - \hat{p}_{eq} = \varepsilon\Omega_{\ell 0}^2Ae^{i\Omega_{\ell 0}t}\frac{1}{(\ell+1)}P_\ell(\cos\theta)r^{-(\ell+1)} + \mathcal{O}(\varepsilon^2)\,. \tag{2.72}$$

Order-of-magnitude analysis

For this case the nondimensional total mechanical energy equation (2.43) reduces to

$$\frac{d}{dt}\{\text{K.E.} + \text{P.E.}\} = 0\,. \tag{2.73}$$

The nondimensional kinetic and potential energies are, respectively,

$$\text{K.E.} = \int_{V_m} \frac{1}{2}|\mathbf{v}|^2\, dV + \frac{\hat{\rho}}{\rho}\int_{\hat{V}_m} \frac{1}{2}|\hat{\mathbf{v}}|^2\, dV \tag{2.74}$$

$$\text{P.E.} = \int_{S_m} dS\,. \tag{2.75}$$

The averaging method requires the time-average of the kinetic and potential energies to be calculated to leading order. For this purpose, the potential flow approximations for the velocity field in each phase are used to calculate the leading order contributions to these quantities. Since the potential flow velocities in each phase are $\mathcal{O}(\varepsilon)$, the integrals over the material volumes in (2.74) may be expanded about a sphere of unit nondimensional radius to yield

$$\int_{V_m} \frac{1}{2}|\mathbf{v}|^2\, dV = \varepsilon^2 \int_0^{2\pi}\int_0^{\pi}\int_0^1 \frac{1}{2}(u_r^2 + u_\theta^2) r^2 \sin\theta dr d\theta d\varphi + \mathcal{O}(\varepsilon^3) \tag{2.76}$$

$$\int_{\hat{V}_m} \frac{1}{2}|\hat{\mathbf{v}}|^2\, dV = \varepsilon^2 \int_0^{2\pi}\int_0^{\pi}\int_1^{\infty} \frac{1}{2}(\hat{u}_r^2 + \hat{u}_\theta^2) r^2 \sin\theta dr d\theta d\varphi + \mathcal{O}(\varepsilon^3)\,, \tag{2.77}$$

where $\mathbf{v} = \varepsilon\mathbf{u}$ and $\hat{\mathbf{v}} = \varepsilon\hat{\mathbf{u}}$.

Without small quantities in the integrand, the evaluation of the integral over the material surface in (2.75) is more complicated. Since the leading-order contribution from the kinetic energies is $\mathcal{O}(\varepsilon^2)$ the contributions from the potential energy are needed up to the same order. The assumed shape in (2.55) does not conserve volume to $\mathcal{O}(\varepsilon^2)$ and must be modified with an $\mathcal{O}(\varepsilon^2)$ correction in order to achieve this. In general, for a regular perturbation expansion of the nondimensional shape disturbance in the form

$$r(\theta, t; \varepsilon) = 1 + \varepsilon f_1(\theta, t) + \varepsilon^2 f_2(\theta, t) + \mathcal{O}(\varepsilon^3) \tag{2.78}$$

the volume of the shape can be shown to be $4\pi/3 + \mathcal{O}(\varepsilon^3)$ if $f_2(\theta, t) = -f_1^2(\theta, t)$. Using this modified shape the integral over the material surface may be expanded about the unit sphere to yield

$$\int_{S_m} dS = \int_0^{2\pi}\int_0^{\pi} \left\{1 + 2\varepsilon f_1 + \frac{\varepsilon^2}{2}\left[\left(\frac{\partial f_1}{\partial\theta}\right)^2 - 2f_1^2\right]\right\} \sin\theta d\varphi d\theta + \mathcal{O}(\varepsilon^3)\,, \tag{2.79}$$

where $f_1(\theta, t) = \Re\{Ae^{i\Omega_{\ell 0}t}\}P_\ell(\cos\theta)$.

An alternate form for the time derivative of the nondimensional potential energy term, obtained with the use of the surface Reynolds Transport Theorem, is

$$\frac{d}{dt}\int_{S_m} dS = \int_{S_m} (\boldsymbol{\nabla}_s \cdot \hat{\mathbf{n}})(\hat{\mathbf{n}} \cdot \mathbf{v})\, dS\,. \tag{2.80}$$

Here the unit normal and twice the mean nondimensional curvature are, respectively,

$$\hat{\mathbf{n}} = \hat{\mathbf{e}}_r - \hat{\mathbf{e}}_\theta \varepsilon \frac{\partial f_1}{\partial\theta}(\theta, t) + \mathcal{O}(\varepsilon^2) \tag{2.81}$$

$$\boldsymbol{\nabla}_s \cdot \hat{\mathbf{n}} = 2 - \varepsilon\left[\frac{\partial^2 f_1}{\partial\theta^2}(\theta, t) + \cot\theta\frac{\partial f_1}{\partial\theta}(\theta, t) + 2f_1(\theta, t)\right] + \mathcal{O}(\varepsilon^2)\,. \tag{2.82}$$

By the divergence theorem and incompressibility, the constant part of the curvature term will not contribute to the surface integral on the right-hand side of (2.80). This allows the time derivative of the nondimensional potential energy to be expanded about a unit sphere in an alternate way

$$\frac{d}{dt}\int_{S_m} dS = -\varepsilon\int_0^{2\pi}\int_0^{\pi}\left[\frac{\partial^2 f_1}{\partial\theta^2} + \cot\theta\frac{\partial f_1}{\partial\theta} + 2f_1\right] v_r \sin\theta d\theta d\varphi + \mathcal{O}(\varepsilon^3)\,, \tag{2.83}$$

which does not require an $\mathcal{O}(\varepsilon^2)$ correction to the shape. The use of the kinematic boundary condition (2.64) and an integration by parts shows that the time derivative of (2.79) is equivalent to (2.83). For consistency in the time-averaging, which is to be discussed next, (2.79) will be used throughout the chapter on theory to calculate the nondimensional surface potential energy.

Time-averaging

Since the shape of the interface and the velocity solutions in each phase are complex functions, their real parts must be used in the integrands. The averaging method further requires only the time-average of the real part of the integrals making up the kinetic and potential energies. For example, the real part of the radial component of velocity in the drop is

$$\Re\{v_r\} = \varepsilon P_\ell(\cos\theta) r^{\ell-1} \frac{1}{2}[i\Omega_{\ell 0} A e^{i\Omega_{\ell 0} t} + \text{c.c.}] + \mathcal{O}(\varepsilon^2)\,. \tag{2.84}$$

Here c.c. refers to the complex conjugate. The nondimensional time-average of the real part of the radial component of velocity squared is

$$\langle \Re\{v_r\}^2 \rangle = \frac{\Omega_{\ell 0}}{2\pi} \int_0^{2\pi/\Omega_{\ell 0}} \Re\{v_r\}^2 \, dt \tag{2.85}$$

$$= \varepsilon^2 P_\ell^2(\cos\theta) r^{2(\ell-1)} \frac{|\Omega_{\ell 0} A|^2}{2} + \mathcal{O}(\varepsilon^3)\,. \tag{2.86}$$

Here $|\ |^2$ denotes the complex amplitude squared. This quantity may now be integrated over the sphere with unit radius to obtain part of the total contribution to the kinetic energy.

$$\frac{1}{2}\int_0^{2\pi}\int_0^{\pi}\int_0^1 \langle \Re\{v_r\}^2 \rangle \, r^2 \sin\theta \, dr d\theta d\varphi = \frac{\varepsilon^2 \pi}{(2\ell+1)^2} |\Omega_{\ell 0} A|^2 + \mathcal{O}(\varepsilon^3)\,. \tag{2.87}$$

Similar operations, taking the real parts before squaring and time-averaging the integrands over one period, may be performed on all the terms in (2.74) and (2.75) to yield

$$\langle \text{K.E.} \rangle = \frac{\varepsilon^2 \pi}{\ell(\ell+1)(2\ell+1)} \left[(\ell+1) + \frac{\hat{\rho}}{\rho}\ell \right] |\Omega_{\ell 0} A|^2 + \mathcal{O}(\varepsilon^3) \tag{2.88}$$

$$\langle \text{P.E.} \rangle = 4\pi + \varepsilon^2 \pi \frac{(\ell-1)(\ell+2)}{(2\ell+1)} |A|^2 + \mathcal{O}(\varepsilon^3)\,. \tag{2.89}$$

Oscillator equation

Following the averaging method, when $a_\ell(t) = \Re\{A e^{i\Omega_{\ell 0} t}\}$, the complex amplitudes, which represent time averages, may be replaced with terms involving $a_\ell(t)$ that would yield the same time average:

$$|\Omega_{\ell 0} A|^2 \rightarrow 2(\dot{a}_\ell)^2 \tag{2.90}$$

$$|A|^2 \rightarrow 2(a_\ell)^2\,. \tag{2.91}$$

Rewriting (2.73) in terms of a_ℓ gives

$$\frac{d}{dt}\left\{ \varepsilon^2 \pi \frac{[(\ell+1) + \ell\hat{\rho}/\rho]}{\ell(\ell+1)(2\ell+1)} 2(\dot{a}_\ell)^2 + 4\pi + \varepsilon^2 \pi \frac{(\ell-1)(\ell+2)}{(2\ell+1)} 2(a_\ell)^2 \right\} = 0\,. \tag{2.92}$$

Expanding and simplifying yields

$$\ddot{a}_\ell + \frac{\ell(\ell-1)(\ell+1)(\ell+2)}{[(\ell+1) + \ell\hat{\rho}/\rho]} a_\ell = \mathcal{O}(\varepsilon)\,. \tag{2.93}$$

Here the nondimensional frequency for the shape oscillations is in agreement with Lamb's result (2.59).

2.4.2 Case 1: "negligible" surfactant effects

This section discusses the viscous drop/medium system with no surfactant effects. The surface properties e_s^*, κ_s^*, and μ_s^* are assumed to be "negligible", or $\mathcal{O}(\alpha^3)$. All the surface dissipation and Marangoni terms on the right-hand side of the total mechanical energy equation (2.43) are neglected in this case.

Due to the complicated forms for the equations and boundary conditions for the drop/medium system, this section calculates the uniformly valid velocity and pressure approximations to an accuracy of $\mathcal{O}(\varepsilon\alpha)$. Unfortunately, this does not allow for the consistent expansion of the leading order nondimensional total mechanical energy equation to $\mathcal{O}(\varepsilon^2\alpha^2)$. This will only affect the calculation of the resulting oscillation frequencies to $\mathcal{O}(\alpha^2)$, leaving the resulting calculation of the damping constant to $\mathcal{O}(\alpha^2)$ unaffected.

Inner equations

Near the interface the radial coordinate may be replaced with $r = R+y$. Thus, y measures the distance away from the interface in the direction of the unit normal. Scaling the full Navier-Stokes equations in the drop using the inertial scales (2.42) with $\delta = (\mu/\rho\omega)^{1/2}$ as the length scale for y introduces a small parameter $\alpha = \delta/R$, the square root of the Reynolds number. α represents the ratio of the Stokes boundary layer thickness in the drop to the equilibrium radius. A similar Stokes boundary layer thickness $\hat{\delta} = (\hat{\mu}/\hat{\rho}\omega)^{1/2}$ and small parameter $\hat{\alpha} = \hat{\delta}/R$ is found in the medium phase. The nondimensional velocity (scaled with ωR) and pressure (scaled with $\rho\omega^2 R^2$) in the drop are written as regular perturbation expansions in α such that

$$\mathbf{V}(y,\theta,t;\varepsilon,\alpha) = \varepsilon[\mathbf{V}_0(y,\theta,t) + \alpha\mathbf{V}_1(y,\theta,t)] + \mathcal{O}(\varepsilon\alpha^2) \tag{2.94}$$

$$P(y,\theta,t;\varepsilon,\alpha) = p_{eq} + \varepsilon[P_0(y,\theta,t) + \alpha P_1(y,\theta,t)] + \mathcal{O}(\varepsilon\alpha^2)\,. \tag{2.95}$$

Similar regular expansions are assumed for the nondimensional velocity $\hat{\mathbf{V}}$ and pressure $\hat{P}$ in the medium in terms of $\hat{\alpha}$. Here p_{eq} (or $\hat{p}_{eq}$) is the reference pressure in the drop (or medium) satisfying the nondimensional Young-Laplace equation $p_{eq} - \hat{p}_{eq}(\hat{\rho}/\rho) = 2$. The size of the deformation is assumed to be small enough that $\varepsilon \ll \alpha^2$ and the fluid properties in each phase are taken to be of the same order in magnitude. With the above expansions the inner equations in the drop phase take the following forms

$$\frac{\partial V_{r0}}{\partial y} = 0 \tag{2.96}$$

$$\frac{\partial P_0}{\partial y} = 0 \tag{2.97}$$

$$\frac{\partial V_{\theta 0}}{\partial t} + \frac{\partial P_0}{\partial \theta} - \frac{\partial^2 V_{\theta 0}}{\partial y^2} = 0\,, \tag{2.98}$$

with similar equations in the medium. These are the standard boundary layer equations for a flat surface driven by a pressure gradient supplied by the outer flow fields. The following boundary conditions hold at the interface

$$V_{r0} = \hat{V}_{r0} = i\Omega_{\ell 0} A e^{i\Omega_{\ell 0} t} P_\ell(\cos\theta) \tag{2.99}$$

$$V_{\theta 0} - \hat{V}_{\theta 0} = 0 \tag{2.100}$$

$$\frac{\partial V_{\theta 0}}{\partial y} - \frac{\alpha}{\hat{\alpha}}\left(\frac{\hat{\mu}}{\mu}\right)^{1/2} \frac{\partial \hat{V}_{\theta 0}}{\partial y} = 0 \tag{2.101}$$

$$P_0 - \frac{\hat{\rho}}{\rho}\hat{P}_0 = (\ell-1)(\ell+2) A e^{i\Omega_{\ell 0} t} P_\ell(\cos\theta)\,. \tag{2.102}$$

These represent, respectively, the kinematic, no-slip, tangential stress balance, and normal stress balance boundary conditions. The prescribed shape perturbation in (2.57) identically satisfies the normal stress balance boundary condition at this order.

The equations for the $\mathcal{O}(\varepsilon\alpha)$ inner variables take the following forms

$$\frac{\partial V_{r1}}{\partial y} = -\frac{\partial V_{\theta 0}}{\partial \theta} - \cot\theta\, V_{\theta 0} - 2V_{r0} \tag{2.103}$$

$$\frac{\partial P_1}{\partial y} = -\frac{\partial V_{r0}}{\partial t} - \frac{\partial^2 V_{r0}}{\partial y^2} \tag{2.104}$$

$$\frac{\partial V_{\theta 1}}{\partial t} + \frac{\partial P_1}{\partial \theta} - \frac{\partial^2 V_{\theta 1}}{\partial y^2} = y\frac{\partial P_0}{\partial \theta} + 2\frac{\partial V_{\theta 0}}{\partial y}\,, \tag{2.105}$$

with similar equations in the medium. The $\mathcal{O}(\varepsilon\alpha)$ variables are subject to the following boundary conditions at the interface

$$V_{r1} = \hat{V}_{r1} = 0 \tag{2.106}$$

$$V_{\theta 1} - \frac{\hat{\alpha}}{\alpha}\hat{V}_{\theta 1} = 0 \tag{2.107}$$

$$\frac{\partial V_{\theta 1}}{\partial y} - \left(\frac{\hat{\mu}}{\mu}\right)^{1/2} \frac{\partial \hat{V}_{\theta 1}}{\partial y} = 0 \tag{2.108}$$

Here the normal stress balance boundary condition is not enforced. Since the shape of the interface has been prescribed, not all of the boundary conditions can be satisfied to $\mathcal{O}(\varepsilon\alpha)$. As is customary in the analysis of drop deformations, see for example [30], the normal stress balance boundary condition is the degree of freedom that is lost.

The boundary conditions far from the interface are replaced by matching conditions with outer velocity and pressure solutions in each phase. For this problem, the leading order matching conditions state that the limit of the inner solution far from the interface must match the limit of the outer solution near the interface. For the higher order matching conditions a more precise definition is needed and the reader is referred to [54] for details.

Outer equations

Far from the interface the full Navier-Stokes equations are nondimensionalized using inertial scales with respect to the drop (2.42). If the nondimensional outer flow is irrotational and given by a scalar velocity potential (scaled with ωR^2), where $\mathbf{v} = \boldsymbol{\nabla}\phi$ in spherical axisymmetric coordinates, the viscous terms in the Navier-Stokes equations for both phases are identically zero. The pressure (scaled with $\rho\omega^2 R^2$) is given by the unsteady Bernoulli equation. Anticipating the matching conditions with the inner viscous flow fields, the outer potential flow fields are written as regular perturbation expansions in the parameter α

$$\phi(r,\theta,t;\varepsilon,\alpha) = \varepsilon[\phi_0(r,\theta,t) + \alpha\phi_1(r,\theta,t)] + \mathcal{O}(\varepsilon\alpha^2) \tag{2.109}$$

$$p(r,\theta,t;\varepsilon,\alpha) = p_{eq} + \varepsilon[p_0(r,\theta,t) + \alpha p_1(r,\theta,t)] + \mathcal{O}(\varepsilon\alpha^2)\,. \tag{2.110}$$

Similar expansions are assumed for $\hat{\phi}$ and $\hat{p}$ in the medium in terms of $\hat{\alpha}$.

The $\mathcal{O}(\varepsilon)$ and $\mathcal{O}(\varepsilon\alpha)$ outer equations are all governed by Laplace's equation in spherical axisymmetric coordinates and the linearized unsteady Bernoulli equation for the pressure

$$\left.\begin{aligned} \nabla^2\phi_i &= 0 \\ p_i &= -\frac{\partial\phi_i}{\partial t} \end{aligned}\right\} \quad \text{for } i = 0, 1\,. \tag{2.111}$$

Similar equations for $\hat{\phi}$ and $\hat{p}$ are used in the medium. The outer fields are subject to the boundary conditions that far from the interface the scalar velocity potential vanishes and the pressure tends to its reference value. The boundary conditions near the interface are replaced by matching conditions with inner velocity and pressure solutions in each phase.

Time-periodic composite solutions

An additive composite expansion [54] is used to obtain uniformly valid approximations for the time-periodic velocity and pressure fields in each phase. These take the following forms

$$\mathbf{v}^{\text{tot}} = \mathbf{v}(r,\theta,t) + \mathbf{V}(r,\theta,t) - \mathbf{v}_{\text{m}}(r,\theta,t) \tag{2.112}$$

$$p^{\text{tot}} = p(r,\theta,t) + P(r,\theta,t) - p_{\text{m}}(r,\theta,t)\,. \tag{2.113}$$

Here $\mathbf{v}^{\text{tot}}$ and p^{tot} represent the total composite fields and $\mathbf{v}_{\text{m}}$ and p_{m} represent the matched outer (or inner) fields in the overlap region. Similar expressions are used to construct the velocity and pressure in the medium. Solving the inner and outer equations in each phase, subject to their boundary and matching conditions, and constructing the uniformly valid solutions in outer variables yields the following approximations for the time-periodic velocity components and pressure. The approximate fields in the drop phase are given by

$$\begin{aligned} v_r^{\text{tot}}(r,\theta,t;\varepsilon,\alpha) = {} & \varepsilon i\Omega_{\ell 0} A e^{i\Omega_{\ell 0}t} P_\ell(\cos\theta)\left\{ r^{\ell-1} \right. \\ & \left. -\alpha\frac{\sqrt{2}}{(1+i)}\frac{1}{\sqrt{\Omega_{\ell 0}}}(\ell+1)C_{\theta 0}[r^{\ell-1} - \text{EXP}]\right\} + \mathcal{O}(\varepsilon\alpha^2)\,, \end{aligned} \tag{2.114}$$

$$v_\theta^{\text{tot}}(r,\theta,t;\varepsilon,\alpha) = \varepsilon i\Omega_{\ell 0} A e^{i\Omega_{\ell 0}t}\frac{1}{\ell}\frac{dP_\ell}{d\theta}(\cos\theta)\left\{ r^{\ell-1} + C_{\theta 0}(2-r)\text{EXP} \right.$$

$$-\alpha\frac{\sqrt{2}}{(1+i)}\frac{1}{\sqrt{\Omega_{\ell 0}}}[(\ell+1)C_{\theta 0}r^{\ell-1}-C_{\theta 1}\mathrm{EXP}]\Bigg\}+\mathcal{O}(\varepsilon\alpha^2)\,, \tag{2.115}$$

$$\begin{aligned} p^{\mathrm{tot}}(r,\theta,t;\varepsilon,\alpha)-p_{eq} &= \varepsilon\Omega_{\ell 0}^2 A e^{i\Omega_{\ell 0}t}\frac{1}{\ell}P_\ell(\cos\theta)\left\{r^\ell\right. \\ &\left.+\alpha\frac{\sqrt{2}}{(1+i)}\frac{1}{\sqrt{\Omega_{\ell 0}}}(\ell+1)C_{\theta 0}r^\ell\right\}+\mathcal{O}(\varepsilon\alpha^2)\,. \end{aligned} \tag{2.116}$$

Similarly, the fields in the medium phase are given by

$$\begin{aligned} \hat{v}_r^{\mathrm{tot}}(r,\theta,t;\varepsilon,\hat{\alpha}) &= \varepsilon i\Omega_{\ell 0}Ae^{i\Omega_{\ell 0}t}P_\ell(\cos\theta)\left\{r^{-(\ell+2)}\right. \\ &\left.-\hat{\alpha}\frac{\sqrt{2}}{(1+i)}\frac{1}{\sqrt{\Omega_{\ell 0}}}\ell\hat{C}_{\theta 0}[r^{-(\ell+2)}-\widehat{\mathrm{EXP}}]\right\}+\mathcal{O}(\varepsilon\hat{\alpha}^2)\,, \end{aligned} \tag{2.117}$$

$$\begin{aligned} \hat{v}_\theta^{\mathrm{tot}}(r,\theta,t;\varepsilon,\hat{\alpha}) &= -\varepsilon i\Omega_{\ell 0}Ae^{i\Omega_{\ell 0}t}\frac{1}{(\ell+1)}\frac{dP_\ell}{d\theta}(\cos\theta)\left\{r^{-(\ell+2)}+\hat{C}_{\theta 0}(2-r)\widehat{\mathrm{EXP}}\right. \\ &\left.-\hat{\alpha}\frac{\sqrt{2}}{(1+i)}\frac{1}{\sqrt{\Omega_{\ell 0}}}[\ell\hat{C}_{\theta 0}r^{-(\ell+2)}+\hat{C}_{\theta 1}\widehat{\mathrm{EXP}}]\right\}+\mathcal{O}(\varepsilon\hat{\alpha}^2)\,, \end{aligned} \tag{2.118}$$

$$\begin{aligned} \hat{p}^{\mathrm{tot}}(r,\theta,t;\varepsilon,\hat{\alpha})-\hat{p}_{eq} &= \varepsilon\Omega_{\ell 0}^2 Ae^{i\Omega_{\ell 0}t}\frac{1}{(\ell+1)}P_\ell(\cos\theta)\left\{r^{-(\ell+1)}\right. \\ &\left.+\hat{\alpha}\frac{\sqrt{2}}{(1+i)}\frac{1}{\sqrt{\Omega_{\ell 0}}}\ell\hat{C}_{\theta 0}r^{-(\ell+1)}\right\}+\mathcal{O}(\varepsilon\hat{\alpha}^2)\,. \end{aligned} \tag{2.119}$$

Here EXP and $\widehat{\mathrm{EXP}}$ are functions that decay exponentially away from the interface in each respective phase. They are given explicitly by:

$$\mathrm{EXP} = \exp\left[\sqrt{\Omega_{\ell 0}}\frac{(1+i)}{\sqrt{2}}\frac{(r-1)}{\alpha}\right] \tag{2.120}$$

$$\widehat{\mathrm{EXP}} = \exp\left[-\sqrt{\Omega_{\ell 0}}\frac{(1+i)}{\sqrt{2}}\frac{(r-1)}{\hat{\alpha}}\right]\,. \tag{2.121}$$

The real constants $C_{\theta 0}$, $C_{\theta 1}$, $\hat{C}_{\theta 0}$, and $\hat{C}_{\theta 1}$ are given in Appendix B.

The above fields contain terms of two types: those that resemble potential flow or those that exponentially decay away from the interface. In the tangential component of the velocity, the exponentially decaying terms appear to leading order, or $\mathcal{O}(\varepsilon)$, in the perturbed fields. In the normal component of the velocity, the exponentially decaying terms do not appear until second order, or $\mathcal{O}(\varepsilon\alpha)$. In the pressure, the exponential decay terms do not appear at all to this order in the expansion.

The above velocity fields in each phase are used to approximate the terms in the energy equation.

Order-of-magnitude analysis

The direct substitution of the uniformly valid velocity approximations in the integrands of the nondimensional total mechanical energy equation leads to very complicated expressions. These expressions can be greatly simplified using an order-of-magnitude analysis to identify the most important terms. For this case the nondimensional total mechanical energy equation (2.43) reduces to

$$\frac{d}{dt}\{\mathrm{K.E.}+\mathrm{P.E.}\} = -\alpha^2\{\mathrm{Bulk\ Diss.}\}\,. \tag{2.122}$$

The nondimensional energies and dissipation may be approximated using the uniformly valid velocity approximations from the matched asymptotic analysis. It is again convenient to use a new notation for the

order-of-magnitudes for the nondimensional velocity in the drop phase:

$$\mathbf{v}^{\text{tot}} = \varepsilon[(\mathbf{u}_0 + \alpha\mathbf{u}_1) + (\mathbf{U}_0 + \alpha\mathbf{U}_1)] + \mathcal{O}(\varepsilon\alpha^2)\,, \tag{2.123}$$

with a similar expression for the medium phase. Here the $\mathbf{u}$'s refer to the potential flow terms in the uniformly valid velocity approximations with small $\mathcal{O}(1)$ gradients in the radial direction. The volume integrals containing these terms will be significant over the nondimensional volume of $\mathcal{O}(1)$.

The $\mathbf{U}$'s refer to the vortical flow terms in the uniformly valid velocity approximations with large $\mathcal{O}(1/\alpha)$ gradients in the radial direction that exponentially decay away from the interface. To distinguish these large gradients, the radial derivatives are recast in terms of the scaled variable $y = (r-1)/\alpha$:

$$\frac{\partial \mathbf{U}}{\partial r}(r,\theta,t) = \frac{1}{\alpha}\frac{\partial \mathbf{U}}{\partial y}(y,\theta,t)\,, \tag{2.124}$$

where $\partial\mathbf{U}/\partial y$ is an $\mathcal{O}(1)$ quantity. The volume integrals containing the components of $\mathbf{U}$ are significant over the nondimensional volume of the boundary layer of $\mathcal{O}(\alpha)$ near the interface in each phase.

The following order-of-magnitude analysis is based on a substitution of these velocities into the integrands of the total mechanical energy equation. The integrals are written in spherical coordinates and expanded about a unit sphere. Only those contributions which are $\mathcal{O}(\varepsilon^2\alpha^2)$ and larger are kept.

The nondimensional kinetic energy in the drop phase is

$$\begin{aligned}
&\int_{V_m} \frac{1}{2}|\mathbf{v}^{\text{tot}}|^2\, dV = \\
&\quad \varepsilon^2 \int_0^{2\pi}\int_0^{\pi}\int_0^{1} \frac{1}{2}\left\{(u_{r0}^2 + u_{\theta 0}^2) + 2\alpha(u_{r0}u_{r1} + u_{\theta 0}u_{\theta 1})\right\} r^2 \sin\theta\, dr\, d\theta\, d\varphi \\
&\quad +\varepsilon^2\alpha \int_0^{2\pi}\int_0^{\pi}\int_{-\infty}^{0} \frac{1}{2}\left\{2(u_{r0}|_{r=1}\, U_{r0} + u_{\theta 0}|_{r=1}\, U_{\theta 0}) + (U_{r0}^2 + U_{\theta 0}^2)\right. \qquad (2.125) \\
&\qquad\qquad \left.\right\} \sin\theta\, dy\, d\theta\, d\varphi + \mathcal{O}(\varepsilon^2\alpha^2)\,. \qquad (2.126)
\end{aligned}$$

A similar expansion for the nondimensional kinetic energy in the medium in terms of $\hat{\alpha}$. There the limits of integration of the potential flow velocity components are from $r = 1$ to $r = \infty$, and the limits of integration for the vortical flow velocity components are from $y = 0$ to $y = \infty$. Here the expansion has been truncated at $\mathcal{O}(\varepsilon^2\alpha^2)$ because the uniformly valid velocity expansions accurate to $\mathcal{O}(\varepsilon\alpha)$ do not contain the $\mathcal{O}(\varepsilon\alpha^2)$ terms required to calculate the nondimensional kinetic energy to $\mathcal{O}(\varepsilon^2\alpha^2)$. The level of algebra needed to construct the uniformly valid velocity to $\mathcal{O}(\varepsilon\alpha^2)$ is enormous and was not attempted. Neglecting the $\mathcal{O}(\varepsilon^2\alpha^2)$ kinetic energy terms is shown below to affect only the calculation of the natural frequency of oscillations at $\mathcal{O}(\alpha^2)$. The calculation of the damping constant to $\mathcal{O}(\alpha^2)$ is unaffected.

The nondimensional bulk viscous dissipation in the drop is

$$\begin{aligned}
&\int_{V_m} 2(\mathbf{E}^{\text{tot}} : \mathbf{E}^{\text{tot}})\, dV = \\
&\quad \varepsilon^2 \int_0^{2\pi}\int_0^{\pi}\int_0^{1} 2\left\{\left(\frac{\partial u_{r0}}{\partial r}\right)^2 + \frac{1}{r^2}\left(\frac{\partial u_{\theta 0}}{\partial \theta} + u_{r0}\right)^2 + \frac{1}{r^2}\left(u_{r0} - \cot\theta\, u_{\theta 0}\right)^2\right. \\
&\qquad\qquad \left. + \frac{1}{2}\left[\frac{\partial u_{\theta 0}}{\partial r} + \frac{1}{r}\left(\frac{\partial u_{r0}}{\partial \theta} - u_{\theta 0}\right)\right]^2\right\} r^2 \sin\theta\, dr\, d\theta\, d\varphi \\
&\quad +\varepsilon^2\alpha \int_0^{2\pi}\int_0^{\pi}\int_{-\infty}^{0} 2\left\{\frac{1}{2\alpha^2}\left(\frac{\partial U_{\theta 0}}{\partial y}\right)^2 + \frac{1}{\alpha}\left(\frac{\partial u_{\theta 0}}{\partial r} + \frac{\partial u_{r0}}{\partial \theta} - u_{\theta 0}\right)\Big|_{r=1} \frac{\partial U_{\theta 0}}{\partial y}\right. \\
&\qquad\qquad \left. + \frac{1}{\alpha} y \left(\frac{\partial U_{\theta 0}}{\partial y}\right)^2\right\} \sin\theta\, dy\, d\theta\, d\varphi + \mathcal{O}(\varepsilon^2\alpha)\,. \qquad (2.127)
\end{aligned}$$

Again, a similar expression is obtained for the bulk viscous dissipation in the medium in terms of $\hat{\alpha}$ and its own limits of integration. Here the leading-order contribution to the nondimensional dissipation is $\mathcal{O}(\varepsilon^2\alpha^{-1})$ and derives from the no-slip boundary condition at the interface.

Time-averaging

The averaging method proceeds by first multiplying the real parts of the velocity components making up the integrands, time-averaging these integrands over one period of oscillation, and finally integrating over the unit sphere. For the terms in the nondimensional total mechanical energy equation (2.122), this procedure yields

$$\begin{aligned}
\langle \text{K.E.} \rangle &= \frac{\varepsilon^2\pi}{\ell(\ell+1)(2\ell+1)}\left\{(\ell+1)+\frac{\hat{\rho}}{\rho}\ell\right. \\
&\quad \left.+\alpha\frac{(2\ell+1)^2}{\sqrt{2}}\frac{\sqrt{\hat{\mu}\hat{\rho}}}{(\sqrt{\mu\rho}+\sqrt{\hat{\mu}\hat{\rho}})^2}\frac{1}{\sqrt{\Omega_{\ell 0}}}\right\}|\Omega_{\ell 0}A|^2+\mathcal{O}(\varepsilon^2\alpha^2) \qquad (2.128)\\
\langle \text{P.E.} \rangle &= 4\pi+\varepsilon^2\pi\frac{(\ell-1)(\ell+2)}{(2\ell+1)}|A|^2+\mathcal{O}(\varepsilon^3) \qquad (2.129)\\
\langle \text{Bulk Diss.} \rangle &= \frac{\varepsilon^2 4\pi}{\ell(\ell+1)}\left\{\frac{1}{\alpha}\frac{(2\ell+1)}{2\sqrt{2}}\frac{\sqrt{\hat{\mu}\hat{\rho}}}{(\sqrt{\mu\rho}+\sqrt{\hat{\mu}\hat{\rho}})}\sqrt{\Omega_{\ell 0}}\right. \\
&\quad +\frac{1}{2(\sqrt{\mu\rho}+\sqrt{\hat{\mu}\hat{\rho}})^2}\left[2(\ell^2-1)\mu\rho+2\ell(\ell+2)\frac{\hat{\mu}^2\hat{\rho}}{\mu}\right. \\
&\quad \left.\left.+\hat{\mu}[(\ell+2)\rho-(\ell-1)\hat{\rho}]\right]\right\}|\Omega_{\ell o}A|^2+\mathcal{O}(\varepsilon^2\alpha)\,. \qquad (2.130)
\end{aligned}$$

The time-average of the total nondimensional potential energy has been calculated as in the base potential flow using (2.79). Note again that the with the $\mathcal{O}(\varepsilon\alpha)$ velocity solutions the time-average of the total nondimensional kinetic energy can only be calculated to $\mathcal{O}(\varepsilon^2\alpha)$. Since the time average of the total nondimensional viscous dissipation rate in the bulk is multiplied by α^2 in the nondimensional total mechanical energy equation, the kinetic energy term is the only quantity not known to at least $\mathcal{O}(\varepsilon^2\alpha^2)$.

Oscillator equation

Following the averaging method with $a_\ell(t) = \Re\{Ae^{i\Omega_{\ell 0}t}\}$, the complex amplitudes in (2.128)–(2.130) are replaced with the quantities

$$\begin{aligned}
|\Omega_{\ell 0}A|^2 &\to 2(\dot{a}_\ell)^2 \qquad (2.131)\\
|A|^2 &\to 2(a_\ell)^2\,. \qquad (2.132)
\end{aligned}$$

After simplifying, the total mechanical energy equation reduces to a damped harmonic oscillator equation of the form

$$(1+\alpha \mathrm{A}_{\ell 1})\,\ddot{a}_\ell+(\alpha \mathrm{B}_{\ell 1}+\alpha^2 \mathrm{B}_{\ell 2})\,\dot{a}_\ell+\Omega_{\ell 0}^2\,a_\ell=0\,. \qquad (2.133)$$

Here,

$$\begin{aligned}
\mathrm{A}_{\ell 1} &= \frac{(2\ell+1)^2}{\sqrt{2}}\frac{1}{[(\ell+1)+\ell\hat{\rho}/\rho]}\frac{\sqrt{\hat{\mu}\hat{\rho}}}{(\sqrt{\mu\rho}+\sqrt{\hat{\mu}\hat{\rho}})}\frac{1}{\sqrt{\Omega_{\ell 0}}} \qquad (2.134)\\
\mathrm{B}_{\ell 1} &= \frac{(2\ell+1)^2}{\sqrt{2}}\frac{1}{[(\ell+1)+\ell\hat{\rho}/\rho]}\frac{\sqrt{\hat{\mu}\hat{\rho}}}{(\sqrt{\mu\rho}+\sqrt{\hat{\mu}\hat{\rho}})}\sqrt{\Omega_{\ell 0}} \qquad (2.135)\\
\mathrm{B}_{\ell 2} &= \frac{(2\ell+1)\{2(\ell^2-1)\mu\rho+2\ell(\ell+2)\hat{\mu}^2\hat{\rho}/\mu+\hat{\mu}[(\ell+2)\rho-(\ell-1)\hat{\rho}]\}}{[(\ell+1)+\ell\hat{\rho}/\rho](\sqrt{\mu\rho}+\sqrt{\hat{\mu}\hat{\rho}})^2}\,. \qquad (2.136)
\end{aligned}$$

If the $\mathcal{O}(\alpha^2)$ added mass terms were calculated, the damped harmonic oscillator equation would take the form

$$(1+\alpha \mathrm{A}_{\ell 1}+\alpha^2 \mathrm{A}_{\ell 2})\,\ddot{a}_\ell+(\alpha \mathrm{B}_{\ell 1}+\alpha^2 \mathrm{B}_{\ell 2})\,\dot{a}_\ell+\Omega_{\ell 0}^2\,a_\ell=0\,. \qquad (2.137)$$

Assuming exponential behavior for the time-dependent oscillation amplitude of the form $a_\ell(t) = e^{i\Omega_\ell t}$, with Ω_ℓ complex, the expressions for the frequency and damping constant can be found to be

$$\Re\{\Omega_\ell\} = \Omega_{\ell 0}\left[1 - \alpha\frac{\mathrm{A}_{\ell 1}}{2} + \alpha^2\left(\frac{3\mathrm{A}_{\ell 1}^2}{8} - \frac{\mathrm{B}_{\ell 1}^2}{8\Omega_{\ell 0}^2} - \frac{\mathrm{A}_{\ell 2}}{2}\right)\right] + \mathcal{O}(\alpha^3) \tag{2.138}$$

$$\Im\{\Omega_\ell\} = -\alpha\frac{\mathrm{B}_{\ell 1}}{2} + \alpha^2\frac{(\mathrm{A}_{\ell 1}\mathrm{B}_{\ell 1} - \mathrm{B}_{\ell 2})}{2} + \mathcal{O}(\alpha^3)\,. \tag{2.139}$$

These show that $\mathrm{A}_{\ell 2}$ contributes only to the expression for the frequency. Therefore, equation (2.133) can be expected to accurately predict frequencies to $\mathcal{O}(\alpha)$ and damping constants to $\mathcal{O}(\alpha^2)$.

Interestingly, the results of (2.138) and (2.139) with $\mathrm{A}_{\ell 2} = 0$ agree with the $\mathcal{O}(\alpha^2)$ frequency and damping constant calculated by Marston [28], who solved the eigenvalue problem for the complex frequencies using a normal mode analysis accurate to $\mathcal{O}(\alpha^2)$. From this comparison it would appear that the $\mathcal{O}(\alpha^2)$ contribution to the added mass is zero.

2.4.3 Case 2: "small" surfactant effects

In this section, the viscous drop in vacuum is analyzed when surfactants are present. For this case, all surface terms on the right-hand side of the nondimensional total mechanical energy equation (2.43) are retained. The surface properties e_s^*, κ_s^*, and μ_s^* are assumed to be "small", or $\mathcal{O}(\alpha^2)$.

This section presents the uniformly valid velocity and pressure approximations to $\mathcal{O}(\varepsilon\alpha^2)$. This allows for the consistent expansion of the nondimensional total mechanical energy equation to $\mathcal{O}(\alpha^2)$, capturing both the frequency shift and damping times to this same order.

Inner equations

As in Case 1, the radial coordinate may be replaced with $r = R + y$ in the inner region, and the full Navier-Stokes equations in the drop using the inertial scales (2.42) with the Stokes' boundary layer thickness as the length scale for y. The nondimensional velocity (scaled with ωR) and pressure (scaled with $\rho\omega^2 R^2$) in the drop and the surfactant concentration at the interface (scaled with its equilibrium value Γ_{eq}) are written as regular perturbation expansions in α such that

$$\mathbf{V}(y,\theta,t;\varepsilon,\alpha) = \varepsilon[\mathbf{V}_0(y,\theta,t) + \alpha\mathbf{V}_1(y,\theta,t) + \alpha^2\mathbf{V}_2(y,\theta,t)] + \mathcal{O}(\varepsilon\alpha^3) \tag{2.140}$$

$$P(y,\theta,t;\varepsilon,\alpha) = p_{eq} + \varepsilon[P_0(y,\theta,t) + \alpha P_1(y,\theta,t) + \alpha^2 P_2(y,\theta,t)] + \mathcal{O}(\varepsilon\alpha^3) \tag{2.141}$$

$$\Gamma(\theta,t;\varepsilon,\alpha) = 1 + \varepsilon[\Gamma_0(\theta,t) + \alpha\Gamma_1(\theta,t) + \alpha^2\Gamma_2(\theta,t)] + \mathcal{O}(\varepsilon\alpha^3)\,. \tag{2.142}$$

The size of the deformation is assumed to be small enough that $\varepsilon \ll \alpha^2$. The inner equations in the drop phase take the following forms at $\mathcal{O}(\varepsilon)$

$$\frac{\partial V_{r0}}{\partial y} = 0 \tag{2.143}$$

$$\frac{\partial P_0}{\partial y} = 0 \tag{2.144}$$

$$\frac{\partial V_{\theta 0}}{\partial t} + \frac{\partial P_0}{\partial \theta} - \frac{\partial^2 V_{\theta 0}}{\partial y^2} = 0 \tag{2.145}$$

$$\frac{\partial \Gamma_0}{\partial t} + M_0 - \frac{1}{\mathrm{Pe}_s}\left(\frac{\partial^2\Gamma_0}{\partial\theta^2} + \cot\theta\frac{\partial\Gamma_0}{\partial\theta}\right) = 0\,, \tag{2.146}$$

where

$$M_0(\theta,t) = \left(\frac{\partial V_{\theta 0}}{\partial\theta} + \cot\theta\, V_{\theta 0} + 2V_{r0}\right)\Big|_{y=0}\,. \tag{2.147}$$

These are the leading-order continuity, radial and tangential components of the linearized momentum equations, and the surfactant transport equation for the perturbed fields. These fields are subject to the kinematic,

tangential stress balance, and normal stress balance boundary conditions at the interface

$$V_{r0} = i\Omega_{\ell 0} A e^{i\Omega_{\ell 0} t} P_\ell(\cos\theta) \tag{2.148}$$

$$\frac{\partial V_{\theta 0}}{\partial y} = 0 \tag{2.149}$$

$$P_0 = (\ell - 1)(\ell + 2) A e^{i\Omega_{\ell 0} t} P_\ell(\cos\theta)\,. \tag{2.150}$$

The prescribed shape in (2.55) identically satisfies the nondimensional normal stress balance boundary condition at this order.

The equations for the $\mathcal{O}(\varepsilon\alpha)$ inner variables take similar forms:

$$\frac{\partial V_{r1}}{\partial y} = -M_0 \tag{2.151}$$

$$\frac{\partial P_1}{\partial y} = -\frac{\partial V_{r0}}{\partial t} - \frac{\partial^2 V_{r0}}{\partial y^2} \tag{2.152}$$

$$\frac{\partial V_{\theta 1}}{\partial t} + \frac{\partial P_1}{\partial \theta} - \frac{\partial^2 V_{\theta 1}}{\partial y^2} = y\frac{\partial P_0}{\partial \theta} + 2\frac{\partial V_{\theta 0}}{\partial y} \tag{2.153}$$

$$\frac{\partial \Gamma_1}{\partial t} + M_1 - \frac{1}{\mathrm{Pe}_s}\left(\frac{\partial^2 \Gamma_1}{\partial \theta^2} + \cot\theta \frac{\partial \Gamma_1}{\partial \theta}\right) = 0\,, \tag{2.154}$$

where now

$$M_1(\theta, t) = \left(\frac{\partial V_{\theta 1}}{\partial \theta} + \cot\theta\, V_{\theta 1} + 2V_{r1}\right)\Big|_{y=0}\,. \tag{2.155}$$

The $\mathcal{O}(\varepsilon\alpha)$ boundary conditions at the interface are

$$V_{r1} = 0 \tag{2.156}$$

$$\frac{\partial V_{\theta 1}}{\partial y} = -\frac{\partial V_{r0}}{\partial \theta} + V_{\theta 0} - \frac{e_s^*}{\alpha^2}\frac{\partial \Gamma_0}{\partial \theta} + \frac{\kappa_s^*}{\alpha^2}\frac{\partial M_0}{\partial \theta} + \frac{\mu_s^*}{\alpha^2}\left(\frac{\partial N_0}{\partial \theta} + 2\cot\theta\, N_0\right) \tag{2.157}$$

$$P_1 = 0\,, \tag{2.158}$$

where

$$N_0(\theta, t) = \left(\frac{\partial V_{\theta 0}}{\partial \theta} - \cot\theta\, V_{\theta 0}\right)\Big|_{y=0}\,. \tag{2.159}$$

Finally, the equations for the $\mathcal{O}(\varepsilon\alpha^2)$ inner variables are

$$\frac{\partial V_{r2}}{\partial y} = -M_1 + yM_0 \tag{2.160}$$

$$\frac{\partial P_2}{\partial y} = -\frac{\partial V_{r1}}{\partial t} - \frac{\partial^2 V_{r1}}{\partial y^2} \tag{2.161}$$

$$\frac{\partial V_{\theta 2}}{\partial t} + \frac{\partial P_2}{\partial \theta} - \frac{\partial^2 V_{\theta 2}}{\partial y^2} = y\frac{\partial P_1}{\partial \theta} + 2\frac{\partial V_{\theta 1}}{\partial y} - y^2\frac{\partial P_0}{\partial \theta} - 2y\frac{\partial V_{\theta 0}}{\partial y} + \frac{\partial M_0}{\partial \theta} \tag{2.162}$$

$$\frac{\partial \Gamma_2}{\partial t} + M_2 - \frac{1}{\mathrm{Pe}_s}\left(\frac{\partial^2 \Gamma_2}{\partial \theta^2} + \cot\theta \frac{\partial \Gamma_2}{\partial \theta}\right) = 0 \tag{2.163}$$

where

$$M_2(\theta, t) = \left(\frac{\partial V_{\theta 2}}{\partial \theta} + \cot\theta\, V_{\theta 2} + 2V_{r2}\right)\Big|_{y=0}\,. \tag{2.164}$$

The $\mathcal{O}(\varepsilon\alpha^2)$ boundary conditions at the interface are again

$$V_{r2} = 0 \tag{2.165}$$

$$\frac{\partial V_{\theta 2}}{\partial y} = -\frac{\partial V_{r1}}{\partial \theta} + V_{\theta 1} - \frac{e_s^*}{\alpha^2}\frac{\partial \Gamma_1}{\partial \theta} + \frac{\kappa_s^*}{\alpha^2}\frac{\partial M_1}{\partial \theta} + \frac{\mu_s^*}{\alpha^2}\left(\frac{\partial N_1}{\partial \theta} + 2\cot\theta N_1\right), \tag{2.166}$$

where

$$N_1(\theta, t) = \left(\frac{\partial V_{\theta 1}}{\partial \theta} - \cot\theta V_{\theta 1}\right)\Big|_{y=0}. \tag{2.167}$$

The normal stress balance boundary condition is not enforced at $\mathcal{O}(\varepsilon\alpha^2)$. This is similar to the loss of the normal stress balance boundary condition at $\mathcal{O}(\varepsilon\alpha)$ in the viscous drop/medium system. The boundary conditions on the inner fields far from the interface are replaced by matching conditions with outer velocity and pressure solutions in each phase.

Outer equations

In the outer region far from the interface the full Navier-Stokes equations are nondimensionalized using inertial scales (2.42). Again, the viscous terms appear at $\mathcal{O}(\alpha^2)$ but are identically zero for an outer potential flow. Anticipating the matching conditions with the inner viscous flow fields motivates writing the outer flow fields as regular perturbation expansions in the parameter α:

$$\phi(r, \theta, t; \varepsilon, \alpha) = \varepsilon[\phi_0(r, \theta, t) + \alpha\phi_1(r, \theta, t) + \alpha^2\phi_2(r, \theta, t)] + \mathcal{O}(\varepsilon\alpha^3) \tag{2.168}$$

$$p(r, \theta, t; \varepsilon, \alpha) = p_{eq} + \varepsilon[p_0(r, \theta, t) + \alpha p_1(r, \theta, t) + \alpha^2 p_2(r, \theta, t)] + \mathcal{O}(\varepsilon\alpha^3). \tag{2.169}$$

Here the arbitrary constant in the scalar velocity potential has been set to zero and p_{eq} is the reference pressure in the drop satisfying the nondimensional Young-Laplace equation $p_{eq} = 2$.

With the above expansions, the $\mathcal{O}(\varepsilon)$, $\mathcal{O}(\varepsilon\alpha)$, and $\mathcal{O}(\varepsilon\alpha^2)$ outer equations are all governed by Laplace's equation in spherical axisymmetric coordinates and the linearized unsteady Bernoulli equation for the pressure

$$\left.\begin{aligned} \nabla^2\phi_i &= 0 \\ p_i &= -\frac{\partial \phi_i}{\partial t} \end{aligned}\right\} \quad \text{for } i = 0, 1, 2. \tag{2.170}$$

These are subject to the boundary conditions that far from the interface the scalar velocity potential vanishes and the pressure tends to its reference value. The boundary conditions near the interface are replaced by matching conditions with inner velocity and pressure solutions in the drop.

Time-periodic composite solutions

As in the Case 1, additive composite expansions are used to obtain uniformly valid approximations for the total time-periodic velocity field $\mathbf{v}^{\text{tot}}$ and pressure field p^{tot} in the drop. Solving the inner and outer equations in the drop, subject to their boundary and matching conditions, and constructing the uniformly valid solutions yields the following approximations for the time-periodic velocity components, pressure, and surfactant concentration written in outer variables:

$$v_r^{\text{tot}}(r, \theta, t; \varepsilon, \alpha) = \varepsilon i\Omega_{\ell 0} A e^{i\Omega_{\ell 0} t} P_\ell(\cos\theta)\left\{ r^{\ell-1} - \alpha^2 \frac{\sqrt{2}}{(1+i)}\frac{1}{\sqrt{\Omega_{\ell 0}}}(\ell+1)C_{\theta 1}[r^{\ell-1} - \text{EXP}]\right\} + \mathcal{O}(\varepsilon\alpha^3), \tag{2.171}$$

$$v_\theta^{\text{tot}}(r, \theta, t; \varepsilon, \alpha) = \varepsilon i\Omega_{\ell 0} A e^{i\Omega_{\ell 0} t}\frac{1}{\ell}\frac{dP_\ell}{d\theta}(\cos\theta)\left\{ r^{\ell-1} + \alpha C_{\theta 1}(2 - r)\text{EXP}\right.$$

$$-\alpha^2\frac{\sqrt{2}}{(1+i)}\frac{1}{\sqrt{\Omega_{\ell 0}}}[(\ell+1)C_{\theta 1}r^{\ell-1}-C_{\theta 2}\mathrm{EXP}]\Bigg\}+\mathcal{O}(\varepsilon\alpha^3)\,, \tag{2.172}$$

$$p^{\mathrm{tot}}(r,\theta,t;\varepsilon,\alpha)-p_{eq} = \varepsilon\Omega_{\ell 0}^2 A e^{i\Omega_{\ell 0}t}\frac{1}{\ell}P_\ell(\cos\theta)\Bigg\{r^\ell$$
$$-\alpha^2\frac{\sqrt{2}}{(1+i)}\frac{1}{\sqrt{\Omega_{\ell 0}}}(\ell+1)C_{\theta 1}r^\ell\Bigg\}+\mathcal{O}(\varepsilon\alpha^3) \tag{2.173}$$

$$\Gamma(\theta,t;\varepsilon,\alpha)-1 = \varepsilon G e^{i\Omega_{\ell 0}t}\left\{1+\alpha C_{g1}+\alpha^2 C_{g2}\right\}P_\ell(\cos\theta)+\mathcal{O}(\varepsilon\alpha^3)\,. \tag{2.174}$$

Here EXP is an exponentially decaying function given by

$$\mathrm{EXP}=\exp\left[\sqrt{\Omega_{\ell 0}}\frac{(1+i)}{\sqrt{2}}\frac{(r-1)}{\alpha}\right]\,. \tag{2.175}$$

The complex constants $C_{\theta 1}$, $C_{\theta 2}$, G, C_{g1}, and C_{g2} are given in the Appendix B.

Again, the above fields contain terms of two types: those that resemble potential flow or those that exponentially decay away from the interface. In the tangential component of the velocity, the exponential decay terms appear at $\mathcal{O}(\varepsilon\alpha)$ in the perturbed fields, which is one order higher in α that in the viscous drop/medium system of Case 1. In the normal component of the velocity, the exponentially decaying terms do not appear until $\mathcal{O}(\varepsilon\alpha^2)$. In the pressure, the exponentially decaying terms do not appear at all to this order.

Order-of-magnitude analysis

As before, the direct substitution of the uniformly valid velocity and surfactant concentration approximations in the integrands of the nondimensional total mechanical energy equation leads to very complicated expressions that can be greatly simplified using an order-of-magnitude analysis. Recall that for this case the nondimensional total mechanical energy equation is

$$\frac{d}{dt}\{\mathrm{K.E.}+\mathrm{P.E.}\} = -\alpha^2\{\mathrm{Bulk\ Diss.}\}$$
$$-\mu_s^*\{\mathrm{Surf.\ Diss.}\}$$
$$+e_s^*\{\mathrm{Marangoni}\}\,. \tag{2.176}$$

The Marangoni term can be written as

$$\{\mathrm{Marangoni}\} = -\frac{d}{dt}\{\mathrm{Mar.\ E.}\}$$
$$-\frac{1}{\mathrm{Pe}_s}\{\mathrm{Mar.\ Diss.}\}$$
$$-\{\mathrm{Remainder}\}\,. \tag{2.177}$$

Equations (2.45)–(2.53), with the fluid properties in the medium set to zero, define the quantities in curly brackets.

The nondimensional energies, dissipation rates, and Marangoni terms may be approximated using the uniformly valid velocity approximations from the matched asymptotic analysis. As before, it is convenient to use a new notation for the order-of-magnitude of the velocity in the drop:

$$\mathbf{v}^{\mathrm{tot}}=\varepsilon[(\mathbf{u}_0+\alpha\mathbf{u}_1+\alpha^2\mathbf{u}_2)+(\mathbf{U}_0+\alpha\mathbf{U}_1+\alpha^2\mathbf{U}_2)]+\mathcal{O}(\varepsilon\alpha^3)\,. \tag{2.178}$$

For this case, the only nonzero components in the expansion (2.178) are u_{r0}, u_{r2}, $u_{\theta 0}$, $u_{\theta 2}$, U_{r2}, $U_{\theta 1}$, and $U_{\theta 2}$. Here the $\mathbf{u}$'s refer to the terms resembling potential flow with small $\mathcal{O}(1)$ gradients. The volume integrals containing these terms will be significant over the nondimensional volume of $\mathcal{O}(1)$. The $\mathbf{U}$'s refer

to the vortical flow terms with large $\mathcal{O}(1/\alpha)$ gradients in the radial direction that decay exponentially away from the interface. The volume integrals containing these terms will be significant over the nondimensional volume of the boundary layer of $\mathcal{O}(\alpha)$ near the interface.

Following the order-of-magnitude analysis of Case 1, keeping only those contributions which are $\mathcal{O}(\varepsilon^2\alpha^2)$ and larger, the nondimensional kinetic energy in the drop is

$$\begin{aligned}\int_{V_m} \frac{1}{2}|\mathbf{v}^{\mathrm{tot}}|^2\, dV = \\ \varepsilon^2 \int_0^{2\pi}\int_0^{\pi}\int_0^1 \frac{1}{2}\left\{(u_{r0}^2 + u_{\theta 0}^2) + 2\alpha^2(u_{r0}u_{r2} + u_{\theta 0}u_{\theta 2})\right\} r^2 \sin\theta dr d\theta d\varphi \\ +\varepsilon^2\alpha \int_0^{2\pi}\int_0^{\pi}\int_{-\infty}^0 \frac{1}{2}\left\{2\alpha\, u_{\theta 0}|_{r=1}\, U_{\theta 1}\right\} \sin\theta dy d\theta d\varphi + \mathcal{O}(\varepsilon^2\alpha^3)\,. \end{aligned} \tag{2.179}$$

Unlike the previous drop/medium case, all the nondimensional kinetic energy terms to $\mathcal{O}(\varepsilon^2\alpha^2)$ may be calculated because the uniformly valid velocity profiles have been determined to $\mathcal{O}(\varepsilon\alpha^2)$. This will allow for the calculation of the frequency shift to $\mathcal{O}(\alpha^2)$.

The bulk viscous dissipation rate in the drop is

$$\begin{aligned}\int_{V_m} 2(\mathbf{E}^{\mathrm{tot}} : \mathbf{E}^{\mathrm{tot}})\, dV = \\ \varepsilon^2 \int_0^{2\pi}\int_0^{\pi}\int_0^1 2\left\{\left(\frac{\partial u_{r0}}{\partial r}\right)^2 + \frac{1}{r^2}\left(\frac{\partial u_{\theta 0}}{\partial \theta} + u_{r0}\right)^2 + \frac{1}{r^2}\left(u_{r0} - \cot\theta u_{\theta 0}\right)^2 \right. \\ \left. + \frac{1}{2}\left[\frac{\partial u_{\theta 0}}{\partial r} + \frac{1}{r}\left(\frac{\partial u_{r0}}{\partial \theta} - u_{\theta 0}\right)\right]^2\right\} r^2 \sin\theta dr d\theta d\varphi \\ + \mathcal{O}(\varepsilon^2\alpha)\,. \end{aligned} \tag{2.180}$$

The surface viscous dissipation rate arising from the surface shear viscosity is

$$\int_{S_m} 2(\mathbf{E}_s^{\mathrm{tot}} : \mathbf{E}_s^{\mathrm{tot}})\, dS = \varepsilon^2 \int_0^{2\pi}\int_0^{\pi} n_0^2 \sin\theta d\theta d\varphi + \mathcal{O}(\varepsilon^2\alpha)\,, \tag{2.181}$$

where

$$n_0(\theta, t) = \left(\frac{\partial u_{\theta 0}}{\partial \theta} - \cot\theta\, u_{\theta 0}\right)\Big|_{r=1}\,. \tag{2.182}$$

The surface viscous dissipation rate arising from the surface dilatational viscosity is similarly:

$$\int_{S_m} (\boldsymbol{\nabla}_s \cdot \mathbf{v}^{\mathrm{tot}})^2\, dS = \varepsilon^2 \int_0^{2\pi}\int_0^{\pi} m_0^2 \sin\theta d\theta d\varphi + \mathcal{O}(\varepsilon^2\alpha)\,, \tag{2.183}$$

where

$$m_0(\theta, t) = \left(\frac{\partial u_{\theta 0}}{\partial \theta} + \cot\theta\, u_{\theta 0} + 2u_{r0}\right)\Big|_{r=1}\,. \tag{2.184}$$

The nondimensional Marangoni term is

$$\int_{S_m} (\Gamma - 1)(\boldsymbol{\nabla}_s \cdot \mathbf{v}^{\mathrm{tot}})\, dS = \varepsilon^2 \int_0^{2\pi}\int_0^{\pi} \Gamma_0 m_0 \sin\theta d\theta d\varphi + \mathcal{O}(\varepsilon^2\alpha)\,. \tag{2.185}$$

The Marangoni stored energy term is

$$\int_{S_m} \frac{1}{2}(\Gamma - 1)^2\, dS = \varepsilon^2 \int_0^{2\pi}\int_0^{\pi} \frac{1}{2}\Gamma_0^2 \sin\theta d\theta d\varphi + \mathcal{O}(\varepsilon^2\alpha)\,. \tag{2.186}$$

Finally, the leading-order Marangoni dissipation rate is given by

$$\int_{S_m} |\boldsymbol{\nabla}_s(\Gamma - 1)|^2 \, dS = \varepsilon^2 \int_0^{2\pi}\int_0^{\pi} \left(\frac{\partial \Gamma_0}{\partial \theta}\right)^2 \sin\theta d\theta d\varphi + \mathcal{O}(\varepsilon^2\alpha) \,. \tag{2.187}$$

The expressions in (2.186) and (2.187) need to be calculated only to $\mathcal{O}(\varepsilon^2)$ since they couple with the nondimensional total mechanical energy equation through the Marangoni term, which is multiplied by e_s^*, an $\mathcal{O}(\alpha^2)$ parameter for this case.

The integrand of the Remainder term is $\mathcal{O}(\varepsilon^3)$ and hence neglected.

Time-averaging

Using the time-averaging procedure as outlined in Case 1, the time-average of the terms in the total mechanical energy equation (2.176) and the Marangoni expression (2.177) are given by

$$\langle \text{K.E.} \rangle = \varepsilon^2 \pi \frac{1}{\ell(2\ell+1)} |\Omega_{\ell 0} A|^2 + \mathcal{O}(\varepsilon^2\alpha^2) \tag{2.188}$$

$$\langle \text{P.E.} \rangle = 4\pi + \varepsilon^2 \pi \frac{(\ell-1)(\ell+2)}{(2\ell+1)} |A|^2 + \mathcal{O}(\varepsilon^3) \tag{2.189}$$

$$\langle \text{Bulk Diss.} \rangle = \varepsilon^2 4\pi \frac{(\ell-1)}{\ell} |\Omega_{\ell 0} A|^2 + \mathcal{O}(\varepsilon^2\alpha) \tag{2.190}$$

$$\langle \text{Surf. Diss.} \rangle = \varepsilon^2 2\pi \frac{(\ell-1)}{\ell(2\ell+1)} \left[(\ell+1)(\ell+2) + \ell(\ell-1)\frac{\kappa_s^*}{\mu_s^*}\right] |\Omega_{\ell 0} A|^2 + \mathcal{O}(\varepsilon^2\alpha) \tag{2.191}$$

$$\langle \text{Marangoni} \rangle = \varepsilon^2 \pi \frac{(\ell-1)}{(2\ell+1)} (i\Omega_{\ell 0} A G^* + \text{c.c.}) + \mathcal{O}(\varepsilon^2\alpha) \tag{2.192}$$

$$\langle \text{M.E.} \rangle = \varepsilon^2 \pi \frac{1}{(2\ell+1)} |G|^2 + \mathcal{O}(\varepsilon^2\alpha) \tag{2.193}$$

$$\langle \text{Mar. Diss.} \rangle = \varepsilon^2 2\pi \frac{\ell(\ell+1)}{(2\ell+1)} |G|^2 + \mathcal{O}(\varepsilon^2\alpha) \,. \tag{2.194}$$

Coupled oscillator equations

Following the averaging method with $a_\ell(t) = \Re\{A e^{i\Omega_{\ell 0} t}\}$ and $g_\ell(t) = \Re\{G e^{i\Omega_{\ell 0} t}\}$, the complex amplitudes in (2.188)–(2.194) are replaced with the quantities

$$|\Omega_{\ell 0} A|^2 \rightarrow 2(\dot{a}_\ell)^2 \tag{2.195}$$

$$|A|^2 \rightarrow 2(a_\ell)^2 \tag{2.196}$$

$$(i\Omega_{\ell 0} A\overline{G} + \text{c.c.}) \rightarrow 2(g_\ell \dot{a}_\ell) \tag{2.197}$$

$$|G|^2 \rightarrow 2(g_\ell)^2 \,. \tag{2.198}$$

These would give the same time average if $a_\ell(t)$ and $g_\ell(t)$ were time-periodic with a nondimensional period $2\pi/\Omega_{\ell 0}$. Simplifying the nondimensional total mechanical energy equation yields the damped harmonic oscillator equation for the nondimensional amplitude of the shape oscillations,

$$\begin{aligned} \ddot{a}_\ell &+ \dot{a}_\ell \left[\alpha^2 2(\ell-1)(2\ell+1) + \kappa_s^* \ell(\ell-1)^2 + \mu_s^*(\ell-1)(\ell+1)(\ell+2)\right] \\ &+ a_\ell \left[(\ell-1)(\ell+2)\right] = -g_\ell \left[\mathrm{e}_s^* \ell(\ell-1)\right] . \end{aligned} \tag{2.199}$$

This oscillator equation is coupled to the simplified Marangoni expression:

$$\dot{g}_\ell + \frac{\ell(\ell+1)}{\mathrm{Pe}_s} g_\ell = (\ell-1)\dot{a}_\ell \,. \tag{2.200}$$

Setting $\alpha^2, \mathrm{e}_s^*, \kappa_s^*$, and μ_s^* to zero reduces the coupled set of equations to a simple harmonic oscillator equation for $a_\ell(t)$, the time-dependent amplitude for the shape oscillations of a drop in vacuum. The

oscillation frequency is in agreement with the results of Lamb [23] when the properties of the medium are negligible compared to those of the drop.

By setting $\mathrm{e}_s^* = 0$ the equations decouple and the oscillator equation for $a_\ell(t)$ contains damping contributions from α^2, κ_s^*, and μ_s^*.

For large surface Peclet number Pe_s, the time-dependence for the surfactant concentration may be seen to be proportional to the time-dependence for the amplitude of the shape oscillations. Therefore the term on the right-hand side of (2.199), which arises from the Marangoni effect, acts to "stiffen" the system and increase the natural frequency of oscillation.

For small Pe_s, equation (2.200) shows that $g_\ell(t)$ is proportional to $\dot{a}_\ell(t)$. The term on the right-hand side of (2.199) thus gives rise to an additional damping mechanism from the irreversible diffusion of surfactant molecules.

For a surface Peclet number of $\mathcal{O}(1)$, the coupled system (2.199) and (2.200) needs to be solved simultaneously to describe the oscillations.

2.4.4 Case 3: "medium" surfactant effects

In this section the presence of the surrounding medium is neglected and the viscous drop in vacuum system when surfactants are present is analyzed. For this case, all terms on the right-hand side of the nondimensional total mechanical energy equation (2.43) are retained. The surface properties e_s^*, κ_s^*, and μ_s^* are assumed to be "medium", or $\mathcal{O}(\alpha)$.

Due to the larger influence of the surfactant monolayer, the uniformly valid velocity and pressure approximations are calculated to an accuracy of $\mathcal{O}(\varepsilon\alpha)$. This allows for a consistent expansion of the total mechanical energy equation to $\mathcal{O}(\alpha)$, capturing both the frequency shift and damping times to this same order.

Inner equations

As before, the inner fields are written as regular perturbation expansions in α in the scaled variable y:

$$\mathbf{V}(y,\theta,t;\varepsilon,\alpha) = \varepsilon[\mathbf{V}_0(y,\theta,t) + \alpha\mathbf{V}_1(y,\theta,t)] + \mathcal{O}(\varepsilon\alpha^2) \tag{2.201}$$

$$P(y,\theta,t;\varepsilon,\alpha) = p_{eq} + \varepsilon[P_0(y,\theta,t) + \alpha P_1(y,\theta,t)] + \mathcal{O}(\varepsilon\alpha^2) \tag{2.202}$$

$$\Gamma(\theta,t;\varepsilon,\alpha) = 1 + \varepsilon[\Gamma_0(\theta,t) + \alpha\Gamma_1(\theta,t)] + \mathcal{O}(\varepsilon\alpha^2) \tag{2.203}$$

With the above expansions, the $\mathcal{O}(\varepsilon)$ and $\mathcal{O}(\varepsilon\alpha)$ inner equations take the same forms as in Case 2 equations (2.143)–(2.146) and (2.151)–(2.154), respectively. The kinematic, tangential stress balance, and normal stress balance boundary conditions at $\mathcal{O}(\varepsilon)$ are

$$V_{r0} = i\Omega_{\ell 0} A e^{i\Omega_{\ell 0} t} P_\ell(\cos\theta) \tag{2.204}$$

$$\frac{\partial V_{\theta 0}}{\partial y} = -\frac{\mathrm{e}_s^*}{\alpha}\frac{\partial \Gamma_0}{\partial \theta} + \frac{\kappa_s^*}{\alpha}\frac{\partial M_0}{\partial \theta} + \frac{\mu_s^*}{\alpha}\left(\frac{\partial N_0}{\partial \theta} + 2\cot\theta N_0\right) \tag{2.205}$$

$$P_0 = (\ell-1)(\ell+2) A e^{i\Omega_{\ell 0} t} P_\ell(\cos\theta)\,. \tag{2.206}$$

N_0 given by (2.159). The prescribed shape (2.55) identically satisfies the normal stress balance boundary condition.

The corresponding boundary conditions at $\mathcal{O}(\varepsilon\alpha)$ are

$$V_{r1} = 0 \tag{2.207}$$

$$\frac{\partial V_{\theta 1}}{\partial y} = -\frac{\partial V_{r0}}{\partial \theta} + V_{\theta 0} - \frac{e_s^*}{\alpha}\frac{\partial \Gamma_1}{\partial \theta} + \frac{\kappa_s^*}{\alpha}\frac{\partial M_1}{\partial \theta} + \frac{\mu_s^*}{\alpha}\left(\frac{\partial N_0}{\partial \theta} + 2\cot\theta N_0\right). \tag{2.208}$$

The normal stress balance boundary condition cannot be satisfied at this order.

Time-periodic composite solutions

The outer equations are identical to those from Case 1. Thus, the composite expansions may be obtained as before and the composite expansions are given by

$$v_r^{\rm tot}(r,\theta,t;\varepsilon,\alpha) = \varepsilon i\Omega_{\ell 0}Ae^{i\Omega_{\ell 0}t}P_\ell(\cos\theta)\left\{r^{\ell-1}\right.$$
$$\left.+\alpha\frac{\sqrt{2}}{(1+i)}\frac{1}{\sqrt{\Omega_{\ell 0}}}(\ell+1)C_{\theta 0}[r^{\ell-1}+{\rm EXP}]\right\}+\mathcal{O}(\varepsilon\alpha^2)\,, \tag{2.209}$$

$$v_\theta^{\rm tot}(r,\theta,t;\varepsilon,\alpha) = \varepsilon i\Omega_{\ell 0}Ae^{i\Omega_{\ell 0}t}\frac{1}{\ell}\frac{dP_\ell}{d\theta}(\cos\theta)\left\{r^{\ell-1}+C_{\theta 0}(2-r){\rm EXP}\right.$$
$$\left.-\alpha\frac{\sqrt{2}}{(1+i)}\frac{1}{\sqrt{\Omega_{\ell 0}}}[(\ell+1)C_{\theta 0}r^{\ell-1}-C_{\theta 1}{\rm EXP}]\right\}+\mathcal{O}(\varepsilon\alpha^2)\,, \tag{2.210}$$

$$p^{\rm tot}(r,\theta,t;\varepsilon,\alpha)-p_{eq} = \varepsilon\Omega_{\ell 0}^2Ae^{i\Omega_{\ell 0}t}\frac{1}{\ell}P_\ell(\cos\theta)\left\{r^\ell\right.$$
$$\left.-\alpha\frac{\sqrt{2}}{(1+i)}\frac{1}{\sqrt{\Omega_{\ell 0}}}(\ell+1)C_{\theta 0}r^\ell\right\}+\mathcal{O}(\varepsilon\alpha^2) \tag{2.211}$$

$$\Gamma(\theta,t;\varepsilon,\alpha)-1 = \varepsilon Ge^{i\Omega_{\ell 0}t}\left\{1+\alpha C_{g1}\right\}P_\ell(\cos\theta)+\mathcal{O}(\varepsilon\alpha^2)\,, \tag{2.212}$$

EXP is the function in (2.120) that decays exponentially away from the interface in the drop. The complex constants $C_{\theta 0}$, $C_{\theta 1}$, G, and C_{g1} are given in the Appendix B.

The fields in (2.209)–(2.211) take the same form as the the fields in the drop phase (2.114)–(2.116) for the drop/medium system considered in Case 1. In Case 1, however, the presence of the $\mathcal{O}(\varepsilon)$ vortical field in the tangential component is traced to the viscous forces between the fluids in each phase in satisfying the no-slip boundary condition at the interface. In this case, on the other hand, its presence comes from the forces exerted between the fluid in the drop and the surfactant monolayer.

Order-of-magnitude analysis

The nondimensional total mechanical energy equation and Marangoni expression are identical to Case 2 equations (2.176) and (2.177).

The energies, dissipation rates and Marangoni terms may be approximated using the uniformly valid velocity approximations from the matched asymptotic analysis. It is again convenient to use a slightly different notation for the order-of-magnitude of the velocity in the drop:

$$\mathbf{v}^{\rm tot} = \varepsilon[(\mathbf{u}_0+\alpha\mathbf{u}_1)+(\mathbf{U}_0+\alpha\mathbf{U}_1)]+\mathcal{O}(\varepsilon\alpha^2)\,. \tag{2.213}$$

For this case, only the U_{r0} component is zero. As before, the $\mathbf{u}$'s refer to the terms resembling potential flow with small $\mathcal{O}(1)$ gradients. The volume integrals containing these terms will be significant over the nondimensional volume of $\mathcal{O}(1)$. The $\mathbf{U}$'s refer to the vortical flow terms with large $\mathcal{O}(1/\alpha)$ gradients in the radial direction that decay exponentially away from the interface. The volume integrals containing these terms will be significant over the nondimensional volume of the boundary layer of $\mathcal{O}(\alpha)$ near the interface.

Substituting the composite expansion into the expression for the kinetic energy and expanding to $\mathcal{O}(\varepsilon^2\alpha)$ yields:

$$\int_{V_m}\frac{1}{2}|\mathbf{v}^{\rm tot}|^2\,dV =$$
$$\varepsilon^2\int_0^{2\pi}\int_0^{\pi}\int_0^1\frac{1}{2}\left\{(u_{ro}^2+u_{\theta o}^2)+2\alpha(u_{ro}u_{r1}+u_{\theta o}u_{\theta 1})\right\}r^2\sin\theta dr d\theta d\varphi$$

$$+\varepsilon^2\alpha\int_0^{2\pi}\int_0^{\pi}\int_{-\infty}^{0}\frac{1}{2}\left\{2\,u_{\theta o}|_{r=1}\,U_{\theta o}+U_{\theta o}^2\right\}\sin\theta dy d\theta d\varphi+\mathcal{O}(\varepsilon^2\alpha^2)\,. \tag{2.214}$$

Similarly, the bulk viscous dissipation rate in the drop is given by:

$$\int_{V_m}2(\mathbf{E}^{\rm tot}:\mathbf{E}^{\rm tot})\,dV = \varepsilon^2\alpha\int_0^{2\pi}\int_0^{\pi}\int_{-\infty}^{0}2\left\{\frac{1}{2\alpha^2}\left(\frac{\partial U_{\theta o}}{\partial y}\right)^2\right\}\sin\theta dy d\theta d\varphi+\mathcal{O}(\varepsilon^2)\,. \tag{2.215}$$

The surface viscous dissipation rate arising from the surface shear viscosity:

$$\int_{S_m}2(\mathbf{E}_s^{\rm tot}:\mathbf{E}_s^{\rm tot})\,dS=\varepsilon^2\int_0^{2\pi}\int_0^{\pi}(n_0+N_0)^2\sin\theta d\theta d\varphi+\mathcal{O}(\varepsilon^2\alpha)\,. \tag{2.216}$$

Here, n_0 and N_0 are given by:

$$n_0(\theta,t) = \left(\frac{\partial u_{\theta 0}}{\partial\theta}-\cot\theta u_{\theta 0}\right)\Big|_{r=1} \tag{2.217}$$

$$N_0(\theta,t) = \left(\frac{\partial U_{\theta 0}}{\partial\theta}-\cot\theta U_{\theta 0}\right)\Big|_{r=1}\,. \tag{2.218}$$

The surface viscous dissipation rate arising from the surface dilatational viscosity is similarly:

$$\int_{S_m}(\boldsymbol{\nabla}_s\cdot\mathbf{v}^{\rm tot})^2\,dS=\varepsilon^2\int_0^{2\pi}\int_0^{\pi}(m_0+M_0)^2\sin\theta d\theta d\varphi+\mathcal{O}(\varepsilon^2\alpha)\,, \tag{2.219}$$

where

$$m_0(\theta,t) = \left(\frac{\partial u_{\theta 0}}{\partial\theta}+\cot\theta u_{\theta 0}+2u_{r0}\right)\Big|_{r=1} \tag{2.220}$$

$$M_0(\theta,t) = \left(\frac{\partial U_{\theta 0}}{\partial\theta}+\cot\theta U_{\theta 0}+2U_{r0}\right)\Big|_{r=1}\,. \tag{2.221}$$

The nondimensional Marangoni term is given by

$$\int_{S_m}(\Gamma-1)(\boldsymbol{\nabla}_s\cdot\mathbf{v}^{\rm tot})\,dS=\varepsilon^2\int_0^{2\pi}\int_0^{\pi}\Gamma_0(m_0+M_0)\sin\theta d\theta d\varphi+\mathcal{O}(\varepsilon^2\alpha)\,. \tag{2.222}$$

The stored Marangoni energy is

$$\int_{S_m}\frac{1}{2}(\Gamma-1)^2\,dS=\varepsilon^2\int_0^{2\pi}\int_0^{\pi}\frac{1}{2}\Gamma_0^2\sin\theta d\theta d\varphi+\mathcal{O}(\varepsilon^2\alpha)\,. \tag{2.223}$$

Finally, the Marangoni dissipation rate is

$$\int_{S_m}|\boldsymbol{\nabla}_s(\Gamma-1)|^2\,dS=\varepsilon^2\int_0^{2\pi}\int_0^{\pi}\left(\frac{\partial\Gamma_0}{\partial\theta}\right)^2\sin\theta d\theta d\varphi+\mathcal{O}(\varepsilon^2\alpha)\,. \tag{2.224}$$

The integrand of the Remainder term is $\mathcal{O}(\varepsilon^3)$ and again neglected.

Time-averaging

As before, the order-of-magnitude estimates for the integrals in the energy equation are time-averaged over one period of oscillation and integrated over the unit sphere. For the terms in the nondimensional total

mechanical energy equation (2.176) and the Marangoni expression (2.177), this procedure yields

$$\langle \text{K.E.} \rangle = \varepsilon^2\pi\frac{1}{\ell(2\ell+1)}\left\{1+\frac{\alpha}{\sqrt{\Omega_{\ell 0}}}\frac{(\ell+1)}{\ell(2\ell+1)}\left[\frac{|C_{\theta 0}|^2}{\sqrt{2}} + \frac{2\ell}{(2\ell+1)}(C_{\theta 0}e^{-i\pi/4}+\text{c.c.})\right]\right\}|\Omega_{\ell 0}A|^2 + \mathcal{O}(\varepsilon^2\alpha^2) \tag{2.225}$$

$$\langle \text{P.E.} \rangle = 4\pi + \varepsilon^2\pi\frac{(\ell-1)(\ell+2)}{(2\ell+1)}|A|^2 + \mathcal{O}(\varepsilon^3) \tag{2.226}$$

$$\langle \text{Bulk Diss.} \rangle = \frac{\varepsilon^2}{\alpha}4\pi\frac{(\ell-1)}{\ell}|C_{\theta 0}|^2|\Omega_{\ell 0}A|^2 + \mathcal{O}(\varepsilon^2) \tag{2.227}$$

$$\langle \text{Surf. Diss.} \rangle = \varepsilon^2 2\pi\frac{(\ell^2-1)}{(2\ell+1)}\left\{\frac{(\ell+2)}{\ell}\left[1+(C_{\theta 0}+\overline{C}_{\theta 0})+|C_{\theta 0}|^2\right] + \left[\frac{(\ell-1)}{(\ell+1)}+(C_{\theta 0}+\overline{C}_{\theta 0})+\frac{(\ell+1)}{(\ell-1)}|C_{\theta 0}|^2\right]\frac{\kappa_s^*}{\mu_s^*}\right\}|\Omega_{\ell 0}A|^2 + \mathcal{O}(\varepsilon^2\alpha) \tag{2.228}$$

$$\langle \text{Marangoni} \rangle = \varepsilon^2\pi\frac{1}{(2\ell+1)}\left[(\ell-1)(i\Omega_{\ell 0}A\overline{G}+\text{c.c.}) + (\ell+1)(i\Omega_{\ell 0}C_{\theta 0}A\overline{G}+\text{c.c.})\right] + \mathcal{O}(\varepsilon^2\alpha) \tag{2.229}$$

$$\langle \text{Mar. E.} \rangle = \varepsilon^2\pi\frac{1}{(2\ell+1)}|G|^2 + \mathcal{O}(\varepsilon^2\alpha) \tag{2.230}$$

$$\langle \text{Mar. Diss.} \rangle = \varepsilon^2 2\pi\frac{\ell(\ell+1)}{(2\ell+1)}|G|^2 + \mathcal{O}(\varepsilon^2\alpha)\,. \tag{2.231}$$

Coupled oscillator equations

Following the averaging method with $a_\ell(t) = \Re\{Ae^{i\Omega_{\ell 0}t}\}$ and $g_\ell(t) = \Re\{Ge^{i\Omega_{\ell 0}t}\}$, the complex amplitudes in (2.225)–(2.231) are replaced with the quantities

$$|\Omega_{\ell 0}A|^2 \rightarrow 2(\dot{a}_\ell)^2 \tag{2.232}$$

$$|A|^2 \rightarrow 2(a_\ell)^2 \tag{2.233}$$

$$(i\Omega_{\ell 0}A\overline{G}+\text{c.c.}) \rightarrow 2g_\ell\dot{a}_\ell \tag{2.234}$$

$$|G|^2 \rightarrow 2(g_\ell)^2 \tag{2.235}$$

which would give the same time average if $a_\ell(t)$ and $g_\ell(t)$ were time-periodic with a nondimensional period $2\pi/\Omega_{\ell 0}$.

Due to the presence of the complex constant $C_{\theta 0}$, it is not clear how to replace the time-averaged quantity $(i\Omega_{\ell 0}C_{\theta 0}A\overline{G}+\text{c.c.})$ in the Marangoni term with terms involving $\dot{a}_\ell$ and g_ℓ. A result may still be extracted from the above analysis if the Gibbs elasticity is set to zero. The limit when $e_s = 0$ corresponds to the case when there is so much insoluble surfactant on the interface that local changes in shape do not change the surfactant concentration appreciably. For this situation the surfactant concentration and surface tension are approximately constant over the interface. The Marangoni term that couples the oscillator equation for the time-dependent amplitude of the shape deformation to the surfactant transport equation then vanishes. The resulting decoupled oscillator equation for $a_\ell(t)$ is given by

$$\ddot{a}_\ell\left\{1+\frac{\alpha}{\sqrt{\Omega_{\ell 0}}}\frac{(\ell+1)}{\ell(2\ell+1)}\left[\frac{|C_{\theta 0}|^2}{\sqrt{2}}+\frac{2\ell}{(2\ell+1)}(C_{\theta 0}e^{-i\pi/4}+\text{c.c.})\right]\right\}$$
$$+\ \dot{a}_\ell\left\{\alpha\sqrt{\Omega_{\ell 0}}\frac{(\ell+1)}{\sqrt{2}}|C_{\theta 0}|^2 + \mu_s^*(\ell-1)(\ell+1)(\ell+2)\left[1+(C_{\theta 0}+\text{c.c.})+|C_{\theta 0}|^2\right] + \kappa_s^*\ell\left[(\ell-1)^2+(\ell-1)(\ell+1)(C_{\theta 0}+\text{c.c.})+(\ell+1)^2|C_{\theta 0}|^2\right]\right\}$$

$$
\begin{aligned}
&+ \quad a_\ell \left[\ell(\ell-1)(\ell+2)\right] \\
&= \quad \mathcal{O}(\alpha^2)\,.
\end{aligned}
\tag{2.236}
$$

Here the complex constant $C_{\theta 0}$ is independent of e_s^* since it has been set to zero. Although the expressions for the $\mathcal{O}(\alpha)$ added mass and damping terms may be found by evaluating the real terms, they are extremely complicated and are not written explicitly here.

If the surface viscosities are zero, the uncoupled oscillator equation reduces to

$$
\ddot{a}_\ell + [\ell(\ell-1)(\ell+2)]a_\ell = \mathcal{O}(\alpha^2) \tag{2.237}
$$

This limit shows that without surface viscosity, the $\mathcal{O}(\alpha)$ added mass and damping terms are shifted to $\mathcal{O}(\alpha^2)$, which is neglected in this leading-order analysis. Without the surface viscosities or Marangoni effects, the viscous bulk fluid in the drop has nothing to "push against" to produce $\mathcal{O}(\alpha)$ dissipation in the boundary layers.

If the bulk viscosity of the drop is neglected, the oscillator equation simplifies to

$$
\begin{aligned}
\ddot{a}_\ell \quad &+ \quad \dot{a}_\ell \left\{ \frac{4\ell(\ell-1)(\ell+2)\mu_s^*\kappa_s^*}{[(\ell-1)(\ell+2)\mu_s^* + \ell(\ell+1)\kappa_s^*]} \right\} \\
&+ \quad a_\ell \left[\ell(\ell-1)(\ell+2)\right] = \mathcal{O}(\alpha^2)\,.
\end{aligned}
\tag{2.238}
$$

Here a damping term remains from the dissipation within the interface due to the surface viscosities. Note that in the limit when one of the surface viscosities is larger than the other, it is the *smaller* of the two surface viscosities which contributes the most to the damping. The natural frequency of oscillation remains unchanged from the Lamb frequency to $\mathcal{O}(\alpha)$, but the presence of the $\mathcal{O}(\alpha)$ damping term in this limit causes a frequency shift at $\mathcal{O}(\alpha^2)$, which has been neglected.

2.4.5 Case 4: "large" surfactant effects

In this section, the leading-order effects of viscosity and surfactants on the drop/medium system are analyzed when the surface properties e_s^*, μ_s^*, and κ_s^* are assumed to be "large", or $\mathcal{O}(1)$.

For this case the viscous dissipation terms in the bulk phases are negligible compared to the surface viscous dissipation and Marangoni effects at the interface. For this reason the uniformly valid velocity profiles in each phase and the analysis of the energy equation using the averaging method is not needed. The dynamics of the drop is determined by the potential flow, but potential flow cannot satisfy the tangential stress balance boundary condition. To treat this, V_θ, the tangential velocity of the interface is introduced. V_θ is distinct from the tangential velocity of the fluid in each phase evaluated at the interface.

The assumed solutions and leading-order field equations are thus of the form:

$$
\begin{aligned}
\phi(r,\theta,t;\varepsilon,\alpha) &= \varepsilon\phi_0(r,\theta,t) + \mathcal{O}(\varepsilon\alpha) && (2.239)\\
p(r,\theta,t;\varepsilon,\alpha) &= p_{eq} + \varepsilon p_0(r,\theta,t) + \mathcal{O}(\varepsilon\alpha) && (2.240)\\
\hat{\phi}(r,\theta,t;\varepsilon,\alpha) &= \varepsilon\hat{\phi}_0(r,\theta,t) + \mathcal{O}(\varepsilon\alpha) && (2.241)\\
\hat{p}(r,\theta,t;\varepsilon,\alpha) &= \hat{p}_{eq} + \varepsilon\hat{p}_0(r,\theta,t) + \mathcal{O}(\varepsilon\alpha) && (2.242)\\
\Gamma(\theta,t;\varepsilon,\alpha) &= 1 + \varepsilon\Gamma_0(\theta,t) + \mathcal{O}(\varepsilon\alpha) && (2.243)\\
V_\theta(\theta,t;\varepsilon,\alpha) &= \varepsilon V_{\theta 0}(\theta,t) + \mathcal{O}(\varepsilon\alpha) && (2.244)
\end{aligned}
$$

$$
\nabla^2\phi_0 = 0\,, \quad p_0 = -\frac{\partial\phi_0}{\partial t} \qquad \text{for } r < 1 \tag{2.245}
$$

$$
\nabla^2\hat{\phi}_0 = 0\,, \quad \hat{p}_0 = -\frac{\hat{\rho}}{\rho}\frac{\partial\hat{\phi}_0}{\partial t} \qquad \text{for } r > 1 \tag{2.246}
$$

$$
\frac{\partial\Gamma_0}{\partial t} + M_0 = \frac{1}{\mathrm{Pe}_s}\left(\frac{\partial^2\Gamma_0}{\partial\theta^2} + \cot\theta\,\frac{\partial\Gamma_0}{\partial\theta}\right) \qquad \text{at } r = 1\,. \tag{2.247}
$$

These are subject to the $\mathcal{O}(\varepsilon)$ kinematic, tangential stress balance, and normal stress balance boundary conditions at $r = 1$, respectively,

$$\frac{\partial \phi_0}{\partial r} = \frac{\partial \hat{\phi}_0}{\partial r} = \frac{\partial f}{\partial t} \tag{2.248}$$

$$0 = -\frac{\mathrm{e}_s^*}{\alpha}\frac{\partial \Gamma_0}{\partial \theta} + \frac{\kappa_s^*}{\alpha}\frac{\partial M_0}{\partial \theta} + \frac{\mu_s^*}{\alpha}\left(\frac{\partial N_0}{\partial \theta} + 2\cot\theta N_0\right) \tag{2.249}$$

$$p_0 - \frac{\hat{\rho}}{\rho}\hat{p}_0 = -\left(\frac{\partial^2 f}{\partial \theta^2} + \cot\theta\frac{\partial f}{\partial \theta} + 2f\right). \tag{2.250}$$

In the above expressions M_0 and N_0 are given by

$$M_0(\theta, t) = \left(\frac{\partial V_{\theta 0}}{\partial \theta} + \cot\theta V_{\theta 0} + 2v_{r0}\right)\Big|_{r=1} \tag{2.251}$$

$$N_0(\theta, t) = \left(\frac{\partial V_{\theta 0}}{\partial \theta} - \cot\theta V_{\theta 0}\right). \tag{2.252}$$

These contain the tangential velocity of the interface $V_{\theta 0}$ and the normal velocity velocity of the fluid evaluated at the interface $v_{r0} = \partial\phi/\partial r$.

The surface deformation $f(\theta, t)$, surfactant concentration $\Gamma_0(\theta, t)$, and the tangential velocity of the interface $V_{\theta 0}$ are assumed to have the forms

$$f(\theta, t) = a_\ell(t) P_\ell(\cos\theta) \tag{2.253}$$

$$\Gamma_0(\theta, t) = g_\ell(t) P_\ell(\cos\theta) \tag{2.254}$$

$$V_{\theta 0} = b_\ell(t)\frac{dP_\ell}{d\theta}(\cos\theta). \tag{2.255}$$

Here a_ℓ, g_ℓ, and b_ℓ are the time-dependent amplitude perturbations for a pure mode. The kinematic boundary condition (2.248) allows a similar modal expansion to be obtained for the velocity potentials ϕ_0 and $\hat{\phi}_0$ with amplitudes proportional to $\dot{a}_\ell$.

Coupled oscillator equations

Substituting the modal expansions (2.253)–(2.255) into the normal stress balance boundary condition (2.250), the tangential stress balance boundary condition (2.249), and the surfactant transport equation (2.247) leads to the three coupled equations:

$$\frac{1}{\ell}\ddot{a}_\ell + \frac{\hat{\rho}}{\rho}\frac{1}{(\ell+1)}\ddot{a}_\ell = -(\ell-1)(\ell+2)a_\ell + 2\mathrm{e}_s^* g_\ell - \kappa_s^*[4\dot{a}_\ell + 2\ell(\ell+1)b_\ell] \tag{2.256}$$

$$0 = -\mathrm{e}_s^* g_\ell + \kappa_s^*[2\dot{a}_\ell - \ell(\ell+1)b_\ell] + \mu_s^*(\ell-1)(\ell+2)b_\ell \tag{2.257}$$

$$\dot{g}_\ell - \ell(\ell+1)b_\ell + 2\dot{a}_\ell = -\frac{\ell(\ell+1)}{\mathrm{Pe}_s} g_\ell. \tag{2.258}$$

Using equation (2.257) to eliminate $b_\ell(t)$ leaves the two coupled equations:

$$\begin{aligned}
\ddot{a}_\ell[(\ell+1) + \ell\hat{\rho}/\rho] &+ \dot{a}_\ell\left\{\frac{4\kappa_s^*\mu_s^*\ell(\ell-1)(\ell+1)(\ell+2)}{[\kappa_s^*\ell(\ell+1) + \mu_s^*(\ell-1)(\ell+2)]}\right\} \\
&+ a_\ell\left[\ell(\ell-1)(\ell+1)(\ell+2)\right] \\
&= g_\ell\left\{\frac{2\mathrm{e}_s^*\mu_s^*\ell(\ell-1)(\ell+1)(\ell+2)}{[\kappa_s^*\ell(\ell+1) + \mu_s^*(\ell-1)(\ell+2)]}\right\}
\end{aligned} \tag{2.259}$$

$$\begin{aligned}
\dot{g}_\ell &+ g_\ell\left\{\frac{\ell(\ell+1)}{\mathrm{Pe}_s} + \frac{\mathrm{e}_s^*\ell(\ell+1)}{[\kappa_s^*\ell(\ell+1) + \mu_s^*(\ell-1)(\ell+2)]}\right\} \\
&= -\dot{a}_\ell\left\{\frac{2\mu_s^*(\ell-1)(\ell+2)}{[\kappa_s^*\ell(\ell+1) + \mu_s^*(\ell-1)(\ell+2)]}\right\}.
\end{aligned} \tag{2.260}$$

Equations (2.259) and (2.260) describe the leading-order dynamics of the system. They neglect all effects at $\mathcal{O}(\alpha)$.

If the surface shear viscosity μ_s^* is set to zero, the oscillator equation for the amplitude of the shape oscillations (2.259) decouples from the surfactant transport equation and reduces to

$$\ddot{a}_\ell + a_\ell \frac{\ell(\ell-1)(\ell+1)(\ell+2)}{[(\ell+1)+\ell\hat{\rho}/\rho]} = \mathcal{O}(\alpha)\,. \tag{2.261}$$

Thus, even when the surface dilatational viscosity is nonzero, or the surface tension depends on surfactant concentration, the leading-order dynamics for the shape oscillations of the system are, in the absence of surface shear viscosity, the same as those for an inviscid drop/medium system.

If the Gibbs elasticity is zero, equations (2.259) and (2.260) decouple. The oscillator equation (2.259) thus reduces to

$$\begin{aligned} \ddot{a}_\ell[(\ell+1)+\ell\hat{\rho}/\rho] \quad &+ \quad \dot{a}_\ell \left\{ \frac{4\kappa_s^*\mu_s^*\ell(\ell-1)(\ell+1)(\ell+2)}{[\kappa_s^*\ell(\ell+1)+\mu_s^*(\ell-1)(\ell+2)]} \right\} \\ &+ \quad a_\ell\,[\ell(\ell-1)(\ell+1)(\ell+2)] = \mathcal{O}(\alpha) \end{aligned} \tag{2.262}$$

Equation (2.262) is valid for a drop/medium system and generalizes the result (2.238) obtained in Case 3, which neglected the bulk viscosities and Gibbs elasticity for a drop in vacuum.

Chapter 3

Numerics

3.1 Governing equations and boundary conditions

Here the potential flow solutions for moderate-amplitude shape oscillations of a drop in vacuum without gravity are considered. The inviscid drop has an unperturbed equilibrium radius R, a density ρ, and a clean interface with constant surface tension σ_o.

As before, the Reynolds number associated with the shape oscillations is assumed large enough that deviations from inviscid flow are present only in thin boundary layers near the surface. This implies that the fluid motion in the bulk of the drop is well approximated as inviscid. For the moderate deformations considered here, the flow is further assumed to be irrotational. The governing equation is then Laplace's equation for a scalar velocity potential ϕ.

Because of their ability to track the position of the interface, boundary integral methods are particularly well suited to this free-surface problem. There are two common boundary integral formulations for Laplace's equation: the single-layer potential representation and the double-layer potential representation. The latter has been shown [42] to be a more accurate and efficient formulation for the numerical simulation of the shape oscillations of two-dimensional drops. This section discusses the extension of the double-layer potential boundary integral formulation to the case of axisymmetric shape oscillations.

3.1.1 Regularized boundary integral representation

The free-space Green's function for Laplace's equation in three dimensions is

$$G(\mathbf{x}_i, \mathbf{x}) = -\frac{1}{4\pi}\frac{1}{|\mathbf{x}-\mathbf{x}_i|} \quad \text{with} \quad \nabla^2 G(\mathbf{x}_i, \mathbf{x}) = \delta(\mathbf{x}-\mathbf{x}_i)\,. \tag{3.1}$$

$\mathbf{x}$ is the field point position vector and $\mathbf{x}_i$ is the source point position vector.

For a source point $\mathbf{x}_i$ located on the boundary of the domain, the double-layer potential boundary integral representation [35]

$$\int_{S(\mathbf{x})} \hat{\mathbf{n}}(\mathbf{x}) \cdot \boldsymbol{\nabla} G(\mathbf{x}_i, \mathbf{x})\, q(\mathbf{x})\, dS(\mathbf{x}) + \frac{1}{2} q(\mathbf{x}_i) = \phi(\mathbf{x}_i)\,, \tag{3.2}$$

expresses the harmonic scalar velocity potential ϕ in terms of a surface distribution of dipole strengths q oriented parallel to the outward pointing unit normal vector $\hat{\mathbf{n}}$. Specifying the scalar velocity potential ϕ reduces the double-layer representation (3.2) to a Fredholm integral equation of the second kind for the dipole strengths q. The dipole density distribution may be used to find a vector velocity potential through the integral relation [35]

$$\boldsymbol{\psi}(\mathbf{x}_i) = -\int_{S(\mathbf{x})} \hat{\mathbf{n}}(\mathbf{x}) \times \boldsymbol{\nabla} G(\mathbf{x}_i, \mathbf{x})\, q(\mathbf{x})\, dS(\mathbf{x})\,. \tag{3.3}$$

The velocity of the interface can be expressed by the two distinct representations: $\mathbf{v} = \boldsymbol{\nabla}\phi = \boldsymbol{\nabla} \times \boldsymbol{\psi}$.

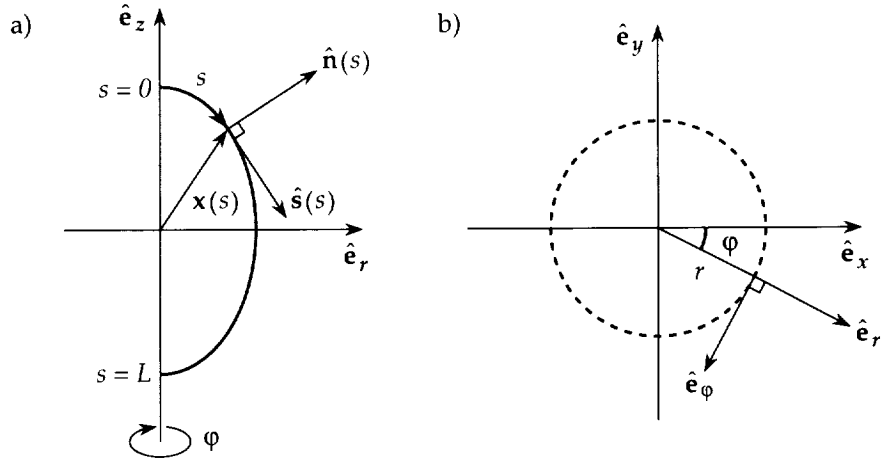

Figure 3.1: a) The local coordinate system in the meridian plane with variable parameterized with arclength s. b) The local coordinate system in a plane perpendicular to the axis of symmetry.

The identities [42]

$$\int_{S(\mathbf{x})} \hat{\mathbf{n}} \cdot \nabla G(\mathbf{x}_i, \mathbf{x})\, dS(\mathbf{x}) = \frac{1}{2} \tag{3.4}$$

$$\int_{S(\mathbf{x})} \hat{\mathbf{n}} \times \nabla G(\mathbf{x}_i, \mathbf{x})\, dS(\mathbf{x}) = \mathbf{0}\,, \tag{3.5}$$

may be used to express the integral representations and relations in their regularized forms

$$\int_{S(\mathbf{x})} \hat{\mathbf{n}}(\mathbf{x}) \cdot \nabla G(\mathbf{x}_i, \mathbf{x})\, [q(\mathbf{x}) - q(\mathbf{x}_i)]\, dS(\mathbf{x}) + q(\mathbf{x}_i) = \phi(\mathbf{x}_i) \tag{3.6}$$

$$\psi(\mathbf{x}_i) = -\int_{S(\mathbf{x})} \hat{\mathbf{n}}(\mathbf{x}) \times \nabla G(\mathbf{x}_i, \mathbf{x})\, [q(\mathbf{x}) - q(\mathbf{x}_i)]\, dS(\mathbf{x})\,. \tag{3.7}$$

The integrands in (3.6) and (3.7) are non-singular everywhere in the integration domain $S(\mathbf{x})$. The regularization of the integral representations and relations, along with the choice of a convenient local coordinate system, to be discussed next, greatly simplifies the numerical problem.

The boundary integral formulation, which reduces the three-dimensional problem to a two-dimensional one, may be further simplified with the assumption of an axisymmetric geometry, which reduces the two-dimensional integrals over the surface to one-dimensional line-integrals over the contour of the domain in a meridian plane. For convenience, a local coordinate system is introduced as illustrated in Figure (3.1). The position vector $\mathbf{x}(s, \varphi) = \hat{\mathbf{e}}_r(\varphi) r(s) + \hat{\mathbf{e}}_z z(s)$ and all other variables are parameterized in terms of arclength s, where $ds^2 = d\mathbf{x} \cdot d\mathbf{x}$ for a fixed meridian angle φ. Note that r represents the distance from the z-axis and not that from the origin. Explicit relations for this local coordinate system are given in Appendix C. For the axisymmetric case, all variables except the unit vectors $\hat{\mathbf{e}}_r$ and $\hat{\mathbf{e}}_\varphi$, are independent of φ. The infinitesimal surface area is $dS = r\, ds d\varphi$ and the φ-dependence may be integrated analytically to give the parameterized forms

$$\int_0^L \hat{\mathbf{n}}(s) \cdot \nabla G(s_i, s)\, r(s)\, [q(s) - q(s_i)]\, ds + q(s_i) = \phi(s_i) \tag{3.8}$$

$$\psi(s_i) = -\int_0^L \hat{\mathbf{e}}_\varphi \cdot [\hat{\mathbf{n}}(s) \times \nabla G(s_i, s)\, r(s)]\, [q(s) - q(s_i)]\, ds\,, \tag{3.9}$$

L is the total arclength between the "poles" of the axisymmetric drop. $\hat{\mathbf{e}}_\varphi$ is evaluated in the meridian plane which contains $\mathbf{x}_i$. The vector velocity potential is $\boldsymbol{\psi} = \hat{\mathbf{e}}_\varphi \psi$. The axisymmetric kernels in (3.8) and (3.9)

can be expressed in terms of the complete elliptic integrals of the first and second kinds. Explicit forms for these weakly singular kernels and their asymptotic behavior as $s \to s_i$ may be found in the Appendix D. Unlike the regularized integrand in (3.8), which is zero at $s = s_i$, analysis of the integrand in (3.9) reveals that as $s \to s_i$

$$\hat{\mathbf{e}}_\varphi \cdot [\hat{\mathbf{n}}(s) \times \boldsymbol{\nabla} G(s_i, s)\, r(s)]\,[q(s) - q(s_i)] \sim \frac{1}{2\pi} \frac{\partial q}{\partial s}(s_i) + \mathcal{O}(s - s_i)\,. \tag{3.10}$$

Since $\mathbf{v} = \boldsymbol{\nabla}\phi = \boldsymbol{\nabla} \times \boldsymbol{\psi}$ the velocity of the interface $\mathbf{v} = \hat{\mathbf{n}}\, v_n + \hat{\mathbf{s}}\, v_s$ has components that may be calculated from derivatives in arclength only

$$v_n(s) = \hat{\mathbf{n}} \cdot (\boldsymbol{\nabla} \times \boldsymbol{\psi}) = \frac{\partial \psi}{\partial s}(s) + \frac{r'(s)}{r(s)} \psi(s) \tag{3.11}$$

$$v_s(s) = \hat{\mathbf{s}} \cdot \boldsymbol{\nabla}\phi = \frac{\partial \phi}{\partial s}(s)\,. \tag{3.12}$$

3.1.2 Boundary conditions

The potential flow solution to the integral representation in (3.8) must satisfy the kinematic and normal stress balance boundary conditions

$$\frac{d\mathbf{x}}{dt} = \hat{\mathbf{n}}\, v_n \tag{3.13}$$

$$p = \sigma_{eq}(\mathcal{C}_s + \mathcal{C}_\varphi)\,. \tag{3.14}$$

Here, $\hat{\mathbf{n}}(s) = -\hat{\mathbf{e}}_r z'(s) + \hat{\mathbf{e}}_z r'(s)$ is the outward pointing unit vector normal to the surface, $p(s)$ is the pressure, and $\mathcal{C}_s(s) = z'(s)r''(s) - r'(s)z''(s)$ and $\mathcal{C}_\varphi(s) = -z'(s)/r(s)$ are the principal radii of the curvature with primes ($'$) denoting differentiation with respect to arclength. The unsteady Bernoulli equation may be used in (3.14) to relate the pressure to ϕ. This gives

$$\left(\frac{D\phi}{Dt}\right)_n = \frac{1}{2}(v_n^2 - v_s^2) - (\mathcal{C}_s + \mathcal{C}_\varphi)\,, \tag{3.15}$$

where the variables have been non-dimensionalized using the inertial scales

$$\text{length} = R \quad \text{mass} = \rho R^3 \quad \text{time} = (\rho R^3/\sigma_{eq})^{1/2}\,. \tag{3.16}$$

The time derivative in (3.15) is with respect to an observer moving with the normal velocity of the interface.

3.2 Numerical procedure

The double-layer potential boundary integral formulation uses equations (3.8), (3.9), (3.11), (3.12), (3.13) and (3.15) to follow the time-evolution of the drop's shape. The equations are discretized by dividing the drop boundary into N equally-spaced nodes, with spacing $\Delta s = L/(N-1)$ in the interval $0 \le s \le L$.

Since the dynamics are driven solely by the curvature variations around the drop, it is important to calculate higher-order arclength derivatives accurately. For this purpose a least-squares spectral transform method [42] is used to represent all the parameterized surface variables. The method approximates each variable by a truncated sine and cosine series that is periodic in twice the total arclength L:

$$f(s) = \frac{a_o}{2} + \sum_{k=1}^{m} a_k \cos\left(\frac{\pi k s}{L}\right) + \sum_{k=1}^{m} b_k \sin\left(\frac{\pi k s}{L}\right) \tag{3.17}$$

$$= \sum_{k=1}^{2m+1} c_k \mathcal{S}_k(s)\,. \tag{3.18}$$

Here $f(s)$ is any variable and $\mathcal{S}_k(s)$ is a sine or cosine shape function with $2m + 1 \equiv N_c$ coefficients c_k. For N discrete nodal values of $f(s_i)$ and assuming $N_c < N$, equation (3.18) represents an over-determined

system of equations for the coefficients. This may be solved in a least-squares sense [42]. The least-squares procedure results in a symmetric and positive-definite $N_c \times N_c$ system of equations for the coefficients c_k. Inverting the coefficient matrix is most efficiently accomplished using a Cholesky decomposition routine [36]. Once the function coefficients are determined, its derivative or integral may be exactly calculated.

Aliasing is a potential problem in the least-squares spectral transform method. It can be avoided by adjusting N_c so that the smallest wavelength represented by the shape functions, $4L/(N_c - 1)$, is larger than four times the largest of the unequally-spaced arclength increments Δs_{max} that appear after each change in the drop's shape. For the simulations shown in this work N_c is chosen to be about half the total number of nodes N in order to accurately resolve the drop shape and eliminate aliasing.

Since the drop is axisymmetric, all the surface variables are either even or odd functions in arclength. For instance, z and ϕ are even functions while r and ψ are odd functions. Higher-order derivatives of these functions are alternately odd or even functions. Neglecting the sine (or cosine) shape functions in (3.17) for even (or odd) variables decreases the size of the $N_c \times N_c$ system of equations for the least-squares spectral coefficients by about a factor of two.

The inverse transform back to the nodal values of the variable involves a matrix multiplication by the discrete shape function matrix $\mathcal{S}_k(s_i)$, as defined in (3.18). To redistribute the nodal values of the variable at equal arclengths the discrete shape function matrix is evaluated at $s_i = (i-1)\Delta s, i = 1, \ldots, N$. Inspection of (3.17) shows that this matrix is independent of the total arclength L, which implies that it need only be calculated once for use in redistributing the variables.

The regularized integral equations are discretized into matrix equations using a trapezoidal quadrature rule. For example, the discrete analog of the integral equation (3.8) takes the form

$$\sum_{j=1}^{N} w_j K(s_i, s_j) q(s_j) = \phi(s_i)\,, \quad \text{for } i = 1, \ldots, N\,, \tag{3.19}$$

with

$$K(s_i, s_j) = \begin{cases} \hat{\mathbf{n}}(s_j) \cdot \boldsymbol{\nabla} G(s_i, s_j)\, r(s_j), & \text{for } j \neq i\,, \\ 1 - \sum_{k=1}^{N} (1 - \delta_{ki}) w_k \hat{\mathbf{n}}(s_k) \cdot \boldsymbol{\nabla} G(s_i, s_k)\, r(s_k)\,, & \text{for } j = i\,. \end{cases} \tag{3.20}$$

Here w_i are the trapezoidal quadrature weights and δ_{ki} is the Kronecker delta symbol. The resulting matrix equation is solved using an LU decomposition routine. The use of regularized integral equations and trapezoidal quadrature weights allows for the complete discretization and solution of the integral equations without the need for explicit interpolations between the nodal values.

The numerical procedure begins by initializing the shape of the drop $\mathbf{x}(s)$ and the scalar velocity potential $\phi(s)$ and calculating arclengths between the possibly unequally-spaced nodes. The arclengths between the nodes are first parameterized with the linear distance between the nodes. This approximation is then improved by: 1) solving for the least-squares spectral coefficients of r and z; 2) calculating their derivatives r' and z' with respect to the parameterization; and 3) integrating the arclength function $[(r')^2 + (z')^2]^{1/2}$ to find the true arclength s at each node.

The curvature, kernel, and tangential velocity at the interface is constructed from the derivative of the position vector and scalar velocity potential with respect to the true arclength. The normal velocity of the interface, however, must be found by solving the matrix equivalents of (3.8) and (3.9) with (3.11). Using the instantaneous velocity and curvature of the interface, the drop shape and scalar velocity potential are updated in time using a Runge-Kutta scheme. To prevent clustering, the nodes are redistributed to equal increments in arclength following each time step.

3.2.1 Base flow: inviscid oscillations

There are several conserved quantities that may be used to measure the accuracy of the numerical calculation. They include the volume, center of mass, and, for inviscid oscillations, the total energy, which is composed of the kinetic and potential energies. The quantities of volume and kinetic energy involve volume integrals, but these may be turned into surface integrals with the Divergence Theorem and the vector identity $\boldsymbol{\nabla} \cdot \mathbf{x} = 3$

in three dimensions. Since $dS = r\,ds d\varphi$, these surface integrals may be turned into line integrals in the axisymmetric coordinate system. Thus, for the calculation of the volume of the drop,

$$V = \frac{1}{3}\int_{V_m} \boldsymbol{\nabla}\cdot\mathbf{x}\,dV = \frac{2\pi}{3}\int_0^L (zr' - rz')r\,ds\,. \tag{3.21}$$

Similarly, for the kinetic energy in the drop, since $v_n = \hat{\mathbf{n}}\cdot(\boldsymbol{\nabla}\times\boldsymbol{\psi}) = \hat{\mathbf{n}}\cdot\boldsymbol{\nabla}\phi$:

$$\text{K.E.} = \int_{V_m}\frac{1}{2}|\mathbf{v}|^2\,dV = \pi\int_0^L \phi v_n r\,ds\,. \tag{3.22}$$

The potential energy is the surface area of the drop

$$\text{P.E.} = \int_{S_m} dS = 2\pi\int_0^L r\,ds\,. \tag{3.23}$$

The initial conditions for the shape of the interface and the scalar velocity potential are taken to be

$$\begin{aligned} |\mathbf{x}(\theta)| &= 1 + \varepsilon P_\ell(\cos\theta) \\ \phi(\theta) &= 0\,. \end{aligned} \tag{3.24}$$

Figure 3.2 shows an example calculation for small-amplitude shape oscillations in the quadrupole mode. Calculations using a fourth-order Runge-Kutta time-stepping scheme did not differ significantly from the calculations using a second-order scheme. The second-order Runge-Kutta scheme was therefore used for all the calculations presented in this thesis. The calculated period of oscillations was found to be 2.22 in excellent agreement with the nondimensional theoretical value of $2\pi/\sqrt{8} \approx 2.221$. The conserved quantities of total energy and volume were found to deviate from their initial values by less than $10^{-7}\%$ and $10^{-8}\%$ respectively.

3.3 Modified boundary conditions

In this section, the base potential flow formulation for the drop in vacuum is modified to incorporate the effects of viscosity and surface rheology. Scaling the governing equations for this problem with the inertial scales, the nondimensional conservation of mass and momentum equations, and the transport equation for an insoluble surfactant take the forms:

$$\boldsymbol{\nabla}\cdot\mathbf{v}^{\text{tot}} = 0\,, \tag{3.25}$$

$$\frac{\partial\mathbf{v}^{\text{tot}}}{\partial t} + \mathbf{v}^{\text{tot}}\cdot\boldsymbol{\nabla}\mathbf{v}^{\text{tot}} = -\boldsymbol{\nabla}p^{\text{tot}} + \alpha^2\nabla^2\mathbf{v}^{\text{tot}}\,, \tag{3.26}$$

$$\frac{\partial\Gamma}{\partial t} + \boldsymbol{\nabla}_s\cdot(\mathbf{v}^{\text{tot}}\Gamma) = \frac{1}{\text{Pe}_s}\nabla_s{}^2\,\Gamma\,. \tag{3.27}$$

Here $\mathbf{v}^{\text{tot}}$ and p^{tot} are temporary notations for the nondimensional velocity and pressure fields. The surfactant transport equation is coupled to the continuity and momentum equations through the boundary conditions and the surface equation of state. Although a nonlinear surface equation of state could be incorporated into the numerical formulation, the linear surface equation of state

$$\sigma(\Gamma) = 1 - \text{e}_s^*(\Gamma - 1) \tag{3.28}$$

is assumed here. This allows for direct comparisons to the corresponding results from the small-amplitude theory. The nondimensional components of the stress balance boundary conditions and the kinematic boundary condition take the respective forms

$$\begin{aligned} p^{\text{tot}} - 2\alpha^2(\hat{\mathbf{n}}\cdot\mathbf{E}^{\text{tot}}\cdot\hat{\mathbf{n}}) &= (\boldsymbol{\nabla}_s\cdot\hat{\mathbf{n}}) - \text{e}_s^*(\boldsymbol{\nabla}_s\cdot\hat{\mathbf{n}})(\Gamma - 1) \\ &\quad + 2\mu_s^*(\boldsymbol{\nabla}_s\cdot\mathbf{E}_s^{\text{tot}})\cdot\hat{\mathbf{n}} + \kappa_s^*(\boldsymbol{\nabla}_s\cdot\hat{\mathbf{n}})(\boldsymbol{\nabla}_s\cdot\mathbf{v}^{\text{tot}}) \end{aligned} \tag{3.29}$$

$$\alpha^2(\hat{\mathbf{n}}\cdot\mathbf{E}^{\text{tot}}\cdot\mathbf{I}_s) = -\text{e}_s^*\boldsymbol{\nabla}_s\Gamma + 2\mu_s^*(\boldsymbol{\nabla}_s\cdot\mathbf{E}_s^{\text{tot}})\cdot\mathbf{I}_s + \kappa_s^*\boldsymbol{\nabla}_s(\boldsymbol{\nabla}_s\cdot\mathbf{v}^{\text{tot}}) \tag{3.30}$$

$$\frac{d\mathbf{x}}{dt} = \hat{\mathbf{n}}\,(\hat{\mathbf{n}}\cdot\mathbf{v}^{\text{tot}})\,. \tag{3.31}$$

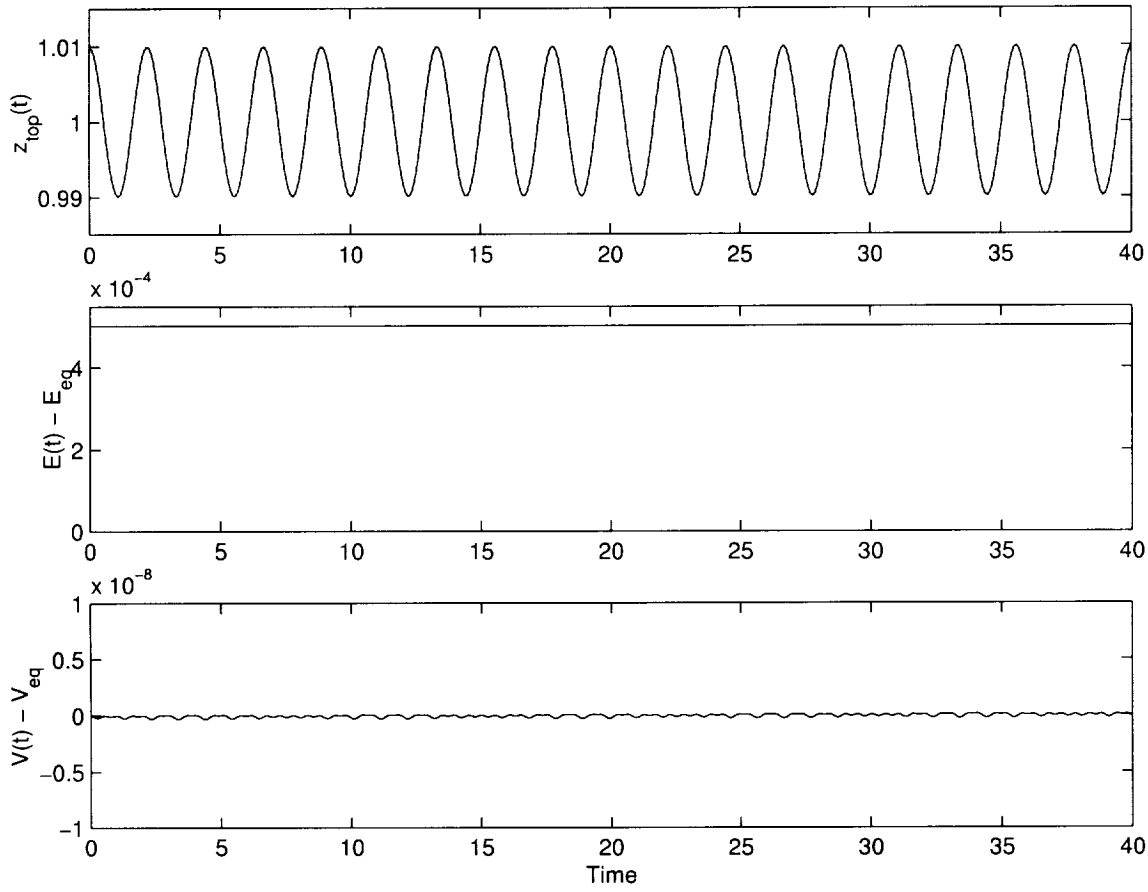

Figure 3.2: Simulations of an initial perturbed inviscid drop in vacuum after the initial conditions $\phi = 0$ and $|\mathbf{x}(\theta)| = R[1 + 0.01P_2(\cos\theta)]$ with $N = 31$, $N_c = 15$, and $\Delta t = 0.001$. The scale factor R in the initial shape ensures that the nondimensional equilibrium volume V_{eq} and the equilibrium energy E_{eq} are $4\pi/3$ and 4π, respectively.

To begin to link the base potential flow formulation of the last section to the equations incorporating viscous and surfactant effects above, the total nondimensional velocity and pressure are separated into two parts

$$\mathbf{v}^{\text{tot}} = \mathbf{v} + \mathbf{V} \tag{3.32}$$

$$p^{\text{tot}} = p + P\,. \tag{3.33}$$

The lower-case letters $(\mathbf{v}, p)$ represent the potential flow velocity and pressure fields while the upper-case letters $(\mathbf{V}, P)$ represent the vortical velocity and pressure fields. The potential flow fields satisfy the irrotational Euler equations

$$\boldsymbol{\nabla}\cdot\mathbf{v} = 0 \tag{3.34}$$

$$\frac{\partial \mathbf{v}}{\partial t} + \mathbf{v}\cdot\boldsymbol{\nabla}\mathbf{v} = -\boldsymbol{\nabla} p\,. \tag{3.35}$$

The vortical velocity and pressure fields satisfy the full Navier-Stokes equations (3.25) and (3.26), after subtracting (3.34) and (3.35):

$$\boldsymbol{\nabla}\cdot\mathbf{V} = 0 \tag{3.36}$$

$$\frac{\partial \mathbf{V}}{\partial t} + \mathbf{v}\cdot\boldsymbol{\nabla}\mathbf{V} + \mathbf{V}\cdot\boldsymbol{\nabla}\mathbf{v} + \mathbf{V}\cdot\boldsymbol{\nabla}\mathbf{V} = -\boldsymbol{\nabla} P + \alpha^2\nabla^2\,\mathbf{v} + \alpha^2\nabla^2\,\mathbf{V}\,. \tag{3.37}$$

Inserting the decomposition (3.32) into the total surfactant transport equation (3.27) yields

$$\frac{\partial \Gamma}{\partial t} + (\mathbf{v}+\mathbf{V})\cdot\boldsymbol{\nabla}_s\Gamma + [\boldsymbol{\nabla}_s\cdot(\mathbf{v}+\mathbf{V})]\Gamma = \frac{1}{\mathrm{Pe}_s}\nabla_s{}^2\,\Gamma\,. \tag{3.38}$$

The boundary conditions (3.29)–(3.31) may also be similarly decomposed, but for clarity this step is postponed for later sections.

The boundary integral representation for the potential flow in the previous section drives this problem. The incorporation of the bulk viscous and surfactant effects comes in by replacing the boundary conditions for potential flow with the total stress balance and kinematic boundary conditions in the boundary integral formulation and keeping only the leading order terms that contribute bulk viscous and surfactant effects. The unknown vortical terms in the boundary conditions are found by satisfying the leading-order equations for the vortical fields.

The vortical fields are assumed to be nonzero only in the thin Stokes boundary layers that form to satisfy the tangential stress balance boundary condition. This leads to considerable simplifications in subsequent sections.

The idea is to use the order of magnitude estimates for the velocity and pressure fields from the small-amplitude theoretical analysis and keep all the terms in the modified boundary conditions (written in local coordinates) up to $\mathcal{O}(\alpha^2)$. These additional terms can be calculated to leading order from the Navier-Stokes equations (3.36) and (3.37). Doing so requires the assumption that the boundary layer fields decay away from the interface.

This section begins by describing a method to include bulk viscosity in what would otherwise be a potential flow calculation for large Reynolds number shape oscillations of a drop in vacuum. The succeeding three cases include increasingly greater effects from the presence of an insoluble surfactant at the interface.

3.3.1 Case 1: "negligible" surfactant effects

This section considers the effects of bulk viscosity on the shape oscillations of a drop in vacuum when the nondimensional surface properties $\mathrm{e}_s^\star$, $\mu_s^\star$, and $\kappa_s^\star$ are "negligible", or $\mathcal{O}(\alpha^3)$. These effects are to be included to leading-order in the numerics by following the procedure just described.

Order-of-magnitude analysis

By using the relations in Appendix B, the nondimensional boundary conditions at the interface may be written in local coordinates as follows

$$p + P - 2\alpha^2\left(\frac{\partial v_n}{\partial n} + \frac{\partial V_n}{\partial n}\right) = \mathcal{C}_s + \mathcal{C}_\varphi\,, \tag{3.39}$$

$$\alpha^2\left[2\left(\frac{\partial v_n}{\partial s}-\mathcal{C}_s v_s\right)+\left(\frac{\partial V_s}{\partial n}+\frac{\partial V_n}{\partial s}-\mathcal{C}_s V_s\right)\right]=0\,, \tag{3.40}$$

$$\frac{dr}{dt} = -\frac{\partial z}{\partial s}(v_n+V_n)\,, \tag{3.41}$$

$$\frac{dz}{dt} = \frac{\partial r}{\partial s}(v_n+V_n)\,. \tag{3.42}$$

Here r and z are the components of the interface shape. In (3.40), the tangential component of the stress balance, the symmetric part of the $\hat{\mathbf{n}}\hat{\mathbf{s}}$ component of the rate of strain tensor corresponding to the potential flow part has been used.

As before, it is convenient to introduce a new notation in the order of magnitude analysis. The small-amplitude analysis in section sec:case1 shows that the potential and vortical flow fields may be written as:

$$\mathbf{v} = \hat{\mathbf{n}}\,(u_{n0}+\alpha^2 u_{n2})+\hat{\mathbf{s}}\,(u_{s0}+\alpha^2 u_{s2})+\mathcal{O}(\alpha^3) \tag{3.43}$$

$$p = p_0+\alpha^2 p_2+\mathcal{O}(\alpha^3) \tag{3.44}$$

$$\mathbf{V} = \hat{\mathbf{n}}\,\alpha^2 U_{n2}+\hat{\mathbf{s}}\,(\alpha U_{s1}+\alpha^2 U_{s2})+\mathcal{O}(\alpha^3) \tag{3.45}$$

$$P = \alpha^2 P_2+\mathcal{O}(\alpha^3)\,. \tag{3.46}$$

As a reminder, the lower case fields $(\mathbf{v}, p)$ represent potential flow and the upper-case fields $(\mathbf{V}, P)$ represent vortical flow. Here the $\mathcal{O}(\alpha^2)$ vortical pressure P_2 has been introduced to account for the nonlinear pressure not appearing in the linear analysis. The potential and vortical fields depend on both n and s. The potential flow fields vary slowly in n and s over a nondimensional length scale of $\mathcal{O}(1)$. The vortical fields, on the other hand, vary rapidly in n, and decay exponentially away from the interface over a nondimensional length scale of $\mathcal{O}(\alpha)$. The normal derivatives of the vortical fields are denoted by a scaled normal coordinate $n \to \alpha N$. For instance, the normal derivative of the $\mathcal{O}(1)$ tangential component of the vortical velocity

$$\frac{\partial U_{s0}}{\partial n}=\frac{1}{\alpha}\frac{\partial U_{s0}}{\partial N}\,, \tag{3.47}$$

where $\partial U_{s0}/\partial N$ is an $\mathcal{O}(1)$ quantity. The order-of-magnitude estimates for the surfactant concentration Γ depend only on s and vary slowly over a nondimensional length scale $\mathcal{O}(1)$. At this stage the only calculable quantities are the $\mathcal{O}(1)$ quantities representing the base potential flow.

Inserting the scales (3.43)–(3.46) into these boundary conditions and expanding yields

$$p_0+\alpha^2\left(p_2+P_2-2\frac{\partial U_{n0}}{\partial N}\right)=\mathcal{C}_s+\mathcal{C}_\varphi+\mathcal{O}(\alpha^3) \tag{3.48}$$

$$\alpha^2\left[2\left(\frac{\partial u_{n0}}{\partial s}-\mathcal{C}_s u_{s0}\right)+\frac{\partial U_{s1}}{\partial N}\right]=0+\mathcal{O}(\alpha^3) \tag{3.49}$$

$$\frac{dr}{dt} = -\frac{\partial z}{\partial s}[u_{n0}+\alpha^2(u_{n2}+U_{n2})]+\mathcal{O}(\alpha^3) \tag{3.50}$$

$$\frac{dz}{dt} = \frac{\partial r}{\partial s}[u_{n0}+\alpha^2(u_{n2}+U_{n2})]+\mathcal{O}(\alpha^3)\,. \tag{3.51}$$

Neglecting the $\mathcal{O}(\alpha^2)$ in these equations reduces them to those for the base potential flow. In order to incorporate the leading order effects of viscosity into the boundary integral formulation, the quantities at $\mathcal{O}(\alpha^2)$ must be determined. Of these, the $\mathcal{O}(\alpha^2)$ corrections to the potential flows, u_{n2} and p_2, may be absorbed into the base flow calculation. Another term which may be treated at this stage is $\partial u_{no}/\partial n$, which may be calculated with the help of $\boldsymbol{\nabla}\cdot\mathbf{v}=0$ written in local coordinates and evaluated at the interface

$$\frac{\partial U_{n0}}{\partial N}+\frac{\partial u_{s0}}{\partial s}+\frac{1}{r}\frac{\partial r}{\partial s}v_{s0}+(\mathcal{C}_s+\mathcal{C}_\varphi)v_{n0}=0\,. \tag{3.52}$$

The three remaining vortical terms, U_{n2}, P_2, and $\partial U_{s1}/\partial N$, must be found from equations (3.36) and (3.37) for the vortical fields $\mathbf{V}$ and P. These fields need only satisfy the leading order equations since their higher order corrections are neglected in the modified boundary conditions above.

From the assumed scaling, the continuity equation can be expanded to $\mathcal{O}(\alpha^2)$

$$\boldsymbol{\nabla}\cdot\mathbf{V} = \alpha\left(\frac{\partial U_{n2}}{\partial N} + \frac{\partial U_{s1}}{\partial s} + \frac{1}{r}\frac{\partial r}{\partial s}U_{s1}\right) = \mathcal{O}(\alpha^2)\,. \tag{3.53}$$

The time derivative of the boundary layer velocity is

$$\frac{\partial \mathbf{V}}{\partial t} = \frac{\partial \hat{\mathbf{s}}}{\partial t}\alpha U_{s1} + \hat{\mathbf{s}}\,\alpha\frac{\partial U_{s1}}{\partial t} + \mathcal{O}(\alpha^2)\,. \tag{3.54}$$

Equation (3.54) involves the time derivative of the unit tangent vector. Since the unit tangent vector is the arclength derivative of the position vector, it can be related to the arclength derivative of the normal velocity through the kinematic boundary condition

$$\frac{\partial \hat{\mathbf{s}}}{\partial t} = \frac{\partial}{\partial t}\left(\frac{\partial \mathbf{x}}{\partial s}\right) = \frac{\partial}{\partial s}\left(\frac{\partial \mathbf{x}}{\partial t}\right) = \frac{\partial}{\partial s}(\hat{\mathbf{n}}\,u_{n0}) + \mathcal{O}(\alpha)\,. \tag{3.55}$$

It follows that

$$\frac{\partial \mathbf{V}}{\partial t} = \hat{\mathbf{n}}\,\alpha\frac{\partial u_{n0}}{\partial s}U_{s1} + \hat{\mathbf{s}}\,\alpha\left(\frac{\partial U_{s1}}{\partial t} + \mathcal{C}_s u_{n0}U_{s1}\right) + \mathcal{O}(\alpha^2)\,. \tag{3.56}$$

The nonlinear terms in (3.37) may be also expanded to give

$$\begin{aligned}\mathbf{v}\cdot\boldsymbol{\nabla}\mathbf{V} &= \hat{\mathbf{n}}\,\alpha\left(u_{n0}\frac{\partial U_{n2}}{\partial N} - \mathcal{C}_s u_{s0}U_{s1}\right)\\ &\quad +\hat{\mathbf{s}}\left[u_{n0}\frac{\partial U_{s1}}{\partial N} + \alpha\left(u_{n0}\frac{\partial U_{s2}}{\partial N} + u_{s0}\frac{\partial U_{s1}}{\partial s}\right)\right] + \mathcal{O}(\alpha^2)\end{aligned} \tag{3.57}$$

$$\begin{aligned}\mathbf{V}\cdot\boldsymbol{\nabla}\mathbf{v} &= \hat{\mathbf{n}}\,\alpha\left(\frac{\partial u_{n0}}{\partial s} - \mathcal{C}_s u_{s0}\right)U_{s1}\\ &\quad +\hat{\mathbf{s}}\,\alpha\left(\frac{\partial u_{s0}}{\partial s} + \mathcal{C}_s u_{n0}\right)U_{s1} + \mathcal{O}(\alpha^2)\end{aligned} \tag{3.58}$$

$$\mathbf{V}\cdot\boldsymbol{\nabla}\mathbf{V} = \mathcal{O}(\alpha^2)\,. \tag{3.59}$$

Similarly, for the pressure and viscous terms

$$\boldsymbol{\nabla}P = \hat{\mathbf{n}}\,\alpha\frac{\partial P_2}{\partial N} + \mathcal{O}(\alpha^2) \tag{3.60}$$

$$\alpha^2\nabla^2\,\mathbf{v} = \mathcal{O}(\alpha^2) \tag{3.61}$$

$$\alpha^2\nabla^2\,\mathbf{V} = \hat{\mathbf{s}}\,\alpha\frac{\partial^2 U_{s1}}{\partial N^2} + \mathcal{O}(\alpha^2)\,. \tag{3.62}$$

Combining (3.54)—(3.62) in the Navier-Stokes equations gives, to leading order:

$$\alpha\left(\frac{\partial U_{n2}}{\partial N} + \frac{\partial U_{s1}}{\partial s} + \frac{1}{r}\frac{\partial r}{\partial s}U_{s1}\right) = 0 + \mathcal{O}(\alpha^2) \tag{3.63}$$

and

$$\alpha u_{n0}\frac{\partial U_{s1}}{\partial s} - \alpha\left[2\left(\frac{\partial u_{n0}}{\partial s} - \mathcal{C}_s u_{s0}\right) - \frac{1}{r}\frac{\partial r}{\partial s}u_{n0}\right]U_{s1} = \alpha\frac{\partial P_2}{\partial N} + \mathcal{O}(\alpha^2) \tag{3.64}$$

$$\alpha\frac{\partial U_{s1}}{\partial t} + u_{n0}\frac{\partial U_{s1}}{\partial N} + \alpha u_{n0}\frac{\partial U_{s2}}{\partial N} + \alpha u_{s0}\frac{\partial U_{s1}}{\partial s} + \alpha\left(\frac{\partial u_{s0}}{\partial s} + 2\mathcal{C}_s u_{n0}\right)U_{s1} = \alpha\frac{\partial^2 U_{s1}}{\partial N^2} + \mathcal{O}(\alpha^2)\,. \tag{3.65}$$

The continuity equation (3.53) may be identically satisfied by defining the vortical part of the boundary layer velocity as the curl of a vector velocity potential $\mathbf{\Psi} = \hat{\mathbf{e}}_\varphi \Psi$. In general $\mathbf{V}$ takes the form

$$\mathbf{V} = \boldsymbol{\nabla} \times \mathbf{\Psi} \tag{3.66}$$

$$= \hat{\mathbf{n}} \left(h_s \frac{\partial \Psi}{\partial s} + \frac{h_s}{h_\varphi} \frac{dh_\varphi}{ds} \Psi \right) + \hat{\mathbf{s}} \left(-h_n \frac{\partial \Psi}{\partial n} - \frac{h_n}{h_\varphi} \frac{\partial h_\varphi}{\partial n} \Psi \right) . \tag{3.67}$$

Here, h_n, h_s, and h_φ are the metrical coefficients for the local coordinate system. To obtain order of magnitude estimates, the vector velocity potential is written $\Psi = \alpha^2 \Psi_2 + \mathcal{O}(\alpha^3)$, with Ψ_2 assumed to have large normal gradients. The velocity magnitudes may be thus restated in terms of Ψ_2 so that

$$U_{n2} = h_s \frac{\partial \Psi_2}{\partial s} - \frac{h_s}{h_\varphi} \frac{\partial h_\varphi}{\partial s} \Psi_2 \tag{3.68}$$

$$U_{s1} = -h_n \frac{\partial \Psi_2}{\partial N} \tag{3.69}$$

$$U_{s2} = \frac{h_n}{h_\varphi} \frac{\partial h_\varphi}{\partial n} \Psi_2 . \tag{3.70}$$

With the continuity equation identically satisfied, these expressions may be substituted into equations (3.63)—(3.65) for the vortical fields. Notice that with these substitutions every term in the equations contains the vector velocity potential, which decays exponentially away from the interface with a decay factor $1/\alpha$, and at least one normal derivative. These observations, and the knowledge that all the other quantities in the equations vary slowly over the thin Stokes boundary, allow for the simplification of the equations through an integration in the normal direction. In a sample term containing an explicit normal derivative, this process proceeds by first expanding the slowly varying terms about their values at the interface,

$$\alpha u_{n0} \frac{\partial U_{s1}}{\partial N} = \alpha \, u_{n0}|_{n=0} \frac{\partial U_{s1}}{\partial N} + \mathcal{O}(\alpha^2) \tag{3.71}$$

and, by integrating over a nondimensional boundary layer thickness α, where the nondimensional variable n is rescaled with α, inside the drop

$$\begin{aligned} \int_{-\infty}^{0} \alpha u_{n0} \frac{\partial U_{s1}}{\partial N} \alpha dN &= \alpha^2 \, u_{n0}|_{n=0} \int_{-\infty}^{0} \frac{\partial U_{s1}}{\partial N} dN + \mathcal{O}(\alpha^3) \\ &= \alpha^2 \, u_{n0}|_{n=0} \left(U_{s1}|_{n=0} - U_{s1}|_{n=-\infty} \right) + \mathcal{O}(\alpha^3) \\ &= -\alpha^2 \left(u_{n0} \frac{\partial \Psi_2}{\partial N} \right) \Big|_{n=0} + \mathcal{O}(\alpha^3) \end{aligned} \tag{3.72}$$

where the last expression on the right-hand side has been evaluated at the interface $n = 0$, where the metric coefficients are known.

Other terms, may be similarly approximated:

$$\begin{aligned} \alpha \frac{\partial u_{s0}}{\partial s} U_{s1} &= -\alpha \frac{\partial u_{s0}}{\partial s} h_n \frac{\partial \Psi_2}{\partial N} \\ &= -\alpha \left. \frac{\partial u_{s0}}{\partial s} \right|_{n=0} \left(h_n \frac{\partial \Psi_2}{\partial N} \right) + \mathcal{O}(\alpha^2) \\ &= -\alpha \left. \frac{\partial u_{s0}}{\partial s} \right|_{n=0} \left[\frac{\partial}{\partial N} (h_n \Psi_2) - \alpha \frac{\partial h_n}{\partial n} \Psi_2 \right] + \mathcal{O}(\alpha^2) . \end{aligned} \tag{3.73}$$

The second term in the square brackets may be neglected. This expression may now be integrated over the nondimensional boundary layer thickness to provide

$$\begin{aligned} \int_{-\infty}^{0} \alpha \frac{\partial u_{s0}}{\partial s} U_{s1} \, \alpha dN &= -\alpha^2 \left. \frac{\partial u_{s0}}{\partial s} \right|_{n=0} \int_{-\infty}^{0} \frac{\partial}{\partial N} (h_n \Psi_2) \, dn + \mathcal{O}(\alpha^3) \\ &= -\alpha^2 \left. \frac{\partial u_{s0}}{\partial s} \right|_{n=0} \left[(h_n \Psi_2)|_{n=0} - (h_n \Psi_2)|_{n=-1} \right] + \mathcal{O}(\alpha^3) \\ &= -\alpha^2 \left(\frac{\partial u_{s0}}{\partial s} \Psi_2 \right) \Big|_{n=0} + \mathcal{O}(\alpha^3) \end{aligned} \tag{3.74}$$

Proceeding similarly for each of the terms in the vortical equations leads to,

$$\alpha^2 P_2 = -\alpha^2 u_{n0}\frac{\partial \Psi_2}{\partial s} + \alpha^2\left[2\left(\frac{\partial u_{n0}}{\partial s} - \mathcal{C}_s u_{s0}\right) - \frac{1}{r}\frac{\partial r}{\partial s}u_{n0}\right]\Psi_2 + \mathcal{O}(\alpha^3) \tag{3.75}$$

$$\begin{aligned}\alpha^2\frac{\partial \Psi_2}{\partial t} + \alpha u_{n0}\frac{\partial \Psi_2}{\partial N} &= -\alpha^2 u_{s0}\frac{\partial \Psi_2}{\partial s} - \alpha^2\left[\frac{\partial u_{s0}}{\partial s} + (2\mathcal{C}_s u_{n0} - \mathcal{C}_\varphi)u_{n0}\right]\Psi_2 \\ &\quad + \alpha^2\frac{\partial^2 \Psi_2}{\partial N^2} + \mathcal{O}(\alpha^3)\,. \end{aligned} \tag{3.76}$$

All the terms up to $\mathcal{O}(\alpha^2)$ are retained and evaluated at the interface. The remaining normal derivatives in these equations can be evaluated as follows. The normal derivative on the left side of (3.76) can be absorbed into the time-derivative of the vector velocity potential with respect to an observer moving at the velocity u_{n0}. The normal derivatives on the right sides of the (3.76) may be found from the tangential stress balance boundary condition.

Modified equations and boundary conditions

Dropping the order of magnitude estimates and reverting to the original notation in terms of $\mathbf{v}$, $\mathbf{V}$, and Ψ yields the following modified boundary conditions for the base potential flow

$$\left(\frac{D\phi}{Dt}\right)_n = \frac{1}{2}(v_n^2 - v_s^2) - (\mathcal{C}_s + \mathcal{C}_\varphi) - 2\alpha^2\frac{\partial v_n}{\partial n} + v_n V_n + P \tag{3.77}$$

$$\left(\frac{D\Psi}{Dt}\right)_n = -v_s\frac{\partial \Psi}{\partial s} - \left[\frac{\partial v_s}{\partial s} + (2\mathcal{C}_s + \mathcal{C}_\varphi)v_n\right]\Psi + \alpha^2\frac{\partial^2 \Psi}{\partial n^2} \tag{3.78}$$

$$\frac{dr}{dt} = -\frac{\partial z}{\partial s}(v_n + V_n) \tag{3.79}$$

$$\frac{dz}{dt} = \frac{\partial r}{\partial s}(v_n + V_n) \tag{3.80}$$

where

$$\alpha^2\frac{\partial v_n}{\partial n} = -\alpha^2\left[\frac{\partial v_s}{\partial s} + \frac{1}{r}\frac{\partial r}{\partial s}v_s + (\mathcal{C}_s + \mathcal{C}_\varphi)v_n\right] \tag{3.81}$$

$$V_n = \frac{\partial \Psi}{\partial s} + \frac{1}{r}\frac{\partial r}{\partial s}\Psi \tag{3.82}$$

$$P = -v_n\frac{\partial \Psi}{\partial s} + \left[2\left(\frac{\partial v_n}{\partial s} - \mathcal{C}_s v_s\right) - \frac{1}{r}\frac{\partial r}{\partial s}v_n\right]\Psi \tag{3.83}$$

$$\alpha^2\frac{\partial^2 \Psi}{\partial n^2} = -2\alpha^2\left(\frac{\partial v_n}{\partial s} - \mathcal{C}_s v_s\right) \tag{3.84}$$

These equations are evaluated at the interface and retain all the leading order viscous terms at $\mathcal{O}(\alpha^2)$, but neglect the higher order contributions. Note that in (3.77), Bernoulli's equation has been used to relate the pressure to the time derivative of the scalar velocity potential and a $V_n(\partial\phi/\partial n) = v_n V_n$, which is an $\mathcal{O}(\alpha^2)$ term, has been added to both sides to ensure that the time derivative is consistent with the kinematic boundary condition. A similar term $V_n(\partial\Psi/\partial n)$ has not been added to (3.78) because it is an $\mathcal{O}(\alpha^3)$ term and may be neglected in the above equations.

The numerical procedure begins by initializing the $r(s)$, $z(s)$, $\phi(s)$, and $\Psi(s)$. After calculating the arclengths, the kernels of the boundary integral formulation are formed and used to calculate the base potential flow velocity components. The potential flow velocity components are used to evaluate the right-hand sides of the evolution equations for r, z, ϕ, and Ψ, which are updated with the Rung-Kutta time stepping scheme.

Figure 3.3 shows an example calculation for small-amplitude quadrupole shape oscillations of a weakly viscous drop. The additional evolution equation and modified boundary conditions were seen to produce an

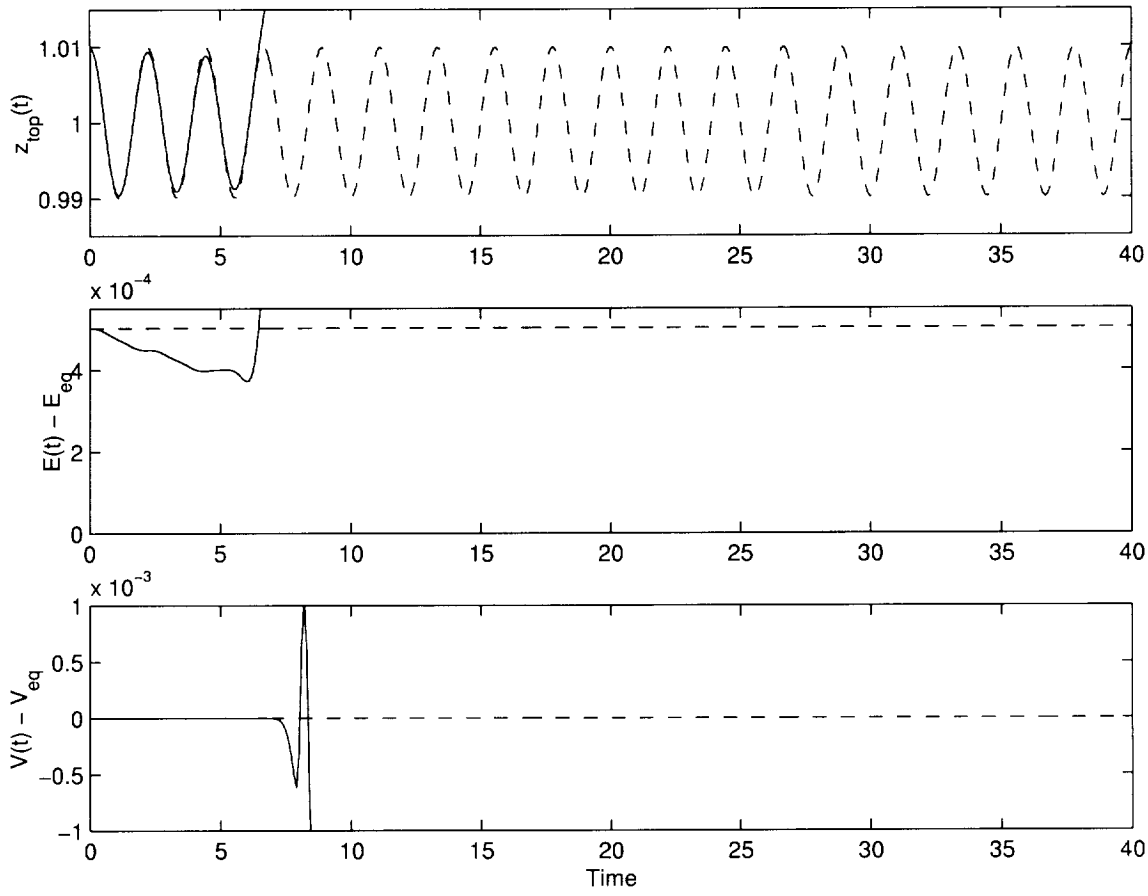

Figure 3.3: Simulations of an weakly viscous drop in vacuum for $\alpha^2 = 0$ (dashed line) and $\alpha^2 = 0.005$ (solid line) after the initial conditions $\phi = 0$ and $|\mathbf{x}(\theta)| = R[1 + 0.01P_2(\cos\theta)]$ with $N = 31$, $N_c = 15$, and $\Delta t = 0.001$. The scale factor R in the initial shape ensures that the nondimensional equilibrium volume V_{eq} and the equilibrium energy E_{eq} are $4\pi/3$ and 4π, respectively.

instability in the simulations. The instability was traced to the variable Ψ, which tended to develop small wavelength disturbances that grew in time. Since Ψ and its first derivatives in arclength are used to calculate V_n, these high wavenumber oscillations eventually contaminated all the variables and the calculations had to be stopped. The calculations were found to be stable in time if the V_n were eliminated from the evolution equations for the shape. The damping constant, which results from the potential flow term $-2\alpha^2\partial v_n/\partial n$, did not correspond to that predicted from theory and, interestingly, was off by a factor of 2 for all axisymmetric mode numbers. The instability arising in the vortical velocity potential Ψ has been well documented in previous work (see, for example [26]). The customary method of correction introduces a "smoothing" parameter D into the problem, where the nodal values of Ψ were replaced with

$$\Psi_i = \Psi_i - D(\Psi_{i-2} - 4\Psi_{i-1} + 6\Psi_i - 4\Psi_{i-1} + \Psi_{i+2}) \tag{3.85}$$

after each time step. This process amounts to placing the negative of a fourth-order derivative with respect to arclength on the right-hand side of the evolution equation for Ψ and acts to smooth out the short wavelength disturbances appearing in the variable.

Preliminary results proved that, with an appropriate choice of the parameter D, the process of smoothing eliminated the instabilities. It was noticed, however, that with a slightly different smoothing algorithm

$$\Psi_i = \Psi_i + D(\Psi_{i-2} + 16\Psi_{i-1} - 30\Psi_i + 16\Psi_{i-1} - \Psi_{i+2})\,, \tag{3.86}$$

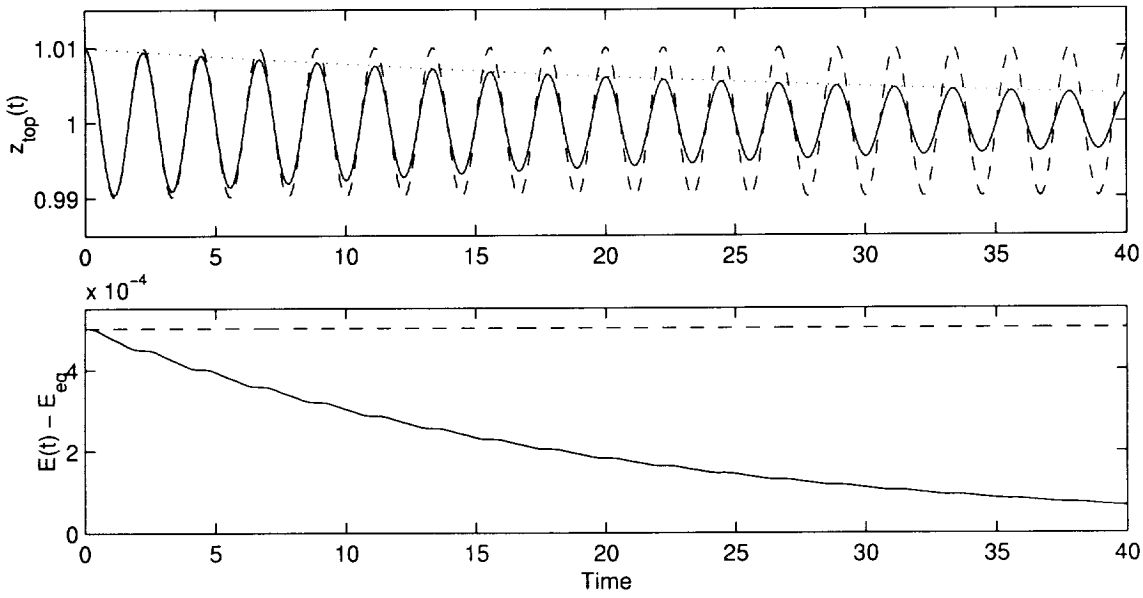

Figure 3.4: Simulations of a weakly viscous drop in vacuum for $\alpha^2 = 0$ (dashed line) and $\alpha^2 = 0.005$ (solid line) after the initial conditions $\phi = 0$ and $|\mathbf{x}(\theta)| = R[1 + 0.01P_2(\cos\theta)]$ with $N = 31$, $N_c = 15$, and $\Delta t = 0.001$. The scale factor R in the initial shape ensures that the nondimensional equilibrium energy E_{eq} is 4π. Also shown is the theoretical prediction for the damped shape in this limit $z_{\rm top}(t) = 1 + [z_{\rm top}(t = 0) - 1]e^{-5\alpha^2 t}$ (dotted line).

the size of the smoothing parameter D could be decreased by two orders of magnitude. This different algorithm amounts to placing a second-order derivative with respect to arclength on the right-hand side of the evolution equation for Ψ. If the smoothing parameter was set too large, the damping constant was less than the theoretical value. A smoothing parameter of $D = 10^{-4}$ was used to produce the weakly viscous simulations in Figure 3.4. With smoothing, the damping rate for the shape oscillations was in good agreement with the theory. As in the base potential flow calculation, the volume was found to deviate by less than $10^{-8}\%$ from its initial value.

3.3.2 Case 2: "small" surfactant effects

This section considers the effects of bulk and surface viscosity and surfactant transport on the shape oscillations of a drop in vacuum when the nondimensional surface properties e_s^*, μ_s^*, and κ_s^* are "small", or $\mathcal{O}(\alpha^2)$. These effects are to be included to leading-order in the numerics by expanding the total decomposition of the boundary conditions in local coordinates to $\mathcal{O}(\alpha^2)$, using the order-of-magnitude estimates from the corresponding section in the theory, and neglecting those terms appearing at $\mathcal{O}(\alpha^3)$ and higher.

Order-of-magnitude analysis

With the velocity and pressure decomposed into potential and vortical fields, the nondimensional forms for the normal stress balance, tangential stress balance, and kinematic boundary conditions in local coordinate are, respectively,

$$p + P - 2\alpha^2\left(\frac{\partial v_n}{\partial n} + \frac{\partial V_n}{\partial n}\right) = (\mathcal{C}_s + \mathcal{C}_\varphi) - \mathrm{e}_s^*(\mathcal{C}_s + \mathcal{C}_\varphi)(\Gamma - 1)$$
$$+\mu_s^*(\mathcal{C}_s - \mathcal{C}_\varphi)(m^- + M^-) + \kappa_s^*(\mathcal{C}_s + \mathcal{C}_\varphi)(m^+ + M^+)\,, \tag{3.87}$$

$$\alpha^2\left[2\left(\frac{\partial v_n}{\partial s}-\mathcal{C}_s v_s\right)+\left(\frac{\partial V_s}{\partial n}+\frac{\partial V_n}{\partial s}-\mathcal{C}_s V_s\right)\right]=-\mathrm{e}_s^*\frac{\partial \Gamma}{\partial s}$$
$$+\mu_s^*\left[\frac{\partial}{\partial s}(m^-+M^-)+\frac{2}{r}\frac{\partial r}{\partial s}(m^-+M^-)\right]+\kappa_s^*\frac{\partial}{\partial s}(m^++M^+)\,, \tag{3.88}$$

and

$$\frac{dr}{dt} = -\frac{\partial z}{\partial s}(v_n+V_n) \tag{3.89}$$
$$\frac{dz}{dt} = \frac{\partial r}{\partial s}(v_n+V_n)\,, \tag{3.90}$$

where

$$m^\pm = \left(\frac{\partial v_s}{\partial s}\pm\frac{1}{r}\frac{\partial r}{\partial s}v_s+(\mathcal{C}_s\pm\mathcal{C}_\varphi)v_n\right)\Big|_{n=0} \tag{3.91}$$
$$M^\pm = \left(\frac{\partial V_s}{\partial s}\pm\frac{1}{r}\frac{\partial r}{\partial s}V_s+(\mathcal{C}_s\pm\mathcal{C}_\varphi)V_n\right)\Big|_{n=0}\,. \tag{3.92}$$

The order-of-magnitude estimates for the potential and vortical flow fields and the surfactant concentration from the corresponding section in the theory yield expansions of the form

$$\mathbf{v} = \hat{\mathbf{n}}\,(u_{n0}+\alpha^2 u_{n2})+\hat{\mathbf{s}}\,(u_{s0}+\alpha^2 u_{s2})+\mathcal{O}(\alpha^3) \tag{3.93}$$
$$p = p_0+\alpha^2 p_2+\mathcal{O}(\alpha^3) \tag{3.94}$$
$$\mathbf{V} = \hat{\mathbf{n}}\,\alpha^2 U_{n2}+\hat{\mathbf{s}}\,(\alpha U_{s1}+\alpha^2 U_{s2})+\mathcal{O}(\alpha^3) \tag{3.95}$$
$$P = \alpha^2 P_2+\mathcal{O}(\alpha^3) \tag{3.96}$$
$$\Gamma = 1+\Gamma_0+\alpha\Gamma_1+\alpha^2\Gamma_2+\mathcal{O}(\alpha^3)\,, \tag{3.97}$$

where, as before, the lower case fields $(\mathbf{v},p)$ refer to those resembling potential flow and the upper-case fields $(\mathbf{V},P)$ refer to those resembling vortical flow. Here the $\mathcal{O}(\alpha)$ vortical pressure P_1 has been introduced to account for the nonlinear pressure not appearing in the linear analysis. The potential and vortical fields depend on both n and s, but unlike the potential flow fields, which vary slowly in n and s over a nondimensional length scale of $\mathcal{O}(1)$, the vortical fields vary rapidly in n, decaying exponentially away from the interface over a nondimensional length scale of $\mathcal{O}(\alpha)$ and slowly in s. The normal derivatives of the vortical fields are denoted by a scaled normal coordinate $n\to\alpha N$. For instance, the normal derivative of the $\mathcal{O}(1)$ tangential component of the vortical velocity

$$\frac{\partial U_{s0}}{\partial n}=\frac{1}{\alpha}\frac{\partial U_{s0}}{\partial N}\,, \tag{3.98}$$

where $\partial U_{s0}/\partial N$ is an $\mathcal{O}(1)$ quantity. The order-of-magnitude estimates for the surfactant concentration Γ depend only on s and vary slowly over a nondimensional length scale $\mathcal{O}(1)$.

Substituting the order-of-magnitude scales (3.93)–(3.97) into the boundary conditions (3.93)–(3.97) and expanding to $\mathcal{O}(\alpha^2)$, noting that a normal derivative of a vortical field introduces a factor of $1/\alpha$, yields

$$p_0+\alpha^2\left(p_2+P_2-2\frac{\partial u_{n0}}{\partial n}\right)=(\mathcal{C}_s+\mathcal{C}_\varphi)-\mathrm{e}_s^*(\mathcal{C}_s+\mathcal{C}_\varphi)(\Gamma_0-1)$$
$$+\mu_s^*(\mathcal{C}_s-\mathcal{C}_\varphi)m_0^-+\kappa_s^*(\mathcal{C}_s+\mathcal{C}_\varphi)m_0^++\mathcal{O}(\alpha^3)\,, \tag{3.99}$$

$$\alpha^2\left[2\left(\frac{\partial u_{n0}}{\partial s}-\mathcal{C}_s u_{s0}\right)+\frac{\partial U_{s1}}{\partial N}\right]=-\mathrm{e}_s^*\frac{d\Gamma_0}{ds}$$
$$+\mu_s^*\left(\frac{\partial m_0^-}{\partial s}+\frac{2}{r}\frac{\partial r}{\partial s}m_0^-\right)+\kappa_s^*\frac{\partial m_0^+}{\partial s}+\mathcal{O}(\alpha^3)\,, \tag{3.100}$$

and

$$\frac{dr}{dt} = -\frac{\partial z}{\partial s}[u_{n0} + \alpha^2(u_{n2} + U_{n2})] + \mathcal{O}(\alpha^3) \tag{3.101}$$

$$\frac{dz}{dt} = \frac{\partial r}{\partial s}[u_{n0} + \alpha^2(u_{n2} + U_{n2})] + \mathcal{O}(\alpha^3)\,, \tag{3.102}$$

where

$$m_0^{\pm} = \left[\frac{\partial u_{s0}}{\partial s} \pm \frac{1}{r}\frac{\partial r}{\partial s}u_{s0} + (\mathcal{C}_s \pm \mathcal{C}_\varphi)u_{n0}\right]\Bigg|_{n=0}\,. \tag{3.103}$$

If the $\mathcal{O}(\alpha^2)$ terms are neglected in these equations, they simplify to those for the base potential flow, provided the unsteady Bernoulli equation is used to relate the pressure to the $\mathcal{O}(1)$ scalar velocity potential. In order to incorporate the leading-order effects of bulk and surface viscosity and surfactant transport into the boundary integral formulation, the quantities at $\mathcal{O}(\alpha^2)$ must be determined. Of these, u_{n2} and p_2 may again be absorbed into the base flow calculation and $\partial u_{no}/\partial n$ calculated from Laplace's equation written in local coordinates and evaluated at the interface. Note that apart from the e_s^* terms all the quantities associated with the surface properties are known from the potential flow and may be readily evaluated.

The unknown quantities still to be determined include the P_2, $\partial U_{s1}/\partial N$, and the two e_s^* terms. Of these P_2 and $\partial U_{s1}/\partial N$ may be found by introducing a vector velocity potential for the vortical velocity and applying an order-of-magnitude analysis to the equations for the vortical fields to determine an evolution equation for the vector velocity potential and an expression for the vortical pressure in terms of this vector velocity potential both evaluated at the interface, as in the previous section.

For the surfactant concentration, an evolution equation may be found from an order of magnitude analysis of the decomposed surfactant transport equation. Inserting the scales into this equation gives, to leading-order,

$$\frac{\partial \Gamma}{\partial t} = \frac{\partial \Gamma_0}{\partial t} + \mathcal{O}(\alpha) \tag{3.104}$$

$$(\mathbf{v} + \mathbf{V}) \cdot \boldsymbol{\nabla}_s \Gamma = u_{s0}\frac{\partial \Gamma_0}{\partial s} + \mathcal{O}(\alpha) \tag{3.105}$$

$$[\boldsymbol{\nabla}_s \cdot (\mathbf{v} + \mathbf{V})]\,\Gamma = m_0^+(1 + \Gamma_0) + \mathcal{O}(\alpha) \tag{3.106}$$

$$\nabla_s{}^2\,\Gamma = \frac{\partial^2 \Gamma_0}{\partial s^2} + \mathcal{O}(\alpha)\,, \tag{3.107}$$

or combining terms and rearranging,

$$\frac{\partial \Gamma_0}{\partial t} = -u_{s0}\frac{\partial \Gamma_0}{\partial s} - m_0^+(1 + \Gamma_0) + \frac{1}{\mathrm{Pe}_s}\frac{\partial^2 \Gamma_0}{\partial s^2} + \mathcal{O}(\alpha) \tag{3.108}$$

Here the time derivative may be rewritten as

$$\frac{\partial \Gamma_0}{\partial t} = \left(\frac{D\Gamma_0}{Dt}\right)_n \tag{3.109}$$

since the insoluble surfactant monolayer has no gradients in the normal direction.

Modified equations and boundary conditions

Dropping the order of magnitude estimates and reverting to the original notation in terms of $\mathbf{v}$, $\mathbf{V}$, Ψ, and Γ yields the following modified boundary conditions for the base potential flow

$$\left(\frac{D\phi}{Dt}\right)_n = \frac{1}{2}(v_n^2 - v_s^2) - (\mathcal{C}_s + \mathcal{C}_\varphi) - 2\alpha^2\frac{\partial v_n}{\partial n} + v_n V_n + P$$
$$-\mu_s^*(\mathcal{C}_s - \mathcal{C}_\varphi)m^- - \kappa_s^*(\mathcal{C}_s + \mathcal{C}_\varphi)m^+ + \mathrm{e}_s^*(\mathcal{C}_s + \mathcal{C}_\varphi)(\Gamma - 1) \tag{3.110}$$

$$\left(\frac{D\Psi}{Dt}\right)_n = -v_s\frac{\partial \Psi}{\partial s} - \left[\frac{\partial v_s}{\partial s} + (2\mathcal{C}_s + \mathcal{C}_\varphi)v_n\right]\Psi + \alpha^2\frac{\partial^2 \Psi}{\partial n^2} \tag{3.111}$$

$$\left(\frac{D\Gamma}{Dt}\right)_n = \frac{1}{\mathrm{Pe}_s}\frac{\partial^2\Gamma}{\partial s^2} - v_s\frac{\partial\Gamma}{\partial s} - m^+\Gamma \tag{3.112}$$

$$\frac{dr}{dt} = -\frac{\partial z}{\partial s}(v_n + V_n) \tag{3.113}$$

$$\frac{dz}{dt} = \frac{\partial r}{\partial s}(v_n + V_n)\,, \tag{3.114}$$

where

$$\alpha^2\frac{\partial v_n}{\partial n} = -\alpha^2 m^+ \tag{3.115}$$

$$V_n = \frac{\partial\Psi}{\partial s} + \frac{1}{r}\frac{\partial r}{\partial s}\Psi \tag{3.116}$$

$$P = -v_n\frac{\partial\Psi}{\partial s} + \left[2\left(\frac{\partial v_n}{\partial s} - \mathcal{C}_s v_s\right) - \frac{1}{r}\frac{\partial r}{\partial s}v_n\right]\Psi \tag{3.117}$$

$$\begin{aligned}\alpha^2\frac{\partial^2\Psi}{\partial n^2} &= -2\alpha^2\left(\frac{\partial v_n}{\partial s} - \mathcal{C}_s v_s\right) - \mathrm{e}_s^*\frac{\partial\Gamma}{\partial s} \\ &\quad +\mu_s^*\left[\frac{\partial m^-}{\partial s} + \frac{2}{r}\frac{\partial r}{\partial s}m^-\right] + \kappa_s^*\frac{\partial m^+}{\partial s}\end{aligned} \tag{3.118}$$

$$m^\pm = \frac{\partial v_s}{\partial s} \pm \frac{1}{r}\frac{\partial r}{\partial s}v_s + (\mathcal{C}_s \pm \mathcal{C}_\varphi)v_n\,. \tag{3.119}$$

These equations are evaluated at the interface and retain all the leading-order bulk and surface viscous and surfactant transport terms at $\mathcal{O}(\alpha^2)$.

The numerical procedure begins by initializing the $r(s)$, $z(s)$, $\phi(s)$, $\Psi(s)$, and $\Gamma(s)$. After calculating the arclengths, the kernels of the boundary integral formulation are formed and used to calculate the base potential flow velocity components. The potential flow velocity components are used to evaluate the right-hand sides of the evolution equations for r, z, ϕ, Ψ, and Γ, which are updated with the Rung-Kutta time stepping scheme.

The simulations including weak bulk viscous and surfactant effects were even more susceptible to the kind of instabilities in the variable Ψ seen in the previous case including weak bulk viscous effects. No value of the smoothing parameter could be found for stable and physically realistic simulations including the surface viscosities and Gibbs elasticity that were of the same order as the inverse of the Reynolds number. For instance, with the Gibbs elasticity set to zero and both the surface viscosities nonzero, the smoothing parameter had to be set so large that the resulting oscillations damped out at a rate smaller than the case without surface viscosities.

There were two limits in which stable and physically realistic simulations could be obtained. These limits set the Gibbs elasticity and one of the surface viscosities to zero. In both example calculations the smoothing parameter was increased to $D = 7.5 \times 10^{-4}$. Figure 3.5 shows the case when the surface shear viscosity is set to zero, but the surface dilatational viscosity is the same order as the inverse of the Reynolds number. The damping constant for small oscillations was found to agree with the theory in that limit. Figure 3.6 shows the case when the surface dilatational viscosity is set to zero, but the surface shear viscosity is the same order as the inverse of the Reynolds number. The damping constant for small oscillations was found to agree with the theory in this limit. For the quadrupole mode, the shear viscosity was seen to have a much larger effect on the damping of the shape oscillations.

3.3.3 Case 3: "medium" surfactant effects

This section considers the effects of bulk and surface viscosity and surfactant transport on the shape oscillations of a drop in vacuum when the nondimensional surface properties e_s^*, μ_s^*, and κ_s^* are "medium", or $\mathcal{O}(\alpha)$. These effects are to be included to leading-order in the numerics by expanding the total decomposition of the boundary conditions in local coordinates to $\mathcal{O}(\alpha)$, using the order-of-magnitude estimates from the corresponding section in the theory, and neglecting those terms appearing at $\mathcal{O}(\alpha^2)$ and higher.

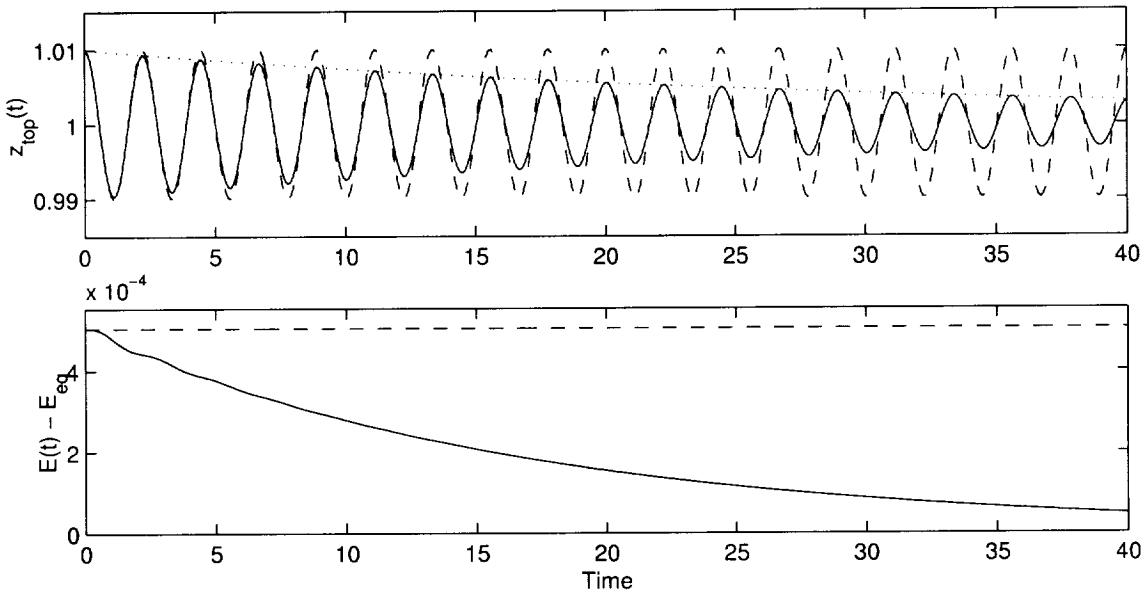

Figure 3.5: Simulations of an initially perturbed weakly viscous drop in vacuum with small surfactant effects for $(\alpha^2, e_s^*, \mu_s^*, \kappa_s^*) = 0$ (dashed line) and $(\alpha^2, \kappa_s^*) = 0.005$ with $(e_s^*, \kappa_s^*, \mu_s^*) = 0$ (solid line). The initial conditions are $(\phi, \Psi) = 0$ and $|\mathbf{x}(\theta)| = R[1 + 0.01P_2(\cos\theta)]$ with $N = 31$, $N_c = 15$, and $\Delta t = 0.001$. The scale factor R in the initial shape ensures that the nondimensional equilibrium energy E_{eq} is 4π. Also shown is the theoretical prediction for the damped shape in this limit $z_{\rm top}(t) = 1 + [z_{\rm top}(t = 0) - 1]e^{-(5\alpha^2+\kappa_s^*)t}$ (dotted line).

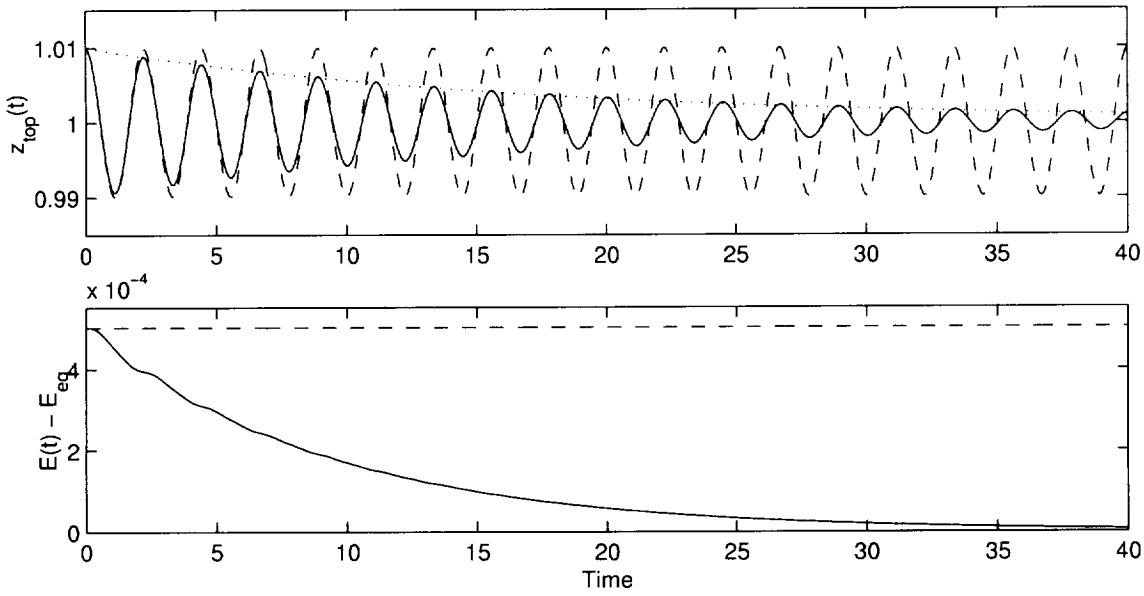

Figure 3.6: Simulations of an initially perturbed weakly viscous drop in vacuum with small surfactant effects for $(\alpha^2, e_s^*, \mu_s^*, \kappa_s^*, Pe_s) = 0$ (dashed line) and $(\alpha^2, \mu_s^*) = 0.005$ with $(e_s^*, \kappa_s^*, Pe_s) = 0$ (solid line). The initial conditions are $(\phi, \Psi) = 0$ and $|\mathbf{x}(\theta)| = R[1 + 0.01P_2(\cos\theta)]$ with $N = 31$, $N_c = 15$, and $\Delta t = 0.001$. The scale factor R in the initial shape ensures that the nondimensional equilibrium energy E_{eq} is 4π. Also shown is the theoretical prediction for the damped shape in this limit $z_{top}(t) = 1 + [z_{top}(t = 0) - 1]e^{-(5\alpha^2 + 12\mu_s^*)t}$ (dotted line).

Order-of-magnitude analysis

This section applies an order of magnitude analysis to the general expressions for the normal and tangential stress balance and kinematic boundary conditions, the equations for the vortical fields and the surfactant transport equation, written in local coordinates.

The order-of-magnitude estimates for the potential and vortical flow fields and the surfactant concentration, obtainted from the corresponding section in the theory, are given by

$$\mathbf{v} = \hat{\mathbf{n}}\,(u_{n0} + \alpha u_{n1}) + \hat{\mathbf{s}}\,(u_{s0} + \alpha u_{s1}) + \mathcal{O}(\alpha^2) \tag{3.120}$$

$$p = p_0 + \alpha p_1 + \mathcal{O}(\alpha^2) \tag{3.121}$$

$$\mathbf{V} = \hat{\mathbf{n}}\,\alpha U_{n1} + \hat{\mathbf{s}}\,(U_{s0} + \alpha^2 U_{s1}) + \mathcal{O}(\alpha^2) \tag{3.122}$$

$$P = \alpha P_1 + \mathcal{O}(\alpha^2) \tag{3.123}$$

$$\Gamma = 1 + \Gamma_0 + \alpha\Gamma_1 + \mathcal{O}(\alpha^2)\,, \tag{3.124}$$

where, as before, the lower case fields $(\mathbf{v}, p)$ refer to those resembling potential flow and the upper-case fields $(\mathbf{V}, P)$ refer to those resembling vortical flow. Here the $\mathcal{O}(\alpha)$ vortical pressure P_1 has been introduced to account for the nonlinear pressure not appearing in the linear analysis. The potential and vortical fields depend on both n and s, but unlike the potential flow fields, which vary slowly in n and s over a nondimensional length scale of $\mathcal{O}(1)$, the vortical fields vary rapidly in n, decaying exponentially away from the interface over a nondimensional length scale of $\mathcal{O}(\alpha)$ and slowly in s. The normal derivatives of the vortical fields are denoted by a scaled normal coordinate $n \to \alpha N$. For instance, the normal derivative of the $\mathcal{O}(1)$ tangential component of the vortical velocity

$$\frac{\partial U_{s0}}{\partial n} = \frac{1}{\alpha}\frac{\partial U_{s0}}{\partial N}\,, \tag{3.125}$$

where $\partial U_{s0}/\partial N$ is an $\mathcal{O}(1)$ quantity. The order-of-magnitude estimates for the surfactant concentration Γ depend only on s and vary slowly over a nondimensional length scale $\mathcal{O}(1)$.

Substituting the order-of-magnitude scales (3.120)–(3.124) into the boundary conditions (3.93)–(3.97) and expanding to $\mathcal{O}(\alpha^2)$, noting that a normal derivative of a vortical field introduces a factor of $1/\alpha$, yields

$$\begin{aligned} p_0 + \alpha\,(p_1 + P_1) &= (\mathcal{C}_s + \mathcal{C}_\varphi) - \mathrm{e}_s^*(\mathcal{C}_s + \mathcal{C}_\varphi)\Gamma_0 \\ &\quad + \mu_s^*(\mathcal{C}_s - \mathcal{C}_\varphi)(m_0^- + M_0^-) + \kappa_s^*(\mathcal{C}_s + \mathcal{C}_\varphi)(m_0^+ + M_0^+) + \mathcal{O}(\alpha^2)\,, \end{aligned} \tag{3.126}$$

$$\begin{aligned} \alpha\frac{\partial U_{s1}}{\partial N} &= -\mathrm{e}_s^*\frac{d\Gamma_0}{ds} \\ &\quad + \mu_s^*\left[\frac{\partial}{\partial s}(m_0^- + M_0^-) + \frac{2}{r}\frac{\partial r}{\partial s}(m_0^- + M_0^-)\right] + \kappa_s^*\frac{\partial}{\partial s}(m_0^+ + M_0^+) + \mathcal{O}(\alpha^2)\,, \end{aligned} \tag{3.127}$$

and

$$\frac{dr}{dt} = -\frac{\partial z}{\partial s}[u_{n0} + \alpha(u_{n1} + U_{n1})] + \mathcal{O}(\alpha^2) \tag{3.128}$$

$$\frac{dz}{dt} = \frac{\partial r}{\partial s}[u_{n0} + \alpha(u_{n1} + U_{n1})] + \mathcal{O}(\alpha^2)\,, \tag{3.129}$$

where

$$m_0^\pm = \left[\frac{\partial u_{s0}}{\partial s} \pm \frac{1}{r}\frac{\partial r}{\partial s}u_{s0} + (\mathcal{C}_s \pm \mathcal{C}_\varphi)u_{n0}\right]\Big|_{n=0} \tag{3.130}$$

$$M_0^\pm = \left(\frac{\partial U_{s0}}{\partial s} \pm \frac{1}{r}\frac{\partial r}{\partial s}U_{s0}\right)\Big|_{n=0}\,. \tag{3.131}$$

If the $\mathcal{O}(\alpha)$ terms are neglected in these equations, they simplify to those for the base potential flow, provided the unsteady Bernoulli equation is used to relate the pressure to the $\mathcal{O}(1)$ scalar velocity potential. In order to

incorporate the leading-order effects of bulk and surface viscosity and surfactant transport into the boundary integral formulation, the quantities at $\mathcal{O}(\alpha^2)$ must be determined. Of these the p_1 may again be absorbed into the base flow calculation.

The unknown quantities still to be determined include the P_1, Γ_0, $\partial V_{s0}/\partial N$, and the two e_s^* terms. Of these P_1 and $\partial V_{s0}/\partial n$ may be found by introducing a vector velocity potential for the vortical velocity and applying an order-of-magnitude analysis to the equations for the vortical fields to determine an evolution equation for the vector velocity potential and an expression for the vortical pressure in terms of this vector velocity potential both evaluated at the interface, as in the previous section. The U_{s0} and its arclength derivatives, however, cannot be determined using the techniques of previous sections. This is because the tangential component of the vortical velocity is defined in terms of the normal derivative of the vector velocity potential, which cannot be determined using any variable known only at the interface. Without the ability to calculate the tangential component of the vortical velocity explicitly, the techniques used in the previous cases may not be used to calculate the numerics for case 3.

Boulton-Stone [12] has developed alternate techniques to solve for the tangential velocity of the interface explicitly, by generating a thin grid near the interface which remains locally orthogonal in the local coordinate system, but this analysis is not attempted in this work.

3.3.4 Case 4: "large" surfactant effects

This section considers the effects of surface viscosity and surfactant transport on the shape oscillations of a drop in vacuum when the nondimensional surface properties e_s^*, μ_s^*, and κ_s^* are "large", or greater than $\mathcal{O}(\alpha)$. The formulation for this case neglects all effects at $\mathcal{O}(\alpha)$ and smaller.

For this case the bulk viscous dissipation and the effects of the vortical fields may be neglected to leading order. The flow field is calculated from potential flow equations and the shape of the interface is updated with the normal velocity from potential flow. Since the bulk viscous forces are neglected the tangential component of the interface velocity, however, is different from the tangential velocity from potential flow.

The governing equations are the regularized integral equations representing Laplace's equation for the potential flow in the drop and the surfactant transport equation. These equations are subject to the normal and tangential components of the leading-order stress balance boundary conditions

$$p = (\mathcal{C}_s + \mathcal{C}_\varphi) - \mathrm{e}_s^*(\mathcal{C}_s + \mathcal{C}_\varphi)(\Gamma - 1) + \mu_s^*(\mathcal{C}_s - \mathcal{C}_\varphi)M^- + \kappa_s^*(\mathcal{C}_s + \mathcal{C}_\varphi)M^+ \tag{3.132}$$

$$0 = -\mathrm{e}_s^*\frac{\partial \Gamma}{\partial s} + \mu_s^*\left(\frac{\partial M^-}{\partial s} + \frac{2}{r}\frac{\partial r}{\partial s}M^-\right) + \kappa_s^*\frac{\partial M^+}{\partial s}\,, \tag{3.133}$$

and the leading-order kinematic boundary condition

$$\frac{dr}{dt} = -\frac{\partial z}{\partial s}[u_{n0} + \alpha(u_{n1} + U_{n1})] + \mathcal{O}(\alpha^2) \tag{3.134}$$

$$\frac{dz}{dt} = \frac{\partial r}{\partial s}[u_{n0} + \alpha(u_{n1} + U_{n1})] + \mathcal{O}(\alpha^2)\,, \tag{3.135}$$

In the stress balance boundary conditions, and in the surfactant transport equation,

$$M^\pm = \left[\left(\frac{\partial V_s}{\partial s} \pm \frac{1}{r}\frac{\partial r}{\partial s}V_s\right) + (\mathcal{C}_s \pm \mathcal{C}_\varphi)v_n\right] \tag{3.136}$$

and is composed of the normal and tangential velocity components of the interface, where the normal interface velocity is the normal component of the potential flow velocity evaluated at the interface.

The tangential stress balance equation may be written in the form of a second-order differential equation for the unknown tangential interface velocity

$$a(s)\frac{\partial^2 V_s}{\partial s^2}(s) + b(s)\frac{\partial V_s}{\partial s}(s) + c(s)V_s(s) = d(s) \tag{3.137}$$

where a, b, c, and d are known functions from the potential flow and the shape. Since the tangential interface velocity is necessarily and odd function in arclength for this axisymmetric problem, it may be expanded in

a truncated sine series

$$V_s(s) = \sum_{k=1}^{N_c} C_k \sin\left(\frac{\pi k s}{L}\right) \tag{3.138}$$

where N_c is the number of coefficients limited by the Nyquist frequency. For discrete nodal values $s_i, i = 1 \ldots N$ in arclength the tangential stress balance boundary condition may be written

$$\sum_{k=1}^{N_c} A_{ik} C_k = d_i \tag{3.139}$$

where

$$A_{ik} = \left[c_i - a_i \left(\frac{\pi k}{L}\right)^2\right] \sin\left(\frac{\pi k s_i}{L}\right) + b_i \left(\frac{\pi k}{L}\right) \cos\left(\frac{\pi k s_i}{L}\right) . \tag{3.140}$$

If $N > N_c$ this equation represents an over-determined system of equations for the coefficients of the tangential interface velocity, and may be solved in a least-squares sense by multiplying each side of the equation by the transpose of A_{ik}. The tangential stress balance boundary condition becomes a matrix equation for the coefficients of the tangential interface velocity.

The modified boundary conditions for this case are

$$\left(\frac{D\phi}{Dt}\right)_n = \frac{1}{2}(v_n^2 - v_s^2) - (\mathcal{C}_s + \mathcal{C}_\varphi) + \mathrm{e}_s^*(\mathcal{C}_s + \mathcal{C}_\varphi)(\Gamma - 1) - \mu_s^*(\mathcal{C}_s - \mathcal{C}_\varphi)M^- - \kappa_s^*(\mathcal{C}_s + \mathcal{C}_\varphi)M^+ \tag{3.141}$$

$$\left(\frac{D\Gamma}{Dt}\right)_n = \frac{1}{\mathrm{Pe}_s}\frac{\partial^2 \Gamma}{\partial s^2} - V_s \frac{\partial \Gamma}{\partial s} - M^+ \Gamma \tag{3.142}$$

$$\frac{dr}{dt} = -\frac{\partial z}{\partial s} v_n \tag{3.143}$$

$$\frac{dz}{dt} = \frac{\partial r}{\partial s} v_n . \tag{3.144}$$

where the discrete form of the tangential stress balance boundary condition (3.140) is used to determine the tangential velocity of the interface.

The numerical procedure begins by initializing the $r(s)$, $z(s)$, $\phi(s)$, and $\Gamma(s)$. After calculating the arclengths, the kernels of the boundary integral formulation are formed and used to calculate the base potential flow velocity components. Using the known interface shape and base potential flow velocity components and the coefficients of the tangential velocity of the interface are found from. Finally, the right-hand sides of the above evolution equations for r, z, ϕ, Ψ, and Γ are updated with the Rung-Kutta time stepping scheme.

Without the need to calculate the vector velocity potential for the vortical velocity contribution, the simulations for this case suffered none of the numerical instabilities seen in the previous cases. The procedure using the tangential stress balance to solve for the tangential velocity of the interface worked well and allowed for the combinations of surface viscous and Marangoni effects to be analyzed.

Figure 3.7 shows a calculation in the limit when the Gibbs elasticity and surface Peclet number are zero with nonzero surface viscosities. Other simulations in this limit with $\mathcal{O}(1)$ surface viscosities showed an over-damped behavior.

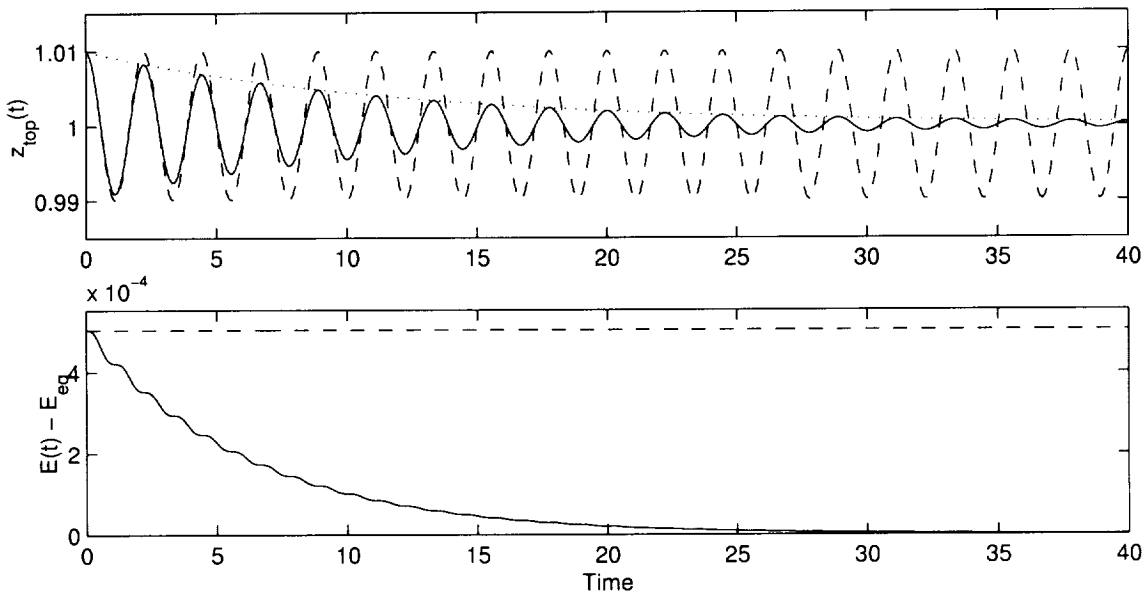

Figure 3.7: Simulations of an initially perturbed inviscid drop in vacuum with large surfactant effects for $(e_s^*, \kappa_s^*, \mu_s^*, Pe_s) = 0$ (dashed line) and $(\kappa_s^*, \mu_s^*) = 0.05$ with $(e_s^*, Pe_s) = 0$ (solid line). The initial conditions are $(\phi, \Psi) = 0$ and $|\mathbf{x}(\theta)| = R[1 + 0.01P_2(\cos\theta)]$ with $N = 31$, $N_c = 15$, and $\Delta t = 0.001$. The scale factor R in the initial shape ensures that the nondimensional equilibrium energy E_{eq} is 4π. Also shown is the theoretical prediction for the damped shape in this limit $z_{top}(t) = 1 + [z_{top}(t = 0) - 1]e^{-[16\kappa_s^*\mu_s^*/(3\kappa_s^* + 2\mu_s^*)]t}$ (dotted line).

Chapter 4

Summary and conclusions

In this research, the dynamics of a drop in a fluid medium with a surfactant contaminated interface are analyzed. The fluids are modeled as Newtonian, and the insoluble surfactant monolayer is modeled as a Boussinesq-Scriven Newtonian surface fluid. Using a linear relationship between the local surface tension and surfactant concentration, an exact mechanical energy equation was derived for the system. The resulting nondimensional total mechanical energy equation is

$$\begin{aligned} \frac{d}{dt}\{\text{K.E.} + \text{P.E.}\} &= -\alpha^2\{\text{Bulk Diss.}\} \\ &\quad -\mu_s^*\{\text{Surf. Diss.}\} \\ &\quad +e_s^*\{\text{Marangoni}\}\,. \end{aligned} \tag{4.1}$$

The terms in (4.1) are clearly identifiable as volume and surface integrals over each phase. In particular, the physical interpretation of the Marangoni term was shown to be a combination of energy storage and dissipation terms whose dominant contributions are controlled by the surface Peclet number.

A novel analysis of the total mechanical energy equation was performed using an averaging method. This method, when complemented with velocity field approximations found using matched asymptotic expansions, allows for the construction of a damped harmonic oscillator equation that approximately describes the dynamics of the system for small-amplitude shape oscillations. For the cases with surfactants this damped harmonic oscillator equation was coupled to a second o.d.e. that describes the surfactant transport.

For inviscid potential flow and a clean interface, the dynamics of the system are approximately described by the simple harmonic oscillator equation:

$$\ddot{a}_\ell + \frac{\ell(\ell-1)(\ell+1)(\ell+2)}{[(\ell+1)+\ell\hat{\rho}/\rho]}\,a_\ell = 0\,. \tag{4.2}$$

The nondimensional frequencies predicted by (4.2) are in agreement with the classical results of Lamb [23].

Adding viscosity to the system with a clean interface introduces damping. As shown in section 2.4.2 (Case 1), the shape oscillations of the viscous system are described by the equation

$$(1+\alpha \mathrm{A}_{\ell 1})\,\ddot{a}_\ell + (\alpha \mathrm{B}_{\ell 1} + \alpha^2 \mathrm{B}_{\ell 2})\,\dot{a}_\ell + \Omega_{\ell 0}^2\,a_\ell = 0\,. \tag{4.3}$$

Equation (4.3) differs from (4.2) in that it contains added mass and damping terms due to the bulk viscosity in both phases. The frequencies and damping constants for this case are accurate to $\mathcal{O}(\alpha^3)$ and agree with the results of Marston [28].

Even small surfactant effects lead to qualitative changes in the system. As shown in section 2.4.3 (Case 2), for a viscous drop in vacuum with weak $\mathcal{O}(\alpha^2)$ surfactant effects the dynamics of the system are described by a *coupled* set of equations:

$$\begin{aligned} \ddot{a}_\ell &+ \dot{a}_\ell\,[\alpha^2 2(\ell-1)(2\ell+1) + \kappa_s^*\ell(\ell-1)^2 + \mu_s^*(\ell-1)(\ell+1)(\ell+2)] \\ &+ a_\ell\,[\ell(\ell-1)(\ell+2)] = -g_\ell\,[\mathrm{e}_s^*\ell(\ell-1)]\,, \end{aligned} \tag{4.4}$$

$$\dot{g}_\ell + \frac{\ell(\ell+1)}{\mathrm{Pe}_s} g_\ell = (\ell-1)\dot{a}_\ell \,. \tag{4.5}$$

In this case, the size of the surface Peclet number Pe_s controls the modification of the frequency and damping constant.

The dynamics of the system becomes more complicated for slightly larger ("medium") surfactant effects. Section 2.4.4 (Case 3) shows that when κ_s^* and μ_s^* are $\mathcal{O}(\alpha)$, a damped harmonic oscillator equation can be found only when the Gibbs elasticity is zero. For the viscous drop in vacuum, that equation is

$$\begin{aligned}
& \ddot{a}_\ell \left\{ 1 + \frac{\alpha}{\sqrt{\Omega_{\ell 0}}} \frac{(\ell+1)}{\ell(2\ell+1)} \left[\frac{|C_{\theta 0}|^2}{\sqrt{2}} + \frac{2\ell}{(2\ell+1)} (C_{\theta 0} e^{-i\pi/4} + \text{c.c.}) \right] \right\} \\
+ \; & \dot{a}_\ell \left\{ \alpha \sqrt{\Omega_{\ell 0}} \frac{(\ell+1)}{\sqrt{2}} |C_{\theta 0}|^2 \right. \\
& \quad + \mu_s^* (\ell-1)(\ell+1)(\ell+2) \left[1 + (C_{\theta 0} + \text{c.c.}) + |C_{\theta 0}|^2 \right] \\
& \quad \left. + \kappa_s^* \ell \left[(\ell-1)^2 + (\ell-1)(\ell+1)(C_{\theta 0} + \text{c.c.}) + (\ell+1)^2 |C_{\theta 0}|^2 \right] \right\} \\
+ \; & a_\ell \left[\ell(\ell-1)(\ell+2) \right] = 0
\end{aligned} \tag{4.6}$$

The added mass and damping terms in this equation are relatively complicated functions of the Reynolds number and surface viscosities.

More straightforward results are available when the surfactant effects are $\mathcal{O}(1)$ and completely dominate the bulk viscous effects in the drop/medium system (Case 4). For that case, the following coupled system of equations is obtained in section 2.4.5:

$$\begin{aligned}
\ddot{a}_\ell [(\ell+1) + \ell\hat{\rho}/\rho] \; & + \; \dot{a}_\ell \left\{ \frac{4\kappa_s^* \mu_s^* \ell(\ell-1)(\ell+1)(\ell+2)}{[\kappa_s^* \ell(\ell+1) + \mu_s^* (\ell-1)(\ell+2)]} \right\} \\
& + \; a_\ell \left[\ell(\ell-1)(\ell+1)(\ell+2) \right] \\
& = \; g_\ell \left\{ \frac{2\mathrm{e}_s^* \mu_s^* \ell(\ell-1)(\ell+1)(\ell+2)}{[\kappa_s^* \ell(\ell+1) + \mu_s^* (\ell-1)(\ell+2)]} \right\}
\end{aligned} \tag{4.7}$$

$$\begin{aligned}
\dot{g}_\ell \; & + \; g_\ell \left\{ \frac{\ell(\ell+1)}{\mathrm{Pe}_s} + \frac{\mathrm{e}_s^* \ell(\ell+1)}{[\kappa_s^* \ell(\ell+1) + \mu_s^* (\ell-1)(\ell+2)]} \right\} \\
& = \; -\dot{a}_\ell \left\{ \frac{2\mu_s^* (\ell-1)(\ell+2)}{[\kappa_s^* \ell(\ell+1) + \mu_s^* (\ell-1)(\ell+2)]} \right\} .
\end{aligned} \tag{4.8}$$

Supplementing the small-amplitude theory just summarized, a numerical boundary integral equation formulation was developed for large-amplitude shape oscillations of a drop in vacuum. With an asymptotic analysis of the weakly singular integrands in the regularized integral equations, a discrete formulation for their solution was developed that only used the nodal values of the variables without special treatment near the singularities. To accurately calculate the higher-order arclength derivatives in the formulation, a least-squares spectral transform technique was used. The least-squares representation allowed for clean coding and gave a continuous, smooth representation of the dependent variables. Such a representation was essential in evaluating derivatives, integrals, and arclengths between unevenly-spaced nodes. It further provided an efficient way of solving for the tangential velocity of the interface when surface parameters were large. The results for the base potential flow calculations were validated with excellent agreement with theory for small-amplitude oscillations. With a second-order Runge-Kutta time-stepping scheme, example calculations for small-amplitude oscillations in the quadrupole mode conserved the total energy and volume with errors of less than $10^{-7}\%$.

Using the order-of-magnitude estimates for the velocity components from the theory, the boundary integral equation formulation for potential flow was extended to approximately include the effects of bulk viscosity, surface viscosity, and surfactant transport. These effects were approximated by including only the dominant terms (in α) in the general viscous boundary conditions at a surfactant-laden interface. For the case including bulk viscous effects with a clean interface, an instability was seen in the calculations. This well-known numerical instability [26, 11, 44] could be controlled with a five-point smoothing algorithm. The resulting calculations gave damping constants that were in excellent agreement with small-amplitude theory.

Section 3.3.2 examined bulk viscous effects and small surfactant effects in the numerics. In this case the numerical instability was much more difficult to control. Only the limit when either one of the surface viscosities was nonzero could be calculated with the smoothing algorithm. The damping constants calculated for each limit were in agreement with small-amplitude theory. For small-amplitude oscillations in the quadrupole mode, the additional damping from surface shear viscosity alone was an order of magnitude larger than that from surface dilatational viscosity.

Case 3 included bulk viscous and surfactant effects assuming the surface properties to be $\mathcal{O}(\alpha)$. The order-of-magnitude analysis for this case revealed that the tangential component of the vortical velocity was needed explicitly in the modified boundary conditions. Since this quantity is not available in the boundary integral formulation presented here, this case could not be treated.

When the surfactant effects were large (Case 4), the vortical velocity contribution could be neglected entirely by assuming that the tangential velocity of the interface was distinct from the underlying potential flow. This tangential velocity could be calculated by integrating the second-order differential equation that resulted from the tangential stress boundary condition. This second-order equation was solved by representing the tangential velocity of the interface as a truncated sine series and solving for the coefficients in a least-squares sense. Once the surface tangential velocity was known, the surfactant transport equation could be used to update the surfactant concentration simultaneously with the remaining surface variables and the drop shape. The resulting calculations for effects of surface viscosity were again found to agree with small-amplitude theory.

Appendix A

Surface theorems

Here the general forms for the Surface Reynolds Transport Theorem and Surface Divergence Theorem are given. The reader is referred to [4, 16, 31] for their derivation.

The Surface Reynolds Transport Theorem for a material surface S_m is:

$$\frac{d}{dt}\int_{S_m} \Phi \, dS = \int_{S_m} \frac{\partial \Phi}{\partial t} + \nabla_s \cdot (\mathbf{v}\Phi) \, dS \, . \tag{A.1}$$

where $\mathbf{\Phi}$ is a scalar, vector, or tensor field.

Referring to Figure A.1, the surface Divergence Theorem for a material surface S_m and material line element C_m is:

$$\int_{S_m} \nabla_s \cdot (\mathbf{I}_s \square \mathbf{\Phi}) \, dS = \int_{C_m} \hat{\boldsymbol{\eta}} \square \mathbf{\Phi} \, dl, \tag{A.2}$$

where $\square$ = " $\cdot$ ", " $\times$ ", or "(blank)".

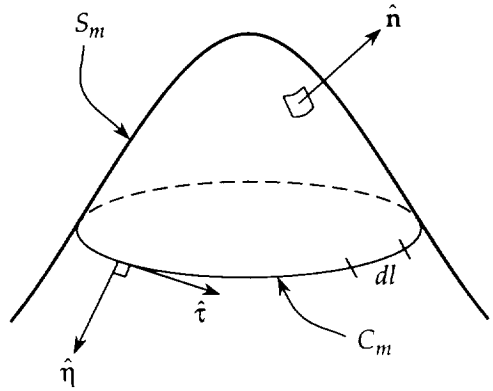

Figure A.1: A material surface S_m bounded by the material line C_m, where $\hat{\boldsymbol{\eta}}$ and $\hat{\tau}$ are perpendicular to the unit normal $\hat{\mathbf{n}}$.

Appendix B

Constants in matched asymptotics

Here the constants in the time-periodic uniformly valid velocity profiles and surfactant concentrations are given explicitly for cases 1-3.

B.1 Case 1: "negligible" surfactant effects

The constants $C_{\theta o}$ and $\hat{C}_{\theta o}$ are

$$C_{\theta o} = -\frac{(2\ell+1)}{(\ell+1)}\frac{\sqrt{\hat{\mu}\hat{\rho}}}{(\sqrt{\mu\rho}+\sqrt{\hat{\mu}\hat{\rho}})} \tag{B.1}$$

$$\hat{C}_{\theta o} = -\frac{(2\ell+1)}{\ell}\frac{\sqrt{\mu\rho}}{(\sqrt{\mu\rho}+\sqrt{\hat{\mu}\hat{\rho}})}\,. \tag{B.2}$$

The constants $C_{\theta 1}$ and $\hat{C}_{\theta 1}$ are given by the solution of the simultaneous equations:

$$\frac{\hat{\alpha}}{\alpha}\ell\hat{C}_{\theta 1} - (\ell+1)C_{\theta 1} = -\left[\frac{\hat{\alpha}}{\alpha}\ell^2\hat{C}_{\theta o} + (\ell+1)^2 C_{\theta o}\right] \tag{B.3}$$

$$\frac{\hat{\mu}}{\mu}\ell\hat{C}_{\theta 1} + (\ell+1)C_{\theta 1} = -\left\{\frac{\hat{\mu}}{\mu}\ell[(\ell+2)+\hat{C}_{\theta o}] - (\ell+1)[(\ell-1)-C_{\theta o}]\right\} \tag{B.4}$$

B.2 Case 2: "small" surfactant effects

The constants $C_{\theta 1}$ and $C_{\theta 2}$ are

$$C_{\theta 1} = \frac{-1}{\sqrt{\Omega_{\ell 0}}}\frac{\sqrt{2}}{(1+i)}\left[2(\ell-1) + \frac{\mathrm{e}_s^*}{\alpha^2}G + \frac{\mu_s^*}{\alpha^2}(\ell-1)(\ell+2) + \frac{\kappa_s^*}{\alpha^2}\ell(\ell+1)\right] \tag{B.5}$$

$$C_{\theta 2} = \frac{1}{\sqrt{\Omega_{\ell 0}}}\frac{\sqrt{2}}{(1+i)}C_{\theta 1}\left[2 - \frac{\mathrm{e}_s^*}{\alpha^2}\frac{C_{g1}}{C_{\theta 1}} - \frac{\mu_s^*}{\alpha^2}(\ell-1)(\ell+2) - \frac{\kappa_s^*}{\alpha^2}\ell(\ell+1)\right]\,. \tag{B.6}$$

The constants G, C_{g1}, and C_{g2} are

$$G = \ell(\ell-1)\mathrm{Pe}_s\left[\frac{\ell(\ell+1) - i\Omega_{\ell 0}\mathrm{Pe}_s}{\ell^2(\ell+1)^2 + \Omega_{\ell 0}^2\mathrm{Pe}_s^2}\right] \tag{B.7}$$

$$C_{g1} = \frac{(\ell+1)}{(\ell-1)}C_{\theta 1} \tag{B.8}$$

$$C_{g2} = \frac{(\ell+1)}{(\ell-1)}\left[C_{\theta 2} - \frac{\sqrt{2}}{(1+i)}(\ell+1)\frac{C_{\theta 1}}{\sqrt{\Omega_{\ell 0}}}\right]\,. \tag{B.9}$$

B.3 Case 3: "medium" surfactant effects

The constant $C_{\theta 0}$ is

$$C_{\theta 0} = \frac{n_1 + n_2 e^{i\pi/2}}{d_1 + d_2 e^{i\pi/4} + d_3 e^{i\pi/2}}, \tag{B.10}$$

where

$$n_1 = -\frac{\mathrm{e}_s^* \mathrm{Pe}_s \ell^2(\ell-1)(\ell+1)}{\ell^2(\ell+1)^2 + \Omega_{\ell 0}^2 \mathrm{Pe}_s^2} - \kappa_s^* \ell(\ell-1) - \mu_s^*(\ell-1)(\ell+2) \tag{B.11}$$

$$n_2 = \frac{\mathrm{e}_s^* \Omega_{\ell 0} \mathrm{Pe}_s^2 \ell(\ell-1)}{\ell^2(\ell+1)^2 + \Omega_{\ell 0}^2 \mathrm{Pe}_s^2} \tag{B.12}$$

$$d_1 = \frac{\mathrm{e}_s^* \mathrm{Pe}_s \ell^2(\ell+1)^2}{\ell^2(\ell+1)^2 + \Omega_{\ell 0}^2 \mathrm{Pe}_s^2} + \kappa_s^* \ell(\ell+1) + \mu_s^*(\ell-1)(\ell+2) \tag{B.13}$$

$$d_2 = \alpha \sqrt{\Omega_{\ell 0}} \tag{B.14}$$

$$d_3 = -\frac{\mathrm{e}_s^* \Omega_{\ell 0} \mathrm{Pe}_s^2 \ell(\ell+1)}{\ell^2(\ell+1)^2 + \Omega_{\ell 0}^2 \mathrm{Pe}_s^2}. \tag{B.15}$$

The constant G is

$$G = \ell(\ell-1)\mathrm{Pe}_s \left[\frac{\ell(\ell+1) - i\Omega_{\ell 0}\mathrm{Pe}_s}{\ell^2(\ell+1)^2 + \Omega_{\ell 0}^2 \mathrm{Pe}_s^2} \right]. \tag{B.16}$$

The constants $C_{\theta 1}$ and C_{g1} take similar but more complicated forms and are not written explicitly here. They are not needed in the leading-order analysis of the energy equation for Case 3.

Appendix C

Local coordinate system

$$\mathbf{x}(s,\varphi) = \hat{\mathbf{e}}_r(\varphi)r(s) + \hat{\mathbf{e}}_z z(s) \tag{C.1}$$
$$\hat{\mathbf{s}}(s,\varphi) = \hat{\mathbf{e}}_r(\varphi)r'(s) + \hat{\mathbf{e}}_z z'(s) \tag{C.2}$$
$$\hat{\mathbf{n}}(s,\varphi) = -\hat{\mathbf{e}}_r(\varphi)z'(s) + \hat{\mathbf{e}}_z r'(s) \tag{C.3}$$

In local coordinates (n, s, φ), the unit tensor, the gradient, operator and their projections onto the interface are given by

$$\mathbf{I} = \hat{\mathbf{n}}\hat{\mathbf{n}} + \hat{\mathbf{s}}\hat{\mathbf{s}} + \hat{\mathbf{e}}_\varphi\hat{\mathbf{e}}_\varphi\,, \tag{C.4}$$
$$\mathbf{I}_s = \mathbf{I} - \hat{\mathbf{n}}\hat{\mathbf{n}} = \hat{\mathbf{s}}\hat{\mathbf{s}} + \hat{\mathbf{e}}_\varphi\hat{\mathbf{e}}_\varphi\,, \tag{C.5}$$
$$\boldsymbol{\nabla} = \hat{\mathbf{n}}\,h_n\frac{\partial}{\partial n} + \hat{\mathbf{s}}\,h_s\frac{\partial}{\partial s} + \hat{\mathbf{e}}_\varphi\,h_\varphi\frac{\partial}{\partial\varphi}\,, \tag{C.6}$$
$$\boldsymbol{\nabla}_s = \mathbf{I}_s\cdot\boldsymbol{\nabla} = \hat{\mathbf{s}}\,h_s\frac{\partial}{\partial s} + \hat{\mathbf{e}}_\varphi\,h_\varphi\frac{\partial}{\partial\varphi}\,, \tag{C.7}$$

where h_n, h_s, and h_φ are metric coefficients that are functions of n, s, and φ in general. For points at a constant meridian angle (φ = constant) and on the interface ($n = 0$), the metrical coefficients and their derivatives are given by

$$\begin{array}{lll}
h_n = 1 & h_s = 1 & h_\varphi = \dfrac{1}{r} \\
\dfrac{\partial h_n}{\partial n} = 0 & \dfrac{\partial h_s}{\partial n} = -\mathcal{C}_s & \dfrac{\partial h_\varphi}{\partial n} = \dfrac{z'}{r^2} \\
\dfrac{\partial h_n}{\partial s} = 0 & \dfrac{\partial h_s}{\partial s} = 0 & \dfrac{\partial h_\varphi}{\partial s} = -\dfrac{r'}{r^2} \\
\dfrac{\partial h_n}{\partial\varphi} = 0 & \dfrac{\partial h_s}{\partial\varphi} = 0 & \dfrac{\partial h_\varphi}{\partial\varphi} = 0 \\
\dfrac{\partial\hat{\mathbf{n}}}{\partial n} = \mathbf{0} & \dfrac{\partial\hat{\mathbf{s}}}{\partial n} = \mathbf{0} & \dfrac{\partial\hat{\mathbf{e}}_\varphi}{\partial n} = \mathbf{0} \\
\dfrac{\partial\hat{\mathbf{n}}}{\partial s} = \hat{\mathbf{s}}\,\mathcal{C}_s & \dfrac{\partial\hat{\mathbf{s}}}{\partial s} = -\hat{\mathbf{n}}\,\mathcal{C}_s & \dfrac{\partial\hat{\mathbf{e}}_\varphi}{\partial s} = \mathbf{0} \\
\dfrac{\partial\hat{\mathbf{n}}}{\partial\varphi} = -\hat{\mathbf{e}}_\varphi z' & \dfrac{\partial\hat{\mathbf{s}}}{\partial\varphi} = \hat{\mathbf{e}}_\varphi r' & \dfrac{\partial\hat{\mathbf{e}}_\varphi}{\partial\varphi} = \hat{\mathbf{n}}\,z' - \hat{\mathbf{s}}\,r'\,,
\end{array} \tag{C.8}$$

where $\mathcal{C}_s = z'r'' - r'z''$ is the curvature in the $\hat{\mathbf{s}}$ direction, and primes denote differentiation with respect to s.

Appendix D

Explicit kernels in numerics

Here the forms of the kernels and their asymptotic behavior as $s \to s_i$ are given explicitly in terms of the axisymmetric arclength parameterization (at constant φ) $\mathbf{x}(s) = \hat{\mathbf{e}}_r r(s) + \hat{\mathbf{e}}_z z(s)$, where $ds^2 = d\mathbf{x} \cdot d\mathbf{x}$. The kernels in the regularized double-layer potential boundary integral representation (3.8) and relation (3.9) take the parameterized forms

$$\begin{aligned}
&\hat{\mathbf{n}}(s) \cdot \nabla G(s_i, s)\, r(s) \;=\; \\
&\quad -\frac{r(s)\{[z(s_i) - z(s)]r'(s) + [r(s_i) + r(s)]z'(s)\}}{\pi\{[r(s_i) + r(s)]^2 + [z(s_i) - z(s)]^2\}^{3/2}} \left[\frac{E(m)}{(1-m)}\right] \\
&\quad +\frac{z'(s)}{2\pi\{[r(s_i) + r(s)]^2 + [z(s_i) - z(s)]^2\}^{1/2}} \left[\frac{E(m)}{(1-m)} - K(m)\right],
\end{aligned} \tag{D.1}$$

$$\begin{aligned}
&\hat{\mathbf{e}}_\varphi \cdot [\hat{\mathbf{n}}(s) \times \nabla G(s_i, s)\, r(s)] \;=\; \\
&\quad \frac{r(s)\{[z(s_i) - z(s)]z'(s) - [r(s_i) + r(s)]r'(s)\}}{\pi\{[r(s_i) + r(s)]^2 + [z(s_i) - z(s)]^2\}^{3/2}} \left[\frac{E(m)}{(1-m)}\right] \\
&\quad -\frac{\{[z(s_i) - z(s)]z'(s) - r(s)r'(s)\}}{2\pi r(s_i)\{[r(s_i) + r(s)]^2 + [z(s_i) - z(s)]^2\}^{1/2}} \left[\frac{E(m)}{(1-m)} - K(m)\right],
\end{aligned} \tag{D.2}$$

where

$$m = m(s_i, s) = \frac{4r(s_i)r(s)}{[r(s_i) + r(s)]^2 + [z(s_i) - z(s)]^2} \tag{D.3}$$

and primes ($'$) denote differentiation with respect to arclength s. $K(m)$ and $E(m)$ are, respectively, the complete elliptic integrals of the first and second kind. Accurate asymptotic expressions for $K(m)$ and $E(m)$ may be found in [1].

As $s \to s_i$ the above kernels have the asymptotic behaviors

$$\begin{aligned}
&\hat{\mathbf{n}}(s) \cdot \nabla G(s_i, s)\, r(s) \;\sim\; \\
&\quad \frac{1}{4\pi}\left\{-\mathcal{C}_\varphi(s_i) \log\left[\frac{(s - s_i)}{4\sqrt{2}r(s_i)}\right] + \mathcal{C}_s(s_i) - \mathcal{C}_\varphi(s_i)\right\} + \mathcal{O}(s - s_i),
\end{aligned} \tag{D.4}$$

$$\begin{aligned}
&\hat{\mathbf{e}}_\varphi \cdot [\hat{\mathbf{n}}(s) \times \nabla G(s_i, s)\, r(s)] \;\sim\; \\
&\quad \frac{1}{2\pi}\left\{\frac{1}{(s - s_i)} + \frac{1}{2}\frac{r'(s_i)}{r(s_i)} \log\left[\frac{(s - s_i)}{4\sqrt{2}r(s_i)}\right]\right\} + \mathcal{O}(s - s_i),
\end{aligned} \tag{D.5}$$

where $\mathcal{C}_s(s) = z'(s)r''(s) - r'(s)z''(s)$ and $\mathcal{C}_\varphi(s) = -z'(s)/r(s)$.

Bibliography

[1] ABRAMOWITZ, M. & STEGUN, I.A. 1965 *Handbook of Mathematical Functions.* Dover.

[2] ALONZO, C.T. 1974 The dynamics of colliding and oscillating drops. In *Proceedings of the International Colloquium on Drops and Bubbles* (ed. Collins, D.J., Plesset, M.S. & Saffren, M.M.), **1**, 139–157. Jet Propulsion Laboratory, Pasadena, CA.

[3] APFEL, R.E., TIAN, Y., JANKOVSKI, J., SHI., T. & CHEN, X. 1997 Free oscillations and surfactant studies of superdeformed drops in microgravity. *Physical Review Letters*, **78**, 1912–1915.

[4] ARIS, R. 1962 *Vectors, Tensors and the Basic Equations of Fluid Mechanics.* Dover.

[5] ASAKI, T.J. & MARSTON, P.L. 1995 The effects of a soluble surfactant on quadrupole shape oscillations and dissolution of bubbles in water. *Journal of the Acoustical Society of America*, **102**(6), 3372–3377.

[6] ASAKI, T.J., MARSTON, P.L. & TRINH, E.H. 1995 Free decay of shape oscillations of bubbles acoustically trapped in sea water. *Journal of Fluid Mechanics*, **300**, 149–167.

[7] BASARAN, A.O. 1992 Nonlinear oscillations of viscous liquid drops. *Journal of Fluid Mechanics*, **241**, 169–198.

[8] BATCHELOR, G.K. 1967 *An Introduction to Fluid Mechanics.* Cambridge University Press.

[9] BECKER, E., HILLER, W.J. & KOWALEWSKI, T.A. 1991 Experimental and theoretical investigation of large-amplitude oscillations of liquid drops. *Journal of Fluid Mechanics*, **231** 189–210

[10] BECKER, E., HILLER, W.J. & KOWALEWSKI, T.A. 1994 Nonlinear dynamics of viscous droplets. *Journal of Fluid Mechanics*, **258**, 191–216.

[11] BOULTON-STONE, J.M. 1993 A comparison of boundary integral methods for studying the motion of a two-dimensional bubble in a infinite fluid. *Computational Methods in Applied Mechanics and Engineering*, **102**, 213-234.

[12] BOULTON-STONE, J.M. 1993 A two-dimensional bubble near a free surface. *Journal of Engineering Mathematics*, **27**, 73–87.

[13] BROSA, U., GROSSMANN, S., MULLER, A. & BECKER, E. 1989 Nuclear scission. *Nuclear Physics A*, **502**, 423c–442c.

[14] CHANDRASEKHAR, S. 1961 *Hydrodynamic and Hydromagnetic Stability.* Dover.

[15] CHEN, X., SHI, T., TIAN, Y., JANKOVSKY, J., HOLT, R.G., APFEL, R.E. 1998 Numerical simulation of superoscillations of a Triton-bearing drop in microgravity. *Journal of Fluid Mechanics*, **367**, 205–220.

[16] EDWARDS, D.A., BRENNER, H. & WASAN, D.T. 1991 *Interfacial Transport Processes and Rheology.* Butterworth-Heinemann, Boston.

[17] FENG, Z.C. & LEAL, L.G. 1997 Nonlinear bubble dynamics. *Annual Review of Fluid Mechanics*, **29**, 201–243.

[18] FENG, J.Q. & BEARD, K.V. 1990 Three-dimensional oscillations of electrostatically deformed drops. *Journal of Fluid Mechanics*, **227**, 429-445.

[19] FOOTE, G.B. 1973 A numerical method for studying simple drop behavior: simple oscillation. *Journal of Computational Physics*, **11**, 507–530.

[20] HSU, C.J. & APFEL, R.E. 1987 Model for the quadrupole oscillations of drops for determining interfacial tension. *Journal of the Acoustical Society of America*, **82**, 2135–2144.

[21] JORDAN, D.W. & SMITH, P. 1987 *Nonlinear Ordinary Differential Equations*, 2nd ed. Clarendon Press. Oxford.

[22] KELVIN, LORD 1890 Oscillations of a liquid sphere. *Mathematical Papers*, Clay & Sons.

[23] LAMB, H. 1932 *Hydrodynamics*, 6th ed. Cambridge University Press. [Reprinted by Dover (1945).]

[24] LEVICH, V.G. 1962 *Physiochemical Hydrodynamics*. Prentice-Hall, New Jersey.

[25] LU, H.L. & APFEL, R.E. 1991 Shape oscillations of drops in the presence of surfactants. *Journal of Fluid Mechanics*, **222**, 351 368.

[26] LUNDGREN, T.S. & MANSOUR, N.N. 1988 Oscillation of drops in zero gravity with weak viscous effects, *Journal of Fluid Mechanics*, **194**, 479–510.

[27] MARSTON, P.L. & APFEL, R.E. 1979 Acoustically-forced shape oscillations of hydrocarbon drops levitated in water. *Journal of Colloid and Interface Science*, **68**, 280–286.

[28] MARSTON, P.L. 1980 Shape oscillation and static deformation of drops and bubbles driven by modulated radiation stresses — theory. *Journal of the Acoustical Society of America*, **67**, 15 26. [Erratum **71**, 511–512, (1982).]

[29] MILLER, C.A. & SCRIVEN, L.E. 1968 The oscillations of a fluid droplet immersed in another fluid. *Journal of Fluid Mechanics*, **32**, 417–435.

[30] NADIM, A. & STONE, H.A. 1990 The motion of small particles and droplets in quadratic flows. *Studies in Applied Mathematics*, **85**, 53.

[31] NADIM, A. 1996 A concise introduction to surface rheology with application to dilute emulsions of viscous drops. *Chemical Engineering Communications*, **148–150**, 391–407.

[32] NADIM, A. & RUSH B.M. 1998 Mechanisms contributing to the damping of shape oscillations of liquid drops. In *Third International Conference on Multiphase Flow*, Lyon, France, June 8–12.

[33] NATARAJAN, R. & BROWN, R.A. 1986 Quadratic resonance in the three-dimensional oscillations of inviscid drops with surface tension. *Phys. Fluids* **29**, 2788–2797.

[34] NATARAJAN, R. & BROWN, R.A. 1987 Third-order resonance effects and the nonlinear stability of drop oscillations. *J. Fluid Mech.* **183**, 95–121.

[35] POZRIKIDIS, C. 1997 *Introduction to Theoretical and Computational Fluid Dynamics*. Oxford University Press, New York.

[36] PRESS, W.H., TEUKOLSKY, S.A., VETTERLING, W.T., & FLANNERY, B.P. 1992 *Numerical Recipes in FORTRAN: The Art of Scientific Computing*, 2nd ed. Cambridge University Press, New York.

[37] PROSPERETTI, A. 1977 Viscous effects on perturbed spherical flows. *Quarterly of Applied Mathematics* **35** 339.

[38] PROSPERETTI, A. 1980 Free oscillations of drops and bubbles: the initial-value problem. *Journal of Fluid Mechanics* **100**, 333–347.

[39] RAYLEIGH, LORD, 1894 *The Theory of Sound*, 2nd ed. Macmillan. [Reprinted by Dover (1945).]

[40] REID, W.H. 1960 The oscillations of a viscous liquid drop. *Quarterly of Applied Mathematics*, **18**, 86–89.

[41] ROBERTS, P.H. & WU, C.C. 1998 The decay of bubble oscillations. *Phys of Fluids*, **10**(12), 3227–3229.

[42] RUSH, B.M. & NADIM, A. 2000 The shape oscillations of a two-dimensional drop including viscous effects. *Engineering Analysis with Boundary Elements*, **24**, 43–51.

[43] SCRIVEN, L.E. 1960 Dynamics of a fluid interface. *Chemical Engineering Science*, **12**, 98–108.

[44] SHI, T. & APFEL, R.E. 1995 Oscillations of a deformed liquid drop in an acoustic field. *Physics of Fluids*, **7**(7), 1545–1552.

[45] TIAN, Y., HOLT, R.G. & APFEL, R.E. 1995 Investigations of liquid surface rheology of surfactant solutions by droplet shape oscillations: Theory. *Physics of Fluids*, **7**(12), 2938–2949.

[46] TRINH, E.H., ZWERN, A. & WANG, T.G. 1982a An experimental study of small-amplitude drop oscillations in immiscible liquid systems. *Journal of Fluid Mechanics*, **115**, 453–474.

[47] TRINH, E.H. & WANG, T.G. 1982b Large-amplitude free and driven drop-shape oscillations: experimental results, *Journal of Fluid Mechanics*, **122**, 315–338.

[48] TRINH, E.H., MARSTON, P.L. & ROBEY, J.L. 1987 Acoustic measurement of the surface tension of levitated drops. *Journal of Colloid and Interface Science*, **124**, 95–103.

[49] TRINH, E.H., HOLT, R.G., & THIESSEN, D.B. 1996 The dynamics of ultrasonically levitated drops in an electric field, *Physics of Fluids*, **6**, 3567–3579.

[50] TRINH, E.H., THIESSEN, D.B., & HOLT, R.G. 1998 Driven and freely decaying nonlinear shape oscillations of drops and bubbles immersed in a liquid: experimental results. *Journal of Fluid Mech.*, **364**, 253–272.

[51] TSAMOPOULOS, J.A. & BROWN, R.A. 1983 Nonlinear oscillations of inviscid drops and bubbles. *Journal of Fluid Mechanics*, **127**, 519–537.

[52] TSAMOPOULOS, J.A. & BROWN, R.A. 1984 Resonant oscillations of inviscid charged drops. *Journal of Fluid Mechanics*, **147**, 373–395.

[53] VALENTINE, R.S., SATHER, N.F. & HEIDEGER, W.J. 1965 The motion of drops in viscous media, *Chemical Engineering Science*, **20**, 719–728.

[54] VAN DYKE, M. 1964 *Perturbation Methods in Fluid Mechanics*. Academic Press, New York.